Title	An investigation of the role of TRIB2 in steady state and stressed haematopoiesis
Author(s)	Liang, Kai Ling
Publication date	2016
Original citation	Liang, K. L. 2016. An investigation of the role of TRIB2 in steady state and stressed haematopoiesis. PhD Thesis, University College Cork.
Type of publication	Doctoral thesis
Rights	© 2016, Kai Ling Liang. http://creativecommons.org/licenses/by-nc-nd/3.0/ ![CC BY NC ND]
Embargo information	No embargo required
Item downloaded from	http://hdl.handle.net/10468/3106

University College Cork, Ireland
Coláiste na hOllscoile Corcaigh

An investigation of the role of TRIB2 in steady state and stressed haematopoiesis

Kai Ling Liang

BSc, MSc

Submitted in fulfilment of the requirements for the degree of

Doctor of Philosophy in Cancer Biology

National University of Ireland, Cork

School of Biochemistry and Cell Biology

August 2016

Head of School: Professor David Sheehan

Supervisors:

Dr. Karen Keeshan & Professor Tommie V. McCarthy

Table of Contents

4

Declaration

The thesis submitted is my own work, except where explicit reference is made to the contribution of others, and has not been submitted for another degree, either at University College Cork or elsewhere.

Signed: _____ (Kai Ling Liang)

Date: __15st AUGUST 2016_

Acknowledgements

First and foremost, I would like to thank my joint supervisors, Dr. Karen Keeshan from University of Glasgow (UoG, UK) and Professor Tommie McCarthy from University College Cork (UCC, Ireland) for their support throughout the duration of my PhD study. This thesis was not possible without their guidance. I enjoyed the time I spent in both laboratories and I am grateful for being given the opportunity to work under their supervision.

I would like to acknowledge people who contributed to the research presented in this thesis. I thank Caitriona O'Connor and Pedro Veiga for their help in collecting the experimental data for bone marrow haematopoiesis at steady state. I thank Joana Campos for providing her experimental data regarding *Trib2* knockdown in U937 cells. I thank all the principal investigators and the technical staffs at Paul O' Gorman Leukaemia Research Centre, UK especially Dr. Alison Michie, Karen Dunn and Hothri Ananyamb Moka. I also thank the technical staffs at the School of Biochemistry and Cell Biology, UCC.

I would like to thank the UoG for appointing me as a visiting postgraduate researcher. This allowed me to do research in Dr. Karen Keeshan's laboratory at Paul O'Gorman Leukaemia Research Centre. All the mice experiments described in this thesis were carried out at Biological Service Unit facilities at the Cancer Research UK Beatson Institute and the UoG Biological Services.

I am indebted to my parents and my brother (Kai Siang) for their support.

Last but not least, I would like to thank Health Research Board Ireland for funding my research through UCC PhD Scholars Program in Cancer Biology. I thank Dr. Kellie Dean, the coordinator of my PhD Program for her support and advice. I thank Professor Rosemary O'Connor, the director and the steering committee of my PhD Program for giving me the opportunity to pursue my PhD at the UCC.

Abstract

TRIB2 is a member of the mammalian Tribbles family of serine/threonine pseudokinases (TRIB1-3). In malignant haematopoiesis, *Trib2* has been identified as an oncogene in myeloid leukaemogenesis. However, *Trib2* is expressed physiologically at high levels in the T cell compartment of normal haematopoiesis and the normal haematopoietic role of TRIB2 remains elusive. Here, we studied murine haematopoiesis after *Trib2* ablation under steady state and proliferative stress conditions, including genotoxic and oncogenic stress.

At the steady state, we found that TRIB2 loss did not adversely affect peripheral blood cell counts and populations. *Trib2*$^{-/-}$ mice had similar bone marrow cellularity compared to wild type mice and no detectable significant differences found in the populations of haematopoietic stem and progenitor cells. However, *Trib2*$^{-/-}$ mice had significantly higher thymic cellularity due to the increased proliferation of *Trib2*$^{-/-}$ developing thymocytes which give rise to increased number of CD4/CD8 double and CD4 single positive mature thymic subsets.

During stress haematopoiesis, *Trib2*$^{-/-}$ developing thymocytes undergo accelerated proliferation and demonstrate hypersensitivity to 5-fluorouracil-induced cell death. Despite the increased cell death post 5-fluorouracil-induced proliferative stress, *Trib2*$^{-/-}$ mice exhibit accelerated thymopoietic recovery post treatment due to expansion of *Trib2*$^{-/-}$ c-Kit$^-$ CD4/CD8 double negative 1 thymic progenitors and increased cell division kinetics of developing thymocytes. The increased proliferation in *Trib2*$^{-/-}$ thymocytes was exacerbated under oncogenic stress. In an experimental murine T-cell acute lymphoblastic leukaemia model, *Trib2*$^{-/-}$ mice had reduced latency *in vivo* which associated with aggressive phenotypes of T-cell acute lymphoblastic leukaemia and impaired activation of mitogen-activated protein

kinase. Gene set enrichment analysis showed that *TRIB2* expression is elevated in immature subtype of human T-cell acute lymphoblastic leukaemia enriched with mitogen-activated protein kinase signalling. However, *TRIB2* expression is suppressed in mature subtype of human T-cell acute lymphoblastic leukaemia associated with impaired mitogen-activated protein kinase signalling. Thus, TRIB2 emerges as a novel regulator of thymocyte cellular proliferation, important for the thymopoietic response to genotoxic and oncogenic stress, and possessing tumour suppressor function.

In *Drosophila*, Tribbles promotes degradation of String which is an orthologue of mammalian CDC25 phosphatases in order to arrest cell cycle during embryonic development. Given the anti-proliferative role we established for *Trib2* in the context of developing thymocytes during intrathymic T-cell development, we also examined if the role of Tribbles-induced degradation of String is conserved in TRIB2. We found that TRIB2 interacts physically with CDC25B/C but not CDC25A isoform. Overexpression of TRIB2 promotes K48-linked polyubiquitination of CDC25C and degradation of CDC25C in the nucleus. Hence, this provides an insight into the molecular mechanism of TRIB2-mediated regulation of cell cycle. Future works are warranted to examine TRIB2-CDC25C interaction in the context of developing thymocytes and in T-cell acute lymphoblastic leukaemia, the malignant counterpart.

List of Abbreviations

4', 6-diamidino-2-phenylindole…………………………………………………...DAPI

5-fluorouracil……………………………………………………………….5-FU

Acute myeloid leukaemia……………………………………………………AML

Adenosine 5'-triphosphate………………………………………………….ATP

Analysis of variance………………………………………………………...ANOVA

Anaphase-promoting complex/cyclosome...APC/C

Asynchronous sample……………………………………………………….AS

Basic Local Alignment Search Tool……………………………………….BLAST

Beta-transducin repeat containing protein..β-TRCP

Bone marrow………………………………………………………………..BM

Bovine serum albumin……………………………………………………….BSA

Breast cancer type 1 susceptibility protein..BRCA

Bromodeoxyuridine………………………………………………………….BrdU

c-Jun N-terminal kinase...JNK

Ca^{2+}/calmodulin-activated serine-threonine kinase...CASK

CCAAT enhancer-binding protein...CEBP

Cell division cycle 25...CDC25

Complementary DNA………………………………………………………..cDNA

Common lymphoid progenitors……………………………………………CLPs

Common myeloid progenitors……………………………………………...CMPs

Constitutive photomorphogenesis 1...COP1

Cyclin dependent kinase……………………………………………………CDK

Dalton……………………………………………………………………….Da

Deoxyribonucleic acid……………………………………………………...DNA

Dimethylsulfoxide…………………………………………………………..DMSO

Double negative……………………………………………………………..DN

Double positive……………………………………………………………...DP

Dulbecco's Modified Eagle Medium……………………………………….DMEM

E2F transcription factor 1...E2F1

Ethylenediaminetetraacetic acid…………………………………………….EDTA

Event-free survival………………………………………………………….EFS

Extracellular signal-regulated kinase..ERK

Fetal bovine serum………………………………………………………….FBS

Fluorescein isothiocyanate………………………………………………….FITC

Fluorescence Minus One……………………………………………………FMO

List of Figures

List of Tables

Related publications (please refer to Appendix)

1   Liang KL, Rishi L, Keeshan K. Tribbles in acute leukemia. *Blood* 2013; **121**:4265-4270.

2   Liang KL, O'Caitriona C, Veiga JP, McCarthy TV, Keeshan K. TRIB2 regulates normal and stress-induced thymocyte proliferation. *Cell Discovery* 2016; **2**: 15050.

3   Liang KL, Paredes R, Carmody R, Eyers PA, Meyer S, McCarthy TV, Keeshan K. Human TRIB2 oscillates during the cell cycle and promotes ubiquitination and degradation of CDC25C. Manuscript under revision.

CHAPTER 1: INTRODUCTION

1.1 Discovery of Tribbles family

The *Tribbles* gene was first discovered in three independent *Drosophila* genetic screens. Two screens (Seher and Leptin, 2000, Grosshans and Wieschaus, 2000) were designed to identify mutations that affect gastrulation, the formation of ventral furrow by mesodermal precursor cells during *Drosophila* embryo development. In *Tribbles* mutants, the precursor cells have premature mitosis and this leads to defective gastrulation. These studies identified Tribbles as an inhibitor of mitosis and suggested that Tribbles inhibits String function, the *Drosophila* ortholog of Cell division cycle 25 (CDC25) phosphatase family that is required to initiate mitosis. The third screen discovered Tribbles as one of the genes that affect oogenesis when being overexpressed (Mata et al., 2000). This study investigated Tribbles in *Drosophila* wing and embryonic developments, and demonstrated that Tribbles coordinates mitosis and morphogenesis by promoting proteasomal dependent degradation of String. Another role of Tribbles in *Drosophila* was found to promote the degradation of Slbo, the *Drosophila* ortholog of CCAAT enhancer-binding protein (CEBP) family of transcription factors during oogenesis (Rorth et al., 2000).
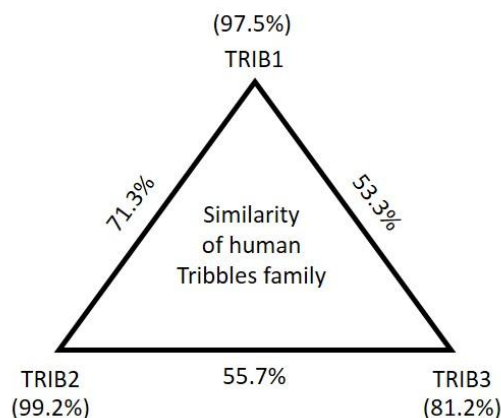
Figure 1.1 │ High degrees of similarity between the amino acid sequences of Tribbles members within the human family. TRIB1 and TRIB2 (71.3%) are more similar compared to TRIB3. The values in parentheses indicate similarity compared to the corresponded mouse Tribbles members.

There are three members (TRIB1-3) for mammalian Tribbles family. All the members are highly conserved between mouse and human (Figure 1.1) and have been identified as important signalling modulators and mediators in various diseases (Yokoyama and Nakamura, 2011). Studies of Tribbles deficient mice are invaluable in this aspect. Satoh and colleagues found that *Trib1* knockout mice have diminished adipose tissue mass due to a defect in the differentiation of tissue-resident M2-like macrophages which regulate lipolysis (Satoh et al., 2013). In contrast, Okamoto and colleagues did not identify any phenotypic defects in *Trib3* knockout mice (Okamoto et al., 2007). Nevertheless, Ord and colleagues showed that mast cells derived from bone marrow cells of *Trib3* knockout mice have increased sensitivity to cell cycle arrest and cell death in response to interleukin (IL)-3 deprivation (Ord et al., 2012). Studies of *Trib2* knockout mice are reviewed in the introduction of Chapter 3. In this chapter, we review mouse and human *Trib2/TRIB2* in-depth.

1.2 Classification of Tribbles family

Drosophila and mammalian Tribbles consist of N-terminal, kinase-like and C-terminal domains. Sequence analysis revealed that although the kinase-like domain of Tribbles is homologous to other serine/theronie kinases, it lacks one (DFG) of the three conserved motifs that are required for catalytic activity (Figure 1.2) (Manning et al., 2002). Hence, Tribbles are considered incapable to phosphorylate substrates and have been termed serine/threonine pseudokinases. This was supported by two studies where kinase activity was not detected in *Drosophila* Tribbles (Grosshans and Wieschaus, 2000) and human TRIB3 (Bowers et al., 2003) using embryo microinjection and *in vitro* kinase assays respectively. However, evidence emerges that pseudokinases could be catalytically active despite lacking conserved motifs. For example, Ca^{2+}/calmodulin-activated serine-threonine kinase (CASK) is classified as pseudokinase because it lacks the DFG motif, which is crucial for Mg^{2+}

binding. Mg^{2+} is required for typical protein kinases to stimulate the transfer of a phosphate from adenosine 5'-triphosphate (ATP) to a protein substrate. However, further studies showed that CASK works independent of Mg^{2+}, and is capable of autophosphorylation and for phosphorylating specific physiological substrate (neurexin-1) (Mukherjee et al., 2008, Mukherjee et al., 2010). Phylogenetic analysis showed that CASK and Tribbles are from the same group (Calmodulin/Calcium regulated kinases) of human kinase superfamily (Manning et al., 2002). Notably, a recent study showed that TRIB2 behaves like CASK that it binds to ATP and autophosphorylates in a metal-independent manner (Bailey et al., 2015). Hence, TRIB2 could be catalytically active and it is important to determine the physiological role of TRIB2 in order to identify its potential substrates which could be cell context specific.

Figure 1.2 │ Tribbles lacks the key enzymatic residues in the DFG motif. Sequence alignment of mammalian Tribbles comparing the three conserved motifs (VAIK, HRD and DFG), located within the catalytic domain, which are essential for ATP, peptide and Mg^{2+} bindings respectively. The amino acid residues in these motifs are conserved in mouse and human orthologs of TRIB1-3. Modified from REF. (Zhang et al., 2012b).

1.3 Cellular functions of TRIB2

TRIB2 acts as a scaffold protein that brings enzymes and their substrates into critical positions to allow cellular reactions to proceed (Zhang et al., 2012b). Due to its scaffolding function, TRIB2 is able to modulate and mediate diverse signalling. In this section, we discuss the functions of TRIB2 identified in different cellular contexts. These studies showed that TRIB2 regulates substrates via either promotion (yes-associated protein (YAP), c-Jun N-terminal kinase (JNK), p38 and

RELB proto-oncogene, NF-kB subunit (RELB)) or inhibition (RAC-beta serine/threonine-protein kinase (AKT), CEBPα, CEBPβ, extracellular signal-regulated kinase (ERK), forkhead box O (FOXO), JNK, myeloid cell leukaemia 1 (MCL1) and p100) of their functions. Enzymes that are required for TRIB2 to regulate these substrates include beta-transducin repeat containing protein (β-TRCP), constitutive photomorphogenesis 1 (COP1), MAPK kinase 1 (MEK1), MAPK kinase 7 (MKK7) and tripartite motif-containing 21 (TRIM21).
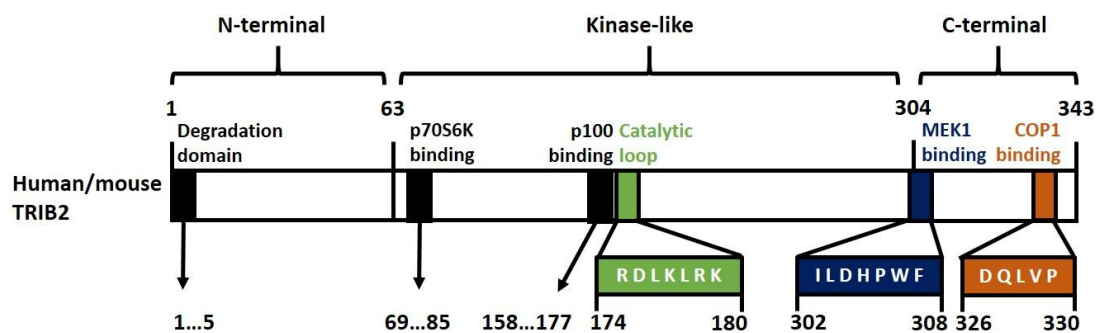
Figure 1.3 │The structure of TRIB2 protein. Catalytic loop (Keeshan et al., 2010), MEK1 binding (Yokoyama et al., 2010) and COP1 (Qi et al., 2006) binding motifs are conserved in TRIB1-3 and *Drosophila* Tribbles (Yokoyama and Nakamura, 2011). Other regions are important for TRIB2 degradation (Wang et al., 2013b), p70S6K binding (Wang et al., 2013b) and p100 binding (Wei et al., 2012), as described in this chapter. Amino acid sequence of these regions and the conserved motifs are identical in human and mouse TRIB2 orthologs.

1.3.1 Autoantigen

TRIB2 was identified as an autoantigen in autoimmune uveitis, a group of inflammatory disorders in the eye by phage display and anti-TRIB2 antibody activities were detected in the patients (Zhang et al., 2005). However, the functional role and expression of TRIB2 in the eye remain unknown. Following that, TRIB2 was implicated in narcolepsy, an excessive daytime sleepiness due to hypocretin deficiency with a dramatic loss in hypothalamic hypocretin-producing neurons. TRIB2 was found to be expressed by these neurons and hence could serve as potential autoimmune targets (Cvetkovic-Lopes et al., 2010). Indeed, high TRIB2-

specific antibody titers were found in narcolepsy patient and these confirm narcolepsy is an autoimmune disease (Cvetkovic-Lopes et al., 2010, Kawashima et al., 2010, Toyoda et al., 2010). This was supported by a recent study that showed passive transfer of anti-TRIB2 autoantibody positive patient immunoglobuline G causes hypothalamic neuron loss and sleep attacks in mice (Katzav et al., 2013). However, the functional role of TRIB2 in hypothalamic neuron remains unknown.

1.3.2 Inhibition of adipogenesis

Activation of AKT and expression of CEBPβ are critical events for adipogenesis. TRIB2 was found to suppress adipocyte differentiation by inhibiting activation of AKT and promoting proteasomal degradation of CEBPβ (Naiki et al., 2007). As such, knockdown of *Trib2* by small-interfering RNAs in mesenchymal stem cells *in vitro* and *in vivo* enhanced adipogenic differentiation (Andersen et al., 2010). However, expression of *TRIB2* influences accumulation of pericardial (Fox et al., 2012) and visceral (Nakayama et al., 2013) fat.

1.3.3 Inhibition of FOXO function

In melanoma cells, TRIB2 abrogates the function of FOXO transcription factors which are tumour suppressive by promoting cytoplasmic sequestration of FOXO (Zanella et al., 2010). TRIB2 expression was found to increase in malignant melanoma and is a biomarker for diagnosis and progression of melanoma (Zanella et al., 2010, Hill et al., 2015).

1.3.4 Inhibition of YAP degradation

In liver cancer, TRIB2 overexpression stabilizes YAP, an oncogenic transcription factor coactivator via two mechanisms. One mechanism includes TRIB2 inhibition of the proteasomal dependent degradation of YAP (Wang et al., 2013a). This requires

binding of β-TRCP, an E3 ubiquitin ligase which was found to modulate TRIB2 in a feedback regulation as described in section 1.4.3 (Wang et al., 2013a, Qiao et al., 2013). Intriguingly, unlike other TRIB2 interacting E3 ligases including COP1 (Keeshan et al., 2010) and TRIM21 (Grandinetti et al., 2011), TRIB2 interaction with β-TRCP leads to inhibition instead of promotion of substrate degradation. It is unclear what influences the outcome of TRIB2 interaction with ubiqutin ligases. Another mechanism of TRIB2-mediated stabilization of YAP is through regulation of CEBPα as described in section 1.3.7 (Wang et al., 2013a).

1.3.5 Modulation of MAPK pathway

TRIB2 has been shown to modulate mitogen-activated protein kinase (MAPK) pathway in different cellular contexts and under different stimuli. Like other Tribbles members, TRIB2 contains a C-terminal conserved motif that is required for MEK1 binding (Figure 1.3) (Yokoyama et al., 2010). In lipopolysaccharide (LPS)-stimulated THP-1 cells, TRIB2 was found to interact with MKK7 and MEK1 to suppress JNK and ERK signalling in order to inhibit IL-8 production (Eder et al., 2008b). However, another study found that modulation of *Trib2* expression doesn't affect low-density lipoprotein uptake by LPS-stimulated THP-1 cells which is regulated by MAPK pathway (Eder et al., 2008a). In epithelials cells stimulated with toll-like receptor (TLR) 5 ligand (flagellin), Trib2 was found to selectively activate p38 and JNK signalling but not ERK (Wei et al., 2012).

1.3.6 Modulation of NFκB pathways

TRIB2 has been shown to modulate both canonical and non-canonical nuclear factor kappa B (NFκB) pathways in different cellular contexts and under different stimuli. In TLR-5 (flagellin)-stimulated epithelial cells, *TRIB2* mRNA expression is induced and TRIB2 protein interacts with p100 (Figure 1.3) to inhibit the canonical

NFκB pathway (Wei et al., 2012). In osteosarcoma cells stimulated with tumour necrosis factor alpha, *TRIB2* mRNA expression is induced and TRIB2 protein upregulates non-canonical NFκB pathway by promoting nuclear retention of RELB (Schoolmeesters et al., 2012).

1.3.7 Promotion of CEBPα degradation

CEBPα belongs to a family of basic region leucine zipper transcription factors. It promotes cell cycle arrest and cell differentiation. Thus, CEBPα pathway is tumour suppressive in many cancers (Koschmieder et al., 2009). In a bone marrow (BM) transplant mouse model, enforced expression of *Trib2* promotes degradation of CEBPα and induces a potent acute myeloid leukaemia (AML) (Keeshan et al., 2006). This is the first study demonstrated that the functional role of *Drosophila* Tribbles is conserved in mammalian Tribbles family. Further study showed that TRIB2-mediated degradation of CEBPα requires COP1 binding which is an E3 ubiquitin ligase to induce AML (Figure 1.3) (Keeshan et al., 2010). In lung cancer, elevated TRIB2 expression contributes to tumourigenesis by also promoting degradation of CEBPα and this requires interaction with a different E3 ligase, TRIM21 instead of COP1 (Grandinetti et al., 2011). In liver cancer, TRIB2 overexpression downregulates CEBPα in a similar way and this in turn relieves CEBPα-mediated inhibition of YAP activity (Wang et al., 2013a).

1.3.8 Promotion of MCL1 degradation

TRIB2 was found to modulate apoptosis of TF-1 cells in response to deprivation of granulocyte-macrophage colony-stimulating factor by promoting proteasomal-independent degradation of MCL1, a pro-survival factor (Lin et al., 2007). The apoptogenic activity of TRIB2 was also found in Me-1 cells when it was overexpressed (Gilby et al., 2010). However, the pro-apoptotic property of TRIB2

which was established in cell lines has yet to be shown to be of relevance in primary cells or in *in vivo* settings.

1.4 Regulation of *Trib2/TRIB2* and TRIB2

1.4.1 Transcription factors

Trib2/TRIB2 was identified as a target gene of several oncogenic transcription factors deregulated in AML, liver cancer and T-cell acute lymphoblastic leukaemia (T-ALL). In homeobox (HOX)-induced murine AML, *Trib2* was identified as a target gene of myeloid ecotropic viral integration site 1 (MEIS1), a HOX co-factor (Argiropoulos et al., 2008) that dimerizes with pre-B-cell leukaemia homeobox 3 (PBX3) (Garcia-Cuellar et al., 2015). In human AML, *TRIB2* expression is upregulated by E2F transcription factor 1 (E2F1) and sustained by an E2F1-CEBPα positive feedback loop to promote leukaemic cell proliferation (Rishi et al., 2014). In liver cancer, *TRIB2* was found as a downstream wingless-type MMTV integration site family (WNT)-β-Catenin target gene and its transcription is coordinated by T-cell factor (TCF) and FOXOA transcription factors (Wang et al., 2013a). In T-ALL, *Trib2* is a direct target of Neurogenic locus notch homolog protein 1 (NOTCH1) (Wouters et al., 2007), pituitary homeobox 1 (PITX1) (Nagel et al., 2011) and T-cell acute lymphocytic leukaemia protein 1 (TAL1) (Sanda et al., 2012). In normal haematopoiesis, *Trib2* is regulated by friend of GATA-1 (FOG-1) which is important in the myelo-erythroid lineage bifurcation (Mancini et al., 2012).

1.4.2 MicroRNAs

Besides transcription factors, *Trib2/TRIB2* expression is also regulated by microRNAs (Table 1.1). These miRNAs were found to be deregulated in different types of cancer and hence contributes to the elevated expression of *Trib2*.

Table 1.1 │ List of microRNAs (miRNAs) that suppress *Trib2/TRIB2* expression.

miRNAs	Cellular context	Functional role of miRNAs	References
let-7c	lung cancer cells	- Inhibition of cell proliferation	(Wang et al., 2013c)
miR-98	Endothelial cells	- not studied	(Xie et al., 2012)
miR-99	Cervical cancer cells	- Inhibition of cell proliferation - Promotion of apoptosis	(Xin et al., 2013)
miR-99a	AML and chronic myeloid leukaemia (CML) cells	- Promotion of cell proliferation - Inhibition of apoptosis	(Zhang et al., 2013)
miR-100	AML cells	- Promotion of cell proliferation - Inhibition of cell differentiation	(Zheng et al., 2012)
miR-155	Flt3 wild type (WT)-AML cells	- Promotion of apoptosis and cell differentiation	(Palma et al., 2014)
miR-511	lung cancer cells	- Promotion of apoptosis - Inhibition of cell proliferation	(Zhang et al., 2014) (Zhang et al., 2012a)
miR-1297	lung cancer cells	- Inhibition of cell proliferation	(Zhang et al., 2012a)

1.4.3 E3 ubiquitin ligases

TRIB2 protein level was found to be elevated in a subset of liver cancers and reported to be critical for liver cancer cell survival and transformation (Wang et al., 2013a). Further study found that TRIB2 has increased protein stability in liver cancer cells compared with other cells and this was due to down regulation of SMAD ubiquitination regulatory factor 1 (SMURF1), an E3 ubiquitin ligase that ubquitinates TRIB2 and promotes its proteasomal dependent degradation (Wang et al., 2013b). SMURF1-mediated ubiquitination requires an intact TRIB2 N-terminus degradation domain and phosphorylation of TRIB2 by p70S6K (Figure 1.3) (Wang et al., 2013b). Like SMURF1, another E3 ubiquitin ligase β-TRCP was shown to regulate stability of TRIB2 in liver cancer cells although TRIB2 phoshorylation was not shown to be a prerequisite (Qiao et al., 2013).

1.5 Steady state haematopoiesis

1.5.1 Bone marrow haematopoiesis

In adults, haematopoiesis takes place in the BM, and is sustained by haematopoietic stem cells (HSCs) which are located atop the haematopoietic hierarchy (Figure 1.4), to produce blood cells of all lineages throughout the life. HSCs are multipotent and reversibly switch from dormancy to self renewal while generating multipotent progenitors (MPPs) (Wilson et al., 2008). However, they cycle infrequently as Wilson and colleagues showed that HSCs are predominantly quiescent with 70% of them are in G_0 phase of cell cycle (Wilson et al., 2008). Based on computational modelling, it is estimated that adult murine HSCs undergo 5-20 divisions over the course of a 2 year life span (Wilson et al., 2008, Foudi et al., 2009). Lineage determination and differentiation are initiated in MPPs which are also multipotent but with reduced self renewal capacity (Reya et al., 2001). Oligopotent common myeloid progenitors (CMPs) gives rise to all myeloid cell types (erythroid cells, megakaryocytes, granulocytes and monocytes) via the commitment to either megakaryocyte-erythroid (MEPs) or granulocyte-macrophage (GMPs) progenitors (Akashi et al., 2000). Likewise, oligopotent common lymphoid progenitors (CLPs) were identified to have the potential to generate cells of lymphoid lineages (T cells, B cells and natural killer cells) *in vivo* (Kondo et al., 1997). Identification of CMP and CLP progenitors marked the branching of MPPs into myelo- and lymphopoiesis respectively. However, the model for haematopoietic blood lineage commitment was revised with the identification of lymphoid-primed multipotent progenitors (LMPPs) which have combined lympho-myeloid differentiation potential but have lost the ability to adopt megakaryocyte and erythroid lineage fates (Adolfsson et al., 2005).
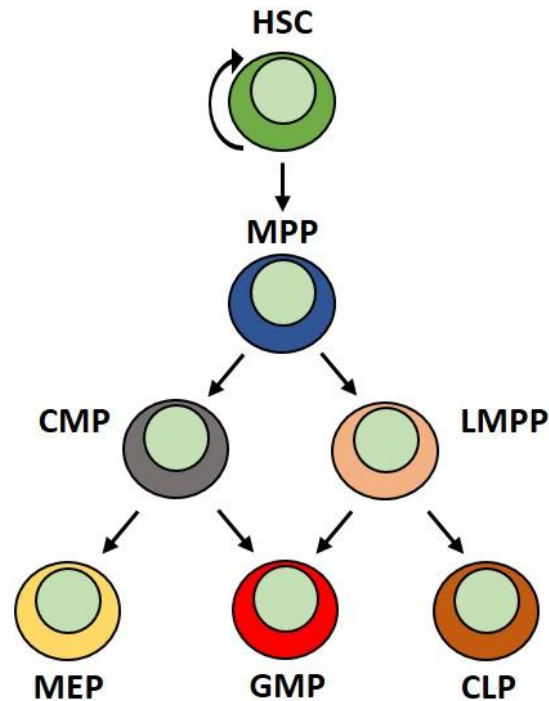
Figure 1.4 │ Model for haematopoietic hierarchy used in this thesis research. MPPs lose their multipotent capacity in a stepwise fashion when they differentiate into oligopotent progenitors (CMPs, LMPPs, MEPs, GMPs and CLPs) which in turn undergo further lineage commitment to produce unipotent progenitors that eventually make all mature blood cells. This model is currently under review due to recent findings in haematopoietic lineage differentiation as described below in the text. HSC, haematopoietic stem cell; MPP, multipotent progenitor; CMP, common myeloid progenitors; LMPP, lymphoid-primed multipotent progenitor; MEP, megakaryocyte-erythroid progenitor; GMP, granulocyte-macrophage progenitor; CLP, common lymphoid progenitor.

While the model described above served as the framework of the research reported in this thesis, findings from recent studies in the past two years, reviewed by Cabezas-Wallscheid and Trumpp (Cabezas-Wallscheid and Trumpp, 2016), suggest a simpler haematopoietic hierarchy. These studies employed single-cell assays to provide strong evidence that either CMPs represent a highly transient cell state, or that such oligopotent cells do not exist in mouse or human BM (Notta et al., 2016, Paul et al., 2015). Rather, mature cells such as megakaryotes are generated from committed unipotent progenitors derived directly from multipotent cells such as HSCs and MPPs (Paul et al., 2015, Notta et al., 2016).

1.5.2 Intrathymic T-cell development

Pre-thymic progenitors are BM-derived progenitors (primarily CLPs (Serwold et al., 2009) and LMPPs (Luc et al., 2012)) that colonize the thymus continuously and sustain thymopoiesis to generate naïve CD4 or CD8 single positive (SP) T-cells. Immature thymocytes are CD4/CD8 double negative (DN) and divided into DN1-DN4 subsets based on their surface expression of CD25 and CD44 markers (Godfrey et al., 1993). DN1 thymocytes are the most immature progenitors and require NOTCH-DLL4 signalling activated by interaction with thymic stromal cells for specification, commitment and development (Pui et al., 1999, Radtke et al., 1999). As such, specification of DN1 thymocytes to DN2 stage involves surface expression of CD25 which is a T-cell marker (Godfrey et al., 1993). DN2a thymocytes commit to T-lineage fate as they develop into DN2b stage with decreasing surface expression of c-Kit which is a BM haematopoietic progenitor marker (Yui et al., 2010). Until the maturation to DN2b stage, the uncommitted cycling DN1 and DN2a progenitors retain the potential to generate dendritic cells, granulocytes, macrophage, natural killer cells and to a lesser extent, B cells (Figure 1.5) (Yui and Rothenberg, 2014). T-cell committed progenitors are then separated into the development of αβ and γδ lineages where the former is predominant in an adult thymus as it contains approximately 300-folds more CD4/CD8 double positive (DP) αβ cells than γδ cells (Prinz et al., 2006). γδ lineage development begins in the DN2b and DN3 cells where productive *Tcrγδ* rearrangements give rise to γδ cells (Carpenter and Bosselut, 2010). However, αβ lineage development begins at DN3 stage. DN3a thymocytes are briefly arrested to undergo *Tcrβ* rearrangement, a checkpoint known as β-selection where productive rearrangements lead to expression of pre-T-cell receptor (TCR) complex and initiation of pre-TCR signalling to turn off NOTCH signalling (Figure 1.5) (Hoffman et al., 1996, Taghon et al., 2006). The pre-TCR signalling drives immature DN3b thymocytes to proliferate and

further differentiate into non-proliferating mature DP thymocytes where they undergo *Tcrα* rearrangements and positive/negative selections to become CD4 or CD8 SP naïve T cells (Figure 1.5) (Carpenter and Bosselut, 2010).
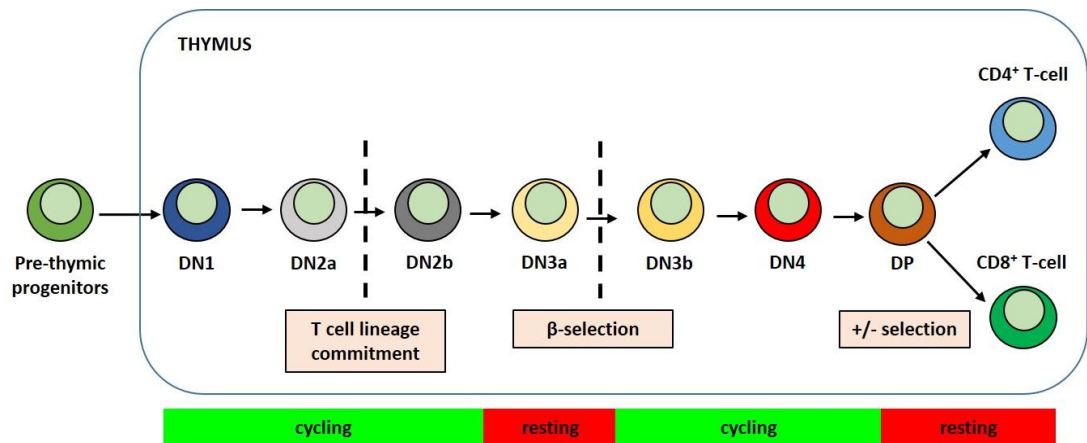
Figure 1.5 │ Overview of murine αβ T-cell development. The main stages of thymocyte development along the αβ T-lineage are depicted. NOTCH signalling is essential for the commitment of thymic progenitors to the T-cell lineage fate. However, NOTCH signalling is switched off in DN3b thymocytes that have passed through the β-selection checkpoint and instead become dependent on Pre-TCR signalling. DN, CD4/CD8 double negative; DP, CD4/CD8 double positive.

It is noteworthy that αβ T-cell development described above is delineated based on mouse studies. Human T-cells undergo the same developmental checkpoints (β-selection and positive/negative selection) during development despite some of the developmental stages being characterized by different phenotypic markers (Taghon et al., 2012). For example, human thymic progenitors undergo T-cell lineage specification and commitment but they are not characterized by the markers CD44 and CD25, and hence are not divided into DN1-4 stages as described in mouse. A detailed discussion of human T-cell development is reviewed here, by Taghon and colleagues (Taghon et al., 2012), and highlights important differences between both species.

1.5.3 TRIB2 in normal haematopoiesis

Trib2 was identified as a direct target gene of FOG-1, a transcription factor that is required for megakaryocyte and erythorid-lineage commitment (Mancini et al., 2012). Indeed, Mancini and colleagues showed that *Trib2* is selectively expressed in murine pre-megakaryocyte/erythroid progenitor cells compared to pre-granulocyte/macrophage and CLP progenitor cells (Mancini et al., 2012). Hence, TRIB2 appears to be an important effector of FOG-1 in suppression of myeloid progenitor specification. This could be attributed to the role of TRIB2 in promoting degradation of CEBPα and CEBPβ which are required for generation of GMPs (Keeshan et al., 2006, Naiki et al., 2007). In accordance with this, a separate study found that CEBPα binds to the promoter region of *Trib2* in murine GMPs to inhibit E2F1-mediated upregulation of *Trib2* expression in order to promote myelopoiesis (Rishi et al., 2014).

Besides the potential role of TRIB2 in myelo-erythroid lineage specification, recent studies also suggest TRIB2 to be important in intrathymic T-cell development. Using whole-transcriptome sequencing, Casero and colleagues studied the transcriptional programs that initiate human lymphopoiesis, and regulate the subsequent B lymphoid and T lymphoid specification (Casero et al., 2015). Human *TRIB2* expression was found to be upregulated more than 10 fold in the earliest BM-derived uncommitted thymic progenitors compared to BM progenitors (HSCs, LMPPs, CLPs and B cell-committed progenitors) (Casero et al., 2015). In murine fetal liver-derived DN1 thymic progenitors, *Trib2* was bound by both GATA3-binding protein 3 (GATA3) and PU.1, two transcription factors with complementary roles in early T-cell development (Zhang et al., 2012d). Hence, it is likely that TRIB2 has a previously unrecognized role in thymopoiesis.

As mentioned earlier in this chapter, Tribbles inhibits String function in *Drosophila* (Seher and Leptin, 2000, Grosshans and Wieschaus, 2000, Mata et al., 2000). The ortholog of String in mammalian is CDC25 phosphatases which are also known as cell cycle activators (Kristjansdottir and Rudolph, 2004) (Chapter Six). It remains unknown if TRIB2 is capable to interact with and regulate CDC25 phosphatases in a similar way in the context of haematopoiesis. The role of CDC25 phosphatases in normal haematopoiesis (BM haematopoiesis and intrathymic T-cell development) is unclear although one of the members (CDC25A) was shown to regulate cell cycle of early erythroid progenitors (Melkun et al., 2002).

1.6 Stressed haematopoiesis

1.6.1 Ageing

Haematopoietic ageing is an evolutionarily conserved process in human and mice that affects the balanced generation of all blood cell lineages. As mice age, HSCs expands numerically due to increased self-renewal but they exhibit functional decline with diminished lymphoid differentiating potential and hence are myeloid-biased (Sudo et al., 2000, Sun et al., 2014, Rossi et al., 2005). Pang and colleagues found the similar features of ageing murine HSCs in older human HSCs (above 65 years) as they showed older human HSCs are increased in frequency and do not engraft or generate lymphoid progeny as efficiently as young human HSCs (20-35 years) in a xenotransplant murine model (Pang et al., 2011). Flach and colleagues showed that the functional decline in murine old HSCs (24 months or greater) is driven by replication stress where the cells have extended S phase and acquisition of chromosomal gaps/break (Flach et al., 2014).

Regression or involution of the thymus is also a feature of haematopoietic ageing. Thymic involution leads to the diminished production of naïve T-cells due to

the age-related changes in thymopoiesis (Palmer, 2013). The thymus is continuously seeded by BM-derived progenitors to sustain thymopoiesis (Serwold et al., 2009, Luc et al., 2012). Hence, any age-related alterations in HSC function would contribute toward thymic involution. As mentioned above, HSCs lose the lymphoid potential as they age (Sudo et al., 2000). In accordance with this, Zediak and colleagues showed that old donor MPPs (24 months) give rise to 2.4 folds fewer DP thymocytes compared to young donor MPPs (2 months) at three weeks after injection into the thymus of non-irradiated recipient mice (Zediak et al., 2007). Furthermore, old mice have fewer numbers of early thymic progenitors, a subset of DN1 progenitors that give rise to subsequent thymocyte subsets (Min et al., 2004, Heng et al., 2005). Min and colleagues showed that old early thymic progenitors (17 months or greater) have reduced thymopoietic potential, reduced proliferation and increased apoptosis compared to young early thymic progenitors (1-2 months) (Min et al., 2004). These physiological age-related changes contribute to the gradual and progressive decline in the number of thymocytes.

1.6.2 Infection

At steady state, bone marrow haematopoiesis generates a balanced supply of granulocytes (granulopoiesis), monocytes/macrophages (myelopoiesis) and B-lymphocytes (B-lymphopoiesis) which are essential for the maintenance of immune homeostasis. The pre-existing pool of granulocytes is usually sufficient to combat local bacteria infection. However, in the setting of systemic infection which is more severe, granulocytes which are short-lived are consumed in large quantities (Manz and Boettcher, 2014). The increase demand for granulocytes during systemically disseminated infection causes the haematopoietic system to switch from steady state to emergency granulopoiesis where HSPCs expand to increase *de novo* generation of granulocytes (Manz and Boettcher, 2014). However, the shift in BM haematopoietic activity towards granulopoiesis results in descreased production of

B-lymphocytes, erythroyctes and megakaryocytes (Glatman Zaretsky et al., 2014). Zhang and colleagues showed that *E. coli*-induced bacterimia in mice caused 10 folds expansion of HSPCs and these cells are committed to granulocyte/macrophage lineage development as assessed by the Colony-Forming Unit assay (Zhang et al., 2008). Cytokines and growth factors play an important role in emergency granulopoiesis. For example, granulocyte-colony stimulating factor level is increased during severe infection to promote myeloid cell production in bone marrow and was shown recently to be secreted by non-haematopoietic cells that sense invading pathogens (Boettcher et al., 2012, Kawakami et al., 1990).

Infection by viruses, bacteria, parasites and fungi is known to cause premature thymic involution (Nunes-Alves et al., 2013). In this context, thymopoiesis is disrupted due to induction of thymocyte (DP primarily) apoptosis by glucocorticoids and pro-inflammatory mediators released by the body in response to systemic infection (Borges et al., 2012, Ashwell et al., 2000). Besides that, thymocytes are also sensitive to toxin and virulence factors that are released by pathogens systemically (Ozeki et al., 1997, Islam et al., 1998). Apoptosis induction of human and murine thymocytes by direct viral infections (Human Immunodeficiency virus (Berkowitz et al., 1998), Murine Leukaemia virus (Yoshimura et al., 1999) and Highly Pathogenic Influenza virus (Vogel et al., 2010)) has also been demontstrated.

1.6.3 Iatrogenic interventions (irradiation and chemotherapy)

Clinically, irradiation and chemotherapy are conventional therapies for patients with cancer since both targets rapidly proliferating cells, one of the hallmarks of cancer (Hanahan and Weinberg, 2011). However, irradiation and chemotherapy induced cytotoxicity are not selective and are known to induce BM suppression which would be life threatening because cycling normal haematopoietic cells are also being

targeted during the course of treatment (Mauch et al., 1995). The resulting clinical symptoms include anaemia, thrombocytopenia, neutropenia and lymphocytopenia due to the disrupted production of RBCs, platelets, granulocytes and B-lymphocytes in the BM respectively. While this side effect is detrimental in the clinical setting, both have been used experimentally to study haematopoiesis during stress and recovery. Li and Slayton showed that although both irradiation and 5-fluorouracil (5-FU, a standard chemotherapy agent which is reviewed further in section 4.1) treatments reduce murine BM cellularity and cause similar morphological changes in BM niche; B lymphocytes are more sensitive to iradiation whereas neutrophils and monocytes are more sensitive to 5-FU treatment (Li and Slayton, 2013). In addition to that, they found that murine haematopoietic system recovered faster following 5-FU treatment, as evidence by the earlier expansion of HSPC populations, compared to irradiation (Li and Slayton, 2013). Shao and colleagues found that sublethal dose of total body irradiation causes long term suppression of murine BM functions because HSCs are induced to senescence prematurely (Shao et al., 2014).

Similar to 5-FU treatment (Aquino Esperanza et al., 2008, Eichhorst et al., 2001), Randle-Barrett and Boyd (Randle-Barrett and Boyd, 1995) showed that sublethal dose of total body irradiation causes reduction of murine thymic cellularity and damages to the murine thymic microenvironment (Randle-Barrett and Boyd, 1995, Aquino Esperanza et al., 2008, Eichhorst et al., 2001). Furthermore, they showed that DP thymocytes are the most sensitive thymic subset to irradiation-induced injury (Randle-Barrett and Boyd, 1995). Thymus recovers at a similar rate in both irradiation and 5-FU murine models (Randle-Barrett and Boyd, 1995, Aquino Esperanza et al., 2008, Eichhorst et al., 2001).

1.7 TRIB2 and acute leukaemia

1.7.1 Acute myeloid leukaemia

AML is a heterogeneous haematological malignancy characterized by the clonal expansion of myeloid blasts due to a differentiation block in haematopoietic stem and progenitor cells (HSPCs). In children, AML is rare with an incidence of 8 cases per million children aged 1-18 years per year (Chaudhury et al., 2015). However, the incidence of AML increases as the population ages. AML occurs at an incidence of 20 cases per million younger adults aged 18-60 years per year and increases to 170 cases per million older adults aged above 60 years per year (Chaudhury et al., 2015). Hence, AML is mainly an adulthood leukaemia. A combination of cytarabine and an anthracycline remains as a standard induction chemotherapy in AML except acute promyelocytic leukaemia which is a distinct entity that can be treated successfully with differentiating therapy (all-*trans* retinoic acid and arsenic trioxide) (Freireich et al., 2014). The five-year overall survival rate for paediatric AML patients is 70-75% but decreases to 45-50% in younger adult AML patients (Chaudhury et al., 2015). Nevertheless, increased understanding of the molecular genetics and pathogenesis of AML has allowed clinical development of new therapeutic drugs (chemotherapies, hypomethylating agents, antibody-drug conjugates and molecularly targeted agents) and this was recently reviewed by Stein and Tallman (Stein and Tallman, 2016).

AML was first classified morphologically based on the lineage-associated phenotype (undifferentiated, myeloid, monoblastic, erythroblastic or megakaryoblastic) and defined according to the French-American-British (FAB) classification (Bennett et al., 1991). In 2001, the World Health Organization (WHO) published a new classification based on not only morphologic but also biologic and genetic features that have proved to have clinical relevance (Vardiman et al., 2002).

In 2008 and 2016, the WHO classification was updated as cytogenetic and molecular genetic studies uncovered more genetic abnormalities in AML (Table 1.2) (Vardiman et al., 2009, Arber et al., 2016). For example, discovery of *Npm1* mutation in AML with normal cytogenetics which has prognostic impact led to the addition of this provisional entity to the current WHO classification (Table 1.2) (Falini et al., 2005). With advances in technologies such as development of whole genome sequencing, whole exome sequencing and RNA sequencing, AML subsets are now defined by cytogenetic and molecular genetic abnormalities which confer independent prognostic information (Table 1.2 and 1.3).

As described above in section 1.3.7, the first cellular function of TRIB2 was demonstrated in myeloid leukaemogenesis where it induces potent murine AML through promotion of CEBPα degradation (Keeshan et al., 2006). TRIB2 was also shown to cooperate with HOXA9 and accelerate the onset of murine AML (Keeshan et al., 2008), and *Trib2* is activated in MEIS1-HOX induced murine AML (Argiropoulos et al., 2008, Garcia-Cuellar et al., 2015) In human AML, *TRIB2* expression is upregulated in a biologically and epigenetically distinct subset of AML characterized with silenced *Cebpα* expression and a mixed myeloid/T-lymphoid phenotype (Wouters et al., 2007, Keeshan et al., 2006). *TRIB2* expression is also higher in promyelocytic leukaemia-retinoic acid receptor alpha positive leukaemia that harbour *FLT3* tyrosine kinase domain mutations compared with promyelocytic leukaemia-retinoic acid receptor alpha negative leukaemias or promyelocytic leukaemia-retinoic acid receptor alpha positive leukaemias with *FLT3* internal tandem duplication mutations (Liang et al., 2013). This could be due to the fact that, unlike Fms-like tyrosine kinase 3 (FLT3) internal tandem duplication mutants, FLT3 tyrosine kinase domain mutants could not repress CEBPα activity and hence necessitate the upregulation of *TRIB2*.

Table 1.2 │ Genetic abnormalities in paediatric and younger adult AML[1].

AML categories	frequency	
	Younger adult (18-60 years)	Paediatric (below 18 years)
WHO 2016 classification		
AML with recurrent genetic abnormalities		
t(8;21)(q22;q22)/*RUNX1-RUNXTt1*	8%	12-14%
inv(16)(p13.1q22) or t(16;16)(p13.1;q22)/*CBFB-MYH11*	5%	8%
t(15;17)(q22;q21)/*PML-RARA*	5-10%	6-10%
t(9;11)(p23;q34.1)/*MLLT3-KMT2A*	2%	7%
t(10;11)(p12;q23)/*Mllt10-Mll*	1%	3% mainly infants
t(6;9)(p23;q34)/*DEK-NUP214*	1%	< 2%
inv(3)(q21.3q26.2) or t(3;3)(q21.3;q26.2)/*GATA2, MECOM*	1%	< 1%
t(1;22)(p13.3;q13.3)/*RBM15-MKL1*	< 1%	AMKL only; infants
mutated *NPM1*	35%	5-10%
biallelic mutations of *CEBPA*	10% in CN	14% in CN
Provisional entity: *BCR-ABL1*	-	-
Provisional entity: mutated *RUNX1*	-	-
Not included in WHO 2016		
Karyotypes/mutations		
t(7;12)(q36;p13)/t(7;12)(q32;p13)	Not in adults	Infants
t(5;11)(q35;p15.5)/*NUP98-NSD1*	Not in adults	Mostly in CN
FLT3-ITD	20-40%	10%
N-RAS	10%	20%
MLL-PTD	3-5%	3%
c-KIT	17% in CBF leukaemia[2]	25% in t(8;21)
WT1	10% in CN	13% in CN
PTPN11	Not in adults	5-21%; infants only
IDH1/2	16%	Rare, 2-3%
TET2	8-17%	Very rare
DNMT3A	20%	Rare
WHO 2016 classification continued		
AML with myelodysplasia-related changes	48%	low
Therapy-related myeloid neoplasms	6%	3.5%
AML, not otherwise specified	17%	15%
Myeloid sarcoma	1%	2-4%
Myeloid proliferations related to Down syndrome		
Transient abnormal myelopoiesis	Not in adults	In 5% of the newborns with Down syndrome
Myeloid-leukaemia associated	Not in adults	400-fold increased risk for AMKL
Acute leukaemias of ambiguous lineage	-	-

Table 1.3 │ Risk stratification for younger adults with AML[†].

Risk group	Cytogenetic/molecular genetic abnormality
Favourable	t(15;17)(q22;q21)/*PML-RARA* t(8;21)(q22;q22)/*RUNX1-RUNX1T1* inv(16)(p13q22)/t(16;16)(p13;q22)/*CBFB-MYH11* *NPM1* mutation (in absence of *FLT3*-ITD or *DNMT3A* mutation) Biallelic *CEBPA* mutation
Intermediate	Cytogenetic/molecular genetic abnormalities not classified as favourable or adverse

Adverse	In the absence of favourable risk cytogenetic/molecular genetic abnormalities
	    abn(3q) [excluding t(3;5)(q21~25;q31~35)/*NPM1-MLF1*
	    inv(3)(q21q26)/t(3;3)(q21;q26)/*GATA2*/*EVI1*
	    add(5q)/del(5q), -5
	    t(5;11)(q35;p15.5)/*NUP98-NSD1*
	    t(6;9)(p23;q34)/*DEK-NUP214*
	    add(7q)/del(7q), -7
	    t(11q23) [excluding t(9;11)(p21~22;q23) and t(11;19)(q23;p13)]
	    t(9;22)(q34;q11)/*BCR-ABL*
	    -17/abn(17q)/*TP53* mutation
	    Complex karyotype (≥4 unrelated abnormalities)
	    ASXL1 mutation
	    DNMT3A mutation
	    FLT3-ITD
	    MLL-PTD
	    RUNX1 mutation

[†] Adapted from (Grimwade et al., 2016).

1.7.2 T-cell acute lymphoblastic leukaemia

In contrast to AML, T-ALL is a heterogenous haematological malignancy caused by the transformation of thymic progenitors. Please refer to the introduction of Chapter 5 where we overviewed the incidence, therapy, oncogenes and molecular subtypes for T-ALL.

In T-ALL, *TRIB2* was identified in a knockdown screen as one of the critical targets of the core transcriptional regulatory circuit controlled by the TAL1 complex comprised of TAL1, GATA3 and Runt-related transcription factor 1 (RUNX1), and TRIB2 was shown to be essential for the growth and survival of human TAL1^{+} T-

ALL cell lines (Sanda et al., 2012). A follow-up study showed that TRIB2 upregulates X-linked inhibitor of apoptosis (XIAP), an anti-apoptotic protein to promote cell survival and regulates the balance between the oncogenic TAL1 complex and the transcription factor E2-alpha (E2A) tumour suppressor (Tan et al., 2015). Although *TRIB2* has also been implicated in NOTCH1^{+} (Hannon et al., 2012) and PITX1^{+} (Nagel et al., 2011) T-ALL as mentioned in section 1.4.1, it remains unclear how TRIB2 contributes to the pathogenesis of T-ALL.

Most of the studies discussed in this chapter examined the pathological roles of TRIB2 in different diseases to understand the contribution of TRIB2 dysregulation, at mRNA and protein levels, to the coordination of signalling networks present in diseased or transformed cells. However, the physiogical role of TRIB2 remains elusive.

1.8 Thesis aims

(i) Investigate the physiological role of TRIB2 in haematopoiesis

Current literature suggests TRIB2 to be important in the specification of megakaryocyte and erythroid lineage as well as in intrathymic T-cell development. To delineate the role of TRIB2 in haematopoiesis, we examined the haematopoietic system of a *Trib2* knockout mouse model.

(ii) Investigate the role of TRIB2 in modulation of haematopoietic stress response

Haematopoiesis at steady state is often perturbed by physiological and external stress. TRIB2 has been implicated in the pathogenesis of both AML and T-ALL indicating a role for TRIB2 in regulating the response of normal haematopoietic cells to oncogenic stress. We aimed to determine if this is linked to the physiological role of TRIB2 in haematopoiesis and if TRIB2 also modulates haematopoietic response to other type of stress.

(iii) Examine the relationship between TRIB2 and CDC25 phosphatases.

Previous studies suggest the functional roles of *Drosophila* Tribbles are evolutionary conserved in mammalian Tribbles. This is illustrated in the relationship between *Drosophila* Tribbles and Slbo. In *Drosophila*, Tribbles also regulates String and hence cellular proliferation, but it is unclear if mammalian Tribbles also interact with CDC25 family. We aimed to examine the relationship between TRIB2 and different members of CDC25 family at the molecular level.

CHAPTER TWO: MATERIALS AND METHODS

2.1 Materials

2.1.1 Antibodies

2.1.1.1 Flow cytometry application

Table 2.1 │ List of antibodies used to stain cells for flow cytometry analysis.

Antibody[†]	Clone
anti-BrdU	BU20A
anti-mouse CD3	17A2
anti-mouse CD4	RM4-5
	GK1.5
anti-mouse CD8α	53-6.7
anti-mouse CD11c	N418
anti-mouse CD16/CD32	93
anti-mouse CD19	eBio1D3 (1D3)
anti-mouse CD25	PC61.5
anti-mouse CD34	RAM34
anti-mouse CD45.1	A20
anti-mouse CD45.2	104
anti-mouse CD48	HM48-1
anti-mouse CD71	R17217
anti-mouse CD150	TC15-12F12.2
anti-mouse c-Kit	2B8
anti-mouse Gr-1	RB6-8C5
anti-mouse IL-7Rα	A7R34
anti-mouse NK1.1	PK136
anti-mouse Sca-1	D7
anti-mouse Ter-119	TER-119
anti-mouse/human B220	RA3-6B2
anti-mouse/human CD11b	M1/70
anti-mouse/human CD44	IM7
anti-mouse/human phosphor-p38 (T180/Y182)	4NIT4KK
anti-mouse/rat Ki-67	SolA15

[†] Antibodies were purchased from BioLegend (London, UK) and eBioscience (Hatfield, UK). Identical clones for all antibodies, as indicated above, were purchased from these two companies. Antibodies were conjugated either with fluorochrome or with biotin, depending on the design of individual multicolour fluorescent antibody panel, and these were specified in section 2.2.10.

2.1.1.2 Western blotting application

Table 2.2 │ List of antibodies used to probe signals for Western blotting.

Antibody	Clone	Company
anti-α-tubulin	B-5-1-2	Sigma-Aldrich (Dorset, UK)
anti-β-actin	AC-15	Sigma-Aldrich
anti-CDC25A	M-191	Santa Cruz Biotechnology (Heidelberg, Germany)
anti-CDC25B	C-20	Santa Cruz Biotechnology
anti-CDC25C	C-20	Santa Cruz Biotechnology
anti-FLAG	M2	Sigma-Aldrich
anti-HA	HA-7	Sigma-Aldrich
anti-HDAC1	H-51	Santa Cruz Biotechnology
anti-JNK1	2C6	Cell Signalling Technology (Leiden, Netherlands)
anti-K48-Ub	Apu2	Millipore (Cork, Ireland)
anti-mouse IgG horseradish peroxidase (HRP)-linked[1]	-	GE Healthcare Life Sciences (Little Chalfont, UK)
anti-MYC	9E10	Santa Cruz Biotechnology
anti-p38	D13E1	Cell Signalling Technology
anti-p44/42	137F5	Cell Signalling Technology
anti-phospho-Histone H3 (S10)	D2C8	Cell Signalling Technology
anti-phospho-JNK (T183/Y185)[2]	-	Cell Signalling Technology
anti-phospho-p38 (T180/Y182)	D3F9	Cell Signalling Technology
anti-phospho-p44/42 (T202/Y204)	D13.14.4E	Cell Signalling Technology
anti-rabbit IgG HRP-linked[3]	-	GE Healthcare Life Sciences
anti-TRIB2	B-06	Santa Cruz Biotechnology

[1] A polyclonal antibody which is identifiable by its catalogue number (NXA931).
[2] A polyclonal antibody which is identifiable by its catalogue number (#9251).
[3] A polyclonal antibody which is identifiable by its catalogue number (NA934).

2.1.2 Bacterial strains

E.coli DH5α strain from the Keeshan and McCarthy labs was used for transformation to replicate plasmids. The bacteria were grown in Luria-Bertani (LB) broth and agar.

2.1.3 Cell lines

Human embryonic kidney (HEK) 293T, 3T3 and U937 cell lines were from the Keeshan lab whereas RPMI-8402 cell line was purchased from DSMZ (Braunschweig, Germany). HeLa cell line was a kind gift from Professor Mary

McCaffrey (UCC, Cork, Ireland). All cell lines were checked for mycoplasma contamination periodically.

2.1.4 Chemicals, consumables and reagents

Table 2.3 │ Essential chemicals, consumables and reagents used in the experiments described in this thesis.

Product	Brand/Company
100 bp and 1 kb deoxyribonucleic acid (DNA) ladder	New England Biolabs (Herts, UK)
30% acrylamide mix	Sigma-Aldrich
384-well plate	Applied Biosystems (Paisley, UK)
4', 6-diamidino-2-phenylindole (DAPI)	Sigma-Aldrich
5-FU solution	Accord Healthcare (North Harrow, UK)
6-well culture plates	Greiner-Bio-One (Gloucestershire, UK)
Agarose powder	Sigma-Aldrich
Ammonium persulfate	Sigma-Aldrich
Aprotinin	Sigma-Aldrich
AsiSI	New England Biolabs
β-mercaptoethanol	Sigma-Aldrich
BD Cytofix/Cytoperm^{TM} Kit	BD Biosciences (Oxford, UK)
BD Pharmingen^{TM} Propidium Iodide (PI)/RNase Staining Buffer	BD Biosciences
Bio-Rad Protein Assay Dye Reagent Concentrate	Bio-Rad (Dublin, Ireland)
Boric acid	Sigma-Aldrich
Bovine serum albumin (BSA)	Sigma-Aldrich
BrdU Labeling Reagent	Invitrogen (Paisley, UK)
Calcium chloride (CaCl$_2$)	Sigma-Aldrich
Carbobenzoxy-Leu-Leu-leucinal (MG132)	Sigma-Aldrich
Cell culture dishes/flasks	Greiner-Bio-One
Cell scrappers	Greiner-Bio-One
Cell strainers	Fisher Scientific (Loughborough, UK)
CL-XPosure^{TM} radiography films	Thermo Scientific (Paisley, UK)
Cryotubes	Greiner-Bio-One
Cytokines (Interleukin (IL)-3, IL-6 and stem cell factor (SCF))	PeproTech (London, UK)
Dimethysulfoxide (DMSO)	Sigma-Aldrich
Disodium phosphate (Na$_2$HPO$_4$)	Sigma-Aldrich
DNase I	STEMCELL Technologies (Grenoble, France)
dNTP	Thermo Scientific
DPX mountant	Sigma-Aldrich
Dulbecco's Modified Eagle Medium (DMEM)	Gibco (Paisley, UK)

Ethanol	Sigma-Aldrich
Ethylenediaminetetraacetic acid (EDTA)	Sigma-Aldrich
FastStart^{TM} High Fidelity PCR Kit	Roche (Dorset, UK)
Fast SYBR$^®$ Green Master Mix	Applied Biosystems
Fetal bovine serum (FBS)	Gibco
Glass slides	VWR (Graumanngasse, Vienna)
Glucose	Sigma-Aldrich
Glycerol	Sigma-Aldrich
Glycine	Sigma-Aldrich
Hank's balanced salt solution	Gibco
High Capacity cDNA Reverse Transcription (RT) Kit	Applied Biosystems
Hydroxyethyl piperazineethanesulfonic acid (HEPES)	Gibco
IGEPAL$^®$ CA-630	Sigma-Aldrich
Leupeptin	Sigma-Aldrich
LB broth (Lennox)	Sigma-Aldrich
LB broth with agar (Lennox)	Sigma-Aldrich
L-glutamine	Gibco
Magnesium chloride (MgCl$_2$)	Sigma-Aldrich
MangoMix^{TM} PCR kit	Bioline (London, UK)
Marvel dried skimmed milk powder	Tesco (Ireland and UK)
Methanol	Sigma-Aldrich
Microvette$^®$ CB 300 K2E	Sarstedt (Leicester, UK)
MluI	New England Biolabs
Monopotassium phosphate (KH$_2$PO$_4$)	Sigma-Aldrich
MycoAlert^{TM} mycoplasma detection Kit	Lonza (Slough, UK)
N-Ethylmaleimide (NEM)	Sigma-Aldrich
Nitrocellulose membrane	Sigma-Aldrich
Nuclear Extract Kit	Active Motif (La Hulpe, Belgium)
Nuclease free water	Sigma-Aldrich
Parafilm	VWR
Paraformaldehyde	Sigma-Aldrich
Penicillin-streptomycin	Gibco
Phenol:chloroform:isoamyl alcohol (25:24:1)	Sigma-Aldrich
Phenylmethylsulfonyl fluoride (PMSF)	Sigma-Aldrich
Polybrene	Sigma-Aldrich
Ponceau S	Thermo Scientific
Potassium chloride (KCl)	Sigma-Aldrich
Precision Plus Protein^{TM} Prestained Standards	Bio-Rad (Hertfordshire, UK)
Primers	Sigma Aldrich IDT (Surrey, UK)
PI	Sigma-Aldrich
Proteinase K	Sigma-Aldrich
Protein G Agarose beads	Millipore (Cork, Ireland)
PureYield^{TM} Plasmid Midiprep System	Promega (Southampton, UK)
Q5$^®$ Hot Start High-Fidelity DNA Polymerase	New England Biolabs
QIAquick Gel Extraction Kit	QIAGEN (Manchester, UK)
QIAquick PCR Purification Kit	QIAGEN
QIAshredder homogenizor	QIAGEN
Restore^{TM} stripping buffer	Thermo Scientific
RNeasy$^®$ Mini Kit	QIAGEN

Roswell Park Memorial Institute (RPMI) medium	Gibco
SafeView Nucleic Acid Stain	NBS Biologicals (Cambridgeshire, UK)
Saponin	Sigma-Aldrich
Shandon^{TM} Kwik-Diff^{TM} Kit	Thermo Scientific
Sodium acetate ($C_2H_3NaO_2$)	Sigma-Aldrich
Sodium chloride (NaCl)	Sigma-Aldrich
Sodium deoxycholate	Sigma-Aldrich
Sodium dodecyl sulphate (SDS)	Sigma-Aldrich
Sodium fluoride (NaF)	Sigma-Aldrich
Sodium hydroxide	Sigma-Aldrich
Sodium orthovanadate (Na_3VO_4)	Sigma-Aldrich
Sticky-end Ligase Master Mix	New England Biolabs
Streptavidin-eFluor® 450	eBioscience
Streptavidin-PerCP-Cy5.5	eBioscience
Streptavidin-phycoerythrin (PE)	eBioscience
SuperSignal^{TM} West Pico and Femto Substrates	Thermo Scientific
Tetramethylethylenediamine (TEMED)	Sigma-Aldrich
Thymidine	Sigma-Aldrich
Trizma® base	Sigma-Aldrich
Trizma® HCl	Sigma-Aldrich
Trypan blue	Sigma-Aldrich
Trypsin-EDTA	Sigma-Aldrich
Tween 20	Sigma-Aldrich
UltraComp eBeads®	eBioscience
Vybrant® DyeCycle Violet Stain	Invitrogen
X-tremeGENE^{TM} HP DNA	Roche

2.1.5 Mice

Trib2 knockout (*Trib2$^{-/-}$*) mice (B6; 129S5-*Trib2^{tm1Lex}*) were purchased from Lexicon Genetics (The Woodlands, TX, USA) and backcrossed onto C57BL/6 background for more than 7 generations. Mice were bred and housed in the biological service unit of the University of Glasgow. Homozygous *Trib2* knockout female mice are infertile. Hence, homozygous *Trib2* knockout male and heterozygous *Trib2* knockout female mice were used as a breeding pair to obtain *Trib2$^{-/-}$* offspring which were identified by genotyping. Mice (B6.SJL-*Ptprc^a Pepc^b*/ BoyJ) used in BM transplantation as recipients were bred and housed in the Beatson Biological Service and Research Units. Age-matched (6-14 weeks old) mice of both genders were used for comparison between wild type (WT) and *Trib2$^{-/-}$* genotypes. All mouse experiments were approved by United Kingdom (UK) Animal Ethical Committees

and performed according to UK Home Office project license #60-4512 (Animal [Scientific Procedures] Act 1986) guidelines.

2.1.6 Plasmids

Table 2.4 │ Plasmids used in the experiments described in this thesis.

Plasmid	Source
MigR1	Keeshan lab
MigR1-ICN1	Keeshan lab
pcDNA3	Keeshan lab
pcDNA3-FLAG-TRIB2	Keeshan lab
pcDNA3-HisA-CDC25C (human)	Requested from Addgene repository (#10964)
pcDNA3-Ub-HA	Keeshan lab
pCMV-Gag-Pol	Keeshan lab
pCMV-VSV-G	Keeshan lab
pCMV6-AC-FLAG	McCarthy lab
pCMV6-CDC25A-FLAG	Sub-cloned from pCMV6-CDC25A-MYC-FLAG
pCMV6-CDC25A-MYC-FLAG	Purchased from OriGene (RC200496)
pCMV6-CDC25B-FLAG	Sub-cloned from pCMV6-CDC25B-MYC-FLAG
pCMV6-CDC25B-MYC-FLAG	Purchased from OriGene (RC207409)
pCMV6-CDC25C (human)-FLAG	Sub-cloned from pcDNA3-HisA-CDC25C
pCMV6-CDC25C (mouse)-FLAG	Sub-cloned from pCMV6-CDC25C
pCMV6-CDC25C (mouse)	Purchased from OriGene (MC200198)
PHMA	Keeshan lab
PHMA-MYC-dC-TRIB2	Keeshan lab
PHMA-MYC-dN-TRIB2	Keeshan lab
PHMA-MYC-FL-TRIB2	Keeshan lab
PHMA-MYC-KD-TRIB2	Keeshan lab

2.2 Methods

2.2.1 Agarose gel electrophoresis

Agarose gel solution was made by dissolving agarose powder in Tris-borate-EDTA (TBE) buffer containing 90 mM Tris-borate and 2 mM EDTA, via microwave heating. 2.5 µL of SafeView Nucleic Acid Stain was added per 50 mL of gel solution and mixed well by shaking before casting. 1x TBE buffer also served as the electrophoresis buffer. Samples were mixed with 6x gel loading dye before loading on agarose gel. Electrophoresis was run at 100 volts and at room temperature. The

electrophoresis was stopped when tracking dye migrated at three quarters of the gel.

2.2.2 Annexin V expression and apoptosis assay

Single cell suspension from thymus was prepared as described in section 2.2.10.1. To enable identification of thymus subsets, cells were stained, as described in section 2.2.10.2, with 50 μL of antibody panel A from Table 2.20. Following that, cell suspension was centrifuged at 350 x g and at 4°C for 5 minutes. 100 μL of Annexin V-fluorescein isothiocyanate (FITC) and DAPI, diluted 1:100 in Hank's balanced salt solution (HBSS), was then added to the cell pellet, mixed by pulsed vortex, and incubated at room temperature in the dark for 15 minutes. The stock concentration for DAPI was 1 mg/mL. After the incubation, 400 μL of HBSS was added. The cell suspension was pulsed vortex before analyzed by flow cytometry.

2.2.3 Bacterial transformation

Competent *E.coli* bacterial cells from the lab stocks were thawed on ice for 5 minutes. 50-100 ng of plasmid DNA was added into 50 µL of competent cells and incubated on ice for 20 minutes. The cells were heat shocked at 42°C for 90 seconds and placed on ice for 90 seconds. 500 µL of SOC medium (LB broth containing 2.5 mM KCl, 10 mM $MgCl_2$ and 20 mM glucose) was added and the cells were incubated in a shaker at 37°C for 45 minutes. For each transformation, 100 µL and 300 µL of cells were plated on two ampicillin-supplemented LB plates. The plates were checked the next morning for the presence of colony.

2.2.4 Blood cell counts

Mice were euthanized by carbon dioxide inhalation and blood was collected by cardiac puncture into EDTA-coated Microvette® CB 300 K2E to prevent coagulation.

Blood was mixed thoroughly by gently flicking and inverting the microvette before analyzed by Hemavet HV950 (Drew Scientific, Miami Lakes, FL, USA) to generate complete blood counts and WBC differential counts (Table 2.5).

Table 2.5 │ Normal haematology profile of a mouse.

Parameter	Units	Normal Range[†]
White blood cell (WBC)	$10^3/\mu L$	1.8 - 10.7
Neutrophil	$10^3/\mu L$	0.1 - 2.4
Lymphocyte	$10^3/\mu L$	0.9 - 9.3
Monocyte	$10^3/\mu L$	0.0 - 0.4
Eosinophil	$10^3/\mu L$	0.0 - 0.2
Basophil	$10^3/\mu L$	0.0 - 0.2
Red blood cell (RBC)	$10^6/\mu L$	6.36 - 9.42
Platelet	$10^3/\mu L$	592 - 2972

[†] Adapted from Hemavet HV950 Product Reference Manual.

2.2.5 Bone marrow transduction and transplantation

2.2.5.1 Production of retroviral supernatants

15×10^6 of 293T cells were seeded in a cell culture dish (150 x 20 mm) the day before transfection. On the transfection day, 1.5 mL of fresh transfection buffer (Table 2.6) and 1.5 mL of DNA cocktail were made (Table 2.8). The existing culture medium was removed from the culture dish followed by addition of 9 mL of pre-warmed fresh culture medium. The DNA cocktail was added drop by drop to the transfection buffer in a 15 mL centrifuge tube. Bubbles were then introduced into the mixture with a pipetting aid equipped with a 1 mL serological pipette for 30 seconds. The mixture was added to the culture dish drop by drop and the dish was tilted gently to distribute the mixture evenly. The next day, with no longer than 16 hours after the addition of transfection mixture, the existing culture medium in the dish was replaced with 13 mL of fresh pre-warmed medium. After 24 hours of culture, the supernatant of transfected cells was collected and another 13 mL of fresh pre-warmed medium was added to the cells. The cells were cultured for another 24

hours before the supernatant was collected. These supernatants contained the retroviral particles. They were syringe-filtered (0.45 μm pore size), aliquoted into 1.5 mL microcentrifuge tubes, and stored at -80°C.

Table 2.6 │ Transfection buffer for retroviral production.

Components	Final concentration
HEPES (pH7.1)	0.05 M
NaCl	0.18 M
Na_2HPO_4	2 mM
Sterile-filtered water	quantity sufficient to 1.5 mL

Table 2.7 │ 10x NaCl-Tris-EDTA (NTE) buffer.

Components	Final concentration
NaCl	1.5 M
Tris-HCl (pH7.4)	0.1 M
EDTA (pH8.0)	10 mM

Table 2.8 │ DNA cocktail for retroviral production.

Components	Final concentration
Sterile-filtered water	quantity sufficient to 1.5 mL
$CaCl_2$	0.25 M
10x NTE bufffer	1x
MigR1 or MigR1-ICN1	45 μg
pCMV-Gag-Pol	30 μg
pCMV-VSV-G	18 μg

2.2.5.2 Determination of retrovirus titer

0.2×10^6 of 3T3 cells in 3 mL of culture medium were seeded per cell culture dish (60 x 15 mm) the day before transduction. On the transduction day, the existing culture medium was replaced with 1 mL of fresh pre-warmed medium containing 4 μg of polybrene. To titre retrovirus supernatant per harvest, 10 μL and 100 μL of the supernatant were added gently to two tilted dishes. The dishes were returned to tissue incubator once the supernatant was added. After 24 hours of culture, 2 mL of fresh medium was added to each dish. Cells were cultured for another 24 hours before harvest. The existing culture medium was removed and cells were washed

once in 1 mL of phosphate buffered saline (PBS) containing 137 mM NaCl, 2.7 mM KCl, 10 mM Na_2HPO_4 and 2 mM KH_2PO_4. 500 μL of trypsin was then added to each dish followed by incubation for 5 minutes at room temperature to detach the cells. 1 mL of 2% FBS-supplemented PBS was added to each dish. The detached cells were pipetted up and down few times to generate single cell suspensions, before being transferred to polystyrene tubes (12 x 75 mm) which were kept on ice. The cells were centrifuged at 350 x g and at 4°C for 5 minutes. The cell pellet was resuspended in 500 μL of 2% FBS-supplemented PBS and was ready for flow cytometry analysis. The retroviral titre is the percentage of green fluorescent protein (GFP) positive 3T3 cells due to transduction by 100 μL of the retroviral supernatant.

2.2.5.3 *Ex vivo* culture and transduction of bone marrow

BM was collected from 6-8 weeks old WT and *Trib2*^{-/-} mice (donor) 4 days after administration of 5-FU (250 mg/kg, i.p.). One donor mouse was required to obtain sufficient cells for transplantation into two recipients. Single cell suspension from WT and *Trib2*^{-/-} BM was generated as described in section 2.2.10.1, resuspended in pre-stimulation medium (Table 2.9) at a density of 4×10^6 cells/mL and was transferred to a 6-well culture plate (up to 4 mL per well) for overnight incubation. The next day, WT and *Trib2*^{-/-} cells were transferred to 50 mL centrifuge tubes and kept on ice. The culture wells were washed thrice with 2 mL of ice-cold PBS and each wash was transferred to the corresponding centrifuge tubes to minimize cell loss. Cell counting was performed to determine the recovery. WT and *Trib2*^{-/-} cell suspensions were divided into halves for transduction with MigR1 and MigR1-ICN1 (total of four transduction conditions) and were centrifuged at 350 x g and at 4°C for 10 minutes. Each cell pellet was resuspended in 3 mL of activation medium (Table 2.10) and transferred to a 6-well culture plate (one well per transduction condition). MigR1 and MigR1-ICN1 retroviral supernatants were thawed on ice and up to 1 mL

of supernatant with a titre of 40% was added into each well. Equal titre was used for MigR1 and MigR1-ICN1 retroviral supernatants and across three independent transplant experiments to ensure similar transduction efficiency of cells. If less than 1 mL of supernatant was added, DMEM was used for compensation. The cells were centrifuged at 1290 x g and at room temperature for 90 minutes (first spin-infection). Following that, the cells were returned to tissue incubator for overnight incubation. The next day, the cells were transferred to 50 mL centrifuge tubes and kept on ice. The culture wells were washed thrice with 2 mL of ice-cold PBS and each wash was transferred to the corresponding centrifuge tubes to minimize cell loss. The cell suspensions were centrifuged at 350 x g and at 4°C for 10 minutes. MigR1 and MigR1-ICN1 retroviral supernatants were thawed on ice and 4 mL of each supernatant, each mL with a titre of 40%, was added into each tube containing the cell pellet. Cytokines (IL-3, IL-6 and SCF from PeproTech, London, UK) and polybrene were added directly to the tube. Their final concentrations were listed in Table 2.10. Cells were resuspended gently and the suspension was transferred to a 6-well culture plate (4 mL per transduction condition per well). The cells were centrifuged at 1290xg and at room temperature for 90 minutes (second spin-infection). Following that, the cells were returned to tissue incubator and incubated for 3 hours. The cells were transferred from each well of the culture plate into individual centrifuge tubes and kept on ice. The culture wells were washed thrice with 2 mL of ice-cold PBS and each wash was transferred to the corresponding centrifuge tubes to minimize cell loss. Cell counting was performed to determine the recovery. Cells were centrifuged at 350 x g and at 4°C for 10 minutes. The cell pellets were washed twice in 20 mL of ice-cold PBS. After that, the cell pellets from all the four transduction conditions were resuspended in ice-cold PBS and adjusted so that all have the equal concentrations (1.25-2.5 x 10^6 cells/mL). The cells were kept on ice and were ready to be transplanted into recipients.

Table 2.9 │ Pre-stimulation medium for retroviral transduction.

Components	Final concentration
DMEM	quantity sufficient to desired volume
Penicillin/streptomycin	100 I.U.mL^{-1}/100 μgmL^{-1}
L-glutamine	2 mM
FBS	15%
IL-3	10 ng/mL
IL-6	10 ng/mL
SCF	100 ng/mL

Table 2.10 │ Activation medium for retroviral transduction.

Components	Final concentration per transduction condition[†]
DMEM	3 mL per transduction condition
Penicillin/streptomycin	100 I.U.mL^{-1}/100 μgmL^{-1}
L-glutamine	2 mM
FBS	15%
IL-3	10 ng/mL
IL-6	10 ng/mL
Polybrene	4 μg/mL
SCF	100 ng/mL

[†] The amount of penicillin/streptomycin, L-glutamine, FBS, polybrene and cytokines added to 3 mL of DMEM was based on the calculation for the final volume (4 mL) of one transduction condition.

2.2.5.4 Transplantation and monitoring for leukaemia development

On the day where donor cells had second spin-infection, recipients were lethally irradiated with two fractionated doses, each 4.25 grays, given three hours apart. 200 μL of donor cells (0.25-0.5 x 10^6 cells) were then injected intravenously into each recipient. The recipients were kept in individually ventilated cages and treated with Baytril antibiotic, administered in the drinking water at a concentration of 80 mg/L, daily for 10 days post transplantation. The recipients were monitored by periodic tail vein bleedings three weeks post transplantation. To count WBC, 97 μL of 3% acetic acid solution was added to 3 μL of blood followed by pipetting up and down for a few times before it was loaded onto a haemocytometer (Hawksley, Lancing, Sussex, UK). To monitor the level of donor engraftment and leukaemia development, the remaining collected blood was used for flow cytometry analysis (Section 2.2.10.2 and Table 2.22). Mice were euthanized when they showed any of

the following symptoms of disease: severe cachexia, lethargy, WBC count more than 20 x 10^6 cells/mL and hunching. Healthy controls were euthanized at the end of experiment when all mice in the test groups succumbed to disease.

2.2.5.5 Analysis for moribund mice

The body weight for each euthanized mouse was measured. Blood, liver, BM and spleen were collected and processed as described in section 2.2.10.1 for flow cytometry analysis using antibody panel C from Table 2.19. Blood cell counts were determined as described in section 2.2.4. Blood smears were made and stained as described in section 2.2.14. BM cells were also lysed in radio immunoprecipitation assay (RIPA) buffer to derive cell lysates for Western blotting analysis (section 2.2.28.1). Spleen was photographed and weighed before being processed for flow cytometry analysis. Genomic DNA was also extracted from spleen cells to verify transplant experimental group based on *Trib2* genotyping (section 2.2.26).

2.2.6 Cell counting by trypan blue exclusion

20 μL of 0.4% trypan blue solution was added to 20 μL of cell suspension and was mixed by pipetting up and down. The mixture was loaded onto a haemocytometer and examined immediately under an inverted microscope at low magnification. Only unstained live cells were counted in two of the large nine squares. The concentration of cells in the original suspension was calculated as below:

$$\left(\frac{\text{number of cells counted}}{2\ \text{large squares}}\right) \times \left(\frac{40\ \mu\text{L}}{20\ \mu\text{L}}\right) = \text{x}10^4\ \text{cells/mL}$$

2.2.7 Co-immunoprecipitation

After 24 hours of transfection, the cells were washed once with ice-cold PBS and harvested by using a cell scraper. The cells were transferred to a microcentrifuge tube and centrifuged at 11,000 x g and at 4°C for 45 seconds. 300 µL of protease inhibitors-supplemented Tris lysis buffer (Table 2.11) were added to the cell pellet. The crude cell lysate was incubated on ice for 30 minutes with vortexing every 5 minutes. After the incubation, the lysate was centrifuged at 21,912 x g and at 4°C for 10 minutes. The supernatant which was the cleared protein lysate was transferred to a new microcentrifuge tube and kept on ice. Protein concentration was determined by using Bio-Rad Protein Assay Dye Reagent Concentrate. 50 µg of the lysate was aliqouted as input. For immunoprecipitation, equal amount of protein lysate for all the conditions were quantified sufficient to 1 mL with protease inhibitors-supplemented Tris lysis buffer (Table 2.11). Prior to immunoprecipitation, the lysate was pre-cleared with addition of 20 µL of Protein G Agarose beads followed by incubation on a rotary tube mixer in a cold room for 30 minutes. The lysate was centrifuged at 21,912 x g and at 4°C for 2 minutes. The supernatant which was the pre-cleared lysate was transferred to a new microcentrifuge tube. 1.5-5 µg of anti-FLAG antibody and 20 µL of Protein G Agarose beads were added to the pre-cleared lysate followed by incubation on a rotary tube mixer in a cold room for overnight. The beads were washed in 1 mL of ice-cold Tris lysis buffer by inverting the tube repeatedly, and centrifugation at maximum speed and at 4°C for 30 seconds. The washing was repeated for three times. In the final wash, residual supernatant was removed by 26 G needle. 25 µL of 2x Laemmli buffer containing 1.5% of fresh β-mercaptoethanol was added to the beads followed by boiling at 95°C for 5 minutes to elute immunoprecipitated proteins. The mixture was vortexed, and centrifuged at maximum speed and at 4°C for 2 minutes. 2x Laemmli buffer containing 1.5% of fresh β-mercaptoethanol was also added to the input followed by

boiling at 95°C for 5 minutes The supernatant and input were analyzed as described in section 2.2.28.2.

Table 2.11 │ Protease inhibitors-supplemented Tris lysis buffer.

Components	Final concentration
Tris buffer [pH 7.4]	50 mM
NaCl	150 mM
IGEPAL® CA-630	0.5 %
Glycerol	5 %
EDTA	1 mM
PMSF[†]	1 mM
Aprotinin[†]	2 μg/mL
Leupeptin[†]	5 μg/mL
Pepstastin[†]	1 μg/mL
Na$_3$VO$_4$[†]	1 mM
NaF[†]	5 mM

[†] Fresh protease inhibitors were added to Tris lysis buffer prior cell lysis.

2.2.8 Cytospin preparation and staining

100 µL of single cell suspension containing 50-100 x 10^3 cells was deposited onto a glass slide using Shandon™ Cytospin™ 4 Cytocentrifuge. The cells were centrifuged at 450 rpm and at room temperature for 4 minutes with medium acceleration rate. The cells deposited onto slide were fixed and stained as described in section 2.2.14 using Shandon™ Kwik-Diff™ Kit.

2.2.9 Detection of endogenous *Tcrb* rearrangements

2.2.9.1 Extraction and clean up of thymic DNA

Unfractionated thymocytes were digested overnight in 500 μL of lysis buffer (Table 2.12) (Wang et al., 2008) at 56°C. The following day, sample was heated at 95°C for 30 minutes to inactivate proteinase K. 500 μL of Phenol:Chloroform:Isoamyl Alcohol (25:24:1) reagent was added to the sample. The mixture was inverted repeatedly to mix homogenously, and centrifuged at maximum speed and at 4°C for

5 minutes. The separated aqueous phase was transferred to a new microcentrifuge tube. 45 μL of 3M sodium acetate (pH 5.2) and 1125 μL of ice-cold absolute ethanol were then added. The mixture was inverted repeatedly to mix homogenously and kept at -20°C for overnight. The following day, it was centrifuged at maximum speed and at 4°C for 10 minutes. The supernatant was removed carefully to leave the DNA pellet undisturbed. 500 μL of 70% ice-cold ethanol was added carefully to leave the DNA pellet undisturbed, and it was centrifuged at maximum speed and at 4°C for 5 minutes. The supernatant was again removed carefully to leave the DNA pellet undisturbed. The DNA pellet was left to air-dry at room temperature for at least 30 minutes. Finally, the DNA pellet was resuspended in 50 μL of nuclease free water and the concentration was determined using NanoDrop® ND-1000 Spectrophotometer. All extracted DNA were stored indefinitely at -20°C.

Table 2.12 │ Lysis buffer to extract thymic DNA.

Components[†]	Final concentration
KCl	50 mM
Tris-HCl (pH8.3)	10 mM
MgCl$_2$	2 mM
IGE	0.45% (vol/vol)
Tween 20	0.4 % (vol/vol)
Proteinase K	60 μg/mL

[†] Fresh lysis buffer was made on the experiment day.

2.2.9.2 Polymerase chain reaction (PCR) amplification of *Tcrb* rearrangements

V(D)J rearrangements of the *Tcrb* locus were amplified by FastStart™ High Fidelity PCR Kit using published primers (Cobaleda et al., 2007). Primer sequences and the annealing temperatures for all amplifications were listed in Table 2.13. All the reagents and DNA were thawed and kept on ice. After thawing, all DNA samples were pre-diluted to 25 ng/μL in nuclease free water and kept on ice. All components, listed in Table 2.14, were added in an order to make a PCR master mix. 22 μL of master mix was aliquoted into individual PCR tubes. 1 μL of pre-

diluted sample (25 ng of DNA input) was then added to the tube. Importantly, 2 μL of primer mix (Table 2.15) was added to the tube in the final step to complete the setup of a PCR reaction. All tubes were pulsed vortexed and spunbriefly with a mini centrifuge before loaded onto a PCR machine. The thermal cycling conditions were listed in Table 2.16. PCR products and 1 kb DNA ladder were separated on a 1.5% agarose gel, detected by SafeView Nucleic Acid Stain, and imaged using Bio-Rad ChemiDoc XRS system.

Table 2.13 │ PCR primers used to detect *Tcrb* rearrangements.

Primer	*Tcrb* locus	5'>3' sequence	Annealing temperature (°C)
Forward	Dβ2	GTAGGCACCTGTGGGGAAGAAACT	58
	Vβ2	GGGTCACTGATACGGAGCTG	58
	Vβ4	GGACAATCAGACTGCCTCAAGT	58
	Vβ5.1	GTCCAACAGTTTGATGACTATCAC	56
	Vβ8	GATGACATCATCAGGTTTTGTC	56
	Vβ14	CTTCTACCTCTGTGCCTGGAGT	58
Reverse	Jβ2	TGAGAGCTGTCTCCTACTATCGATT	According to forward primer

Table 2.14 │ PCR master mix for detection of *Tcrb* rearrangements.

Components	volume per reaction (μL)	Final concentration
Nuclear free water	18.5	-
10x buffer[†]	2.5	1.8 mM MgCl$_2$
dNTP	0.5	200 μM
Enzyme[†]	0.5	2.5 U

[†] Provided in the FastStart High Fidelity PCR kit.

Table 2.15 │ PCR Primer mix for detection of *Tcrb* rearrangements.

Primer	volume per reaction (μL)	Final concentration
Forward	1	0.4 μM
Reverse	1	0.4 μM

Table 2.16 │ PCR thermal cycling conditions for detection of *Tcrb* rearrangements.

Steps	Number of cycles	Duration	Temperature (°C)
Initial denaturation	1	2 minutes	95
Denaturation		30 seconds	95
Annealing	35	30 seconds	refer to Table 2.4
Elongation		3 minutes	72
Final elongation	1	7 minutes	72
Cooling	unlimited	indefinite	4

2.2.10 Flow cytometry

2.2.10.1 Preparation for primary cells

Pelvises, femurs and tibias collected from euthanized mice were dissected free of muscle tissues and tendons. The bones were crushed in 2% (vol/vol) FBS-supplemented PBS using a mortar and pestle. The resulting BM cell suspension was filtered through a cell strainer. Whole spleen and thymus were isolated and grinded directly onto a pre-wet cell strainer and washed with 2% FBS-supplemented PBS to generate single cell suspensions. Cell suspension from liver was derived in a similar way except that a cut piece instead of whole organ was used. All the cell suspensions were centrifuged at 350 x g and at 4°C for 5 minutes. The cell pellets were resuspended in 1 mL homemade ammonium-chloride-potassium lysing buffer containing 10 mM $KHCO_3$, 150 mM NH_4Cl and 0.1 mM EDTA, and incubated on ice for 5 minutes to lyse RBCs. This was followed by washing and resuspension in 2% FBS-supplemented PBS. The RBC lysing procedure was repeated once when the cell pellet remained to be visibly red. Live cell count was then determined by trypan blue exclusion.

2.2.10.2 Surface staining

Cell suspensions were centrifuged at 350 x g and at 4°C for 5 minutes. 50-100 μL of antibody cocktails, diluted in 2% FBS-supplemented FBS, were added to the cell

pellets, mixed by pulsed vortex and incubated on ice for 30 minutes. Following that, the cells were washed once and resuspended in 2% FBS-supplemented PBS. The surface-stained cells were kept on ice and were ready for (i) secondary staining with fluorochrome-conjugated streptavidin, (ii) intracellular staining or (iii) flow cytometry analysis.

Table 2.17 │ Multicolour fluorescent antibody panel to detect HSCs.

Antibody	Fluorochrome	Dilution
anti-mouse CD3 anti-mouse CD4 anti-mouse CD8α anti-mouse CD45.1[1] anti-mouse Gr-1 anti-mouse Ter-119 anti-mouse/human B220 anti-mouse/human CD11b	Biotin[2]	1:200
anti-mouse CD48	PE	1:600
anti-mouse CD16/CD32	APC	1:100
anti-mouse c-Kit	APC-Cy7	1:200
anti-mouse Sca-1	PE-Cy7	1:200

[1] Included only for whole BM transplant experiment to exclude CD45.1^{+} donor cells from analysis.
[2] Biotinylated primary antibodies were revealed by streptavidin-eFluor® 450.

Table 2.18 │ Multicolour fluorescent antibody panel to detect haematopoietic progenitor cells.

Antibody	Fluorochrome	Dilution
anti-mouse CD3 anti-mouse CD4 anti-mouse CD8α anti-mouse CD45.1[1] anti-mouse Gr-1 anti-mouse Ter-119 anti-mouse/human B220 anti-mouse/human CD11b	Biotin[2]	1:200
anti-mouse c-Kit	APC-Cy7	1:200
anti-mouse CD16/CD32	APC	1:100
anti-mouse CD34	FITC	1:100
anti-mouse IL-7Rα	PE	1:100
anti-mouse Sca-1	PE-Cy7	1:200

[1] Included only for whole BM transplant experiment to exclude CD45.1^{+} donor cells from analysis.
[2] Biotinylated primary antibodies were revealed by streptavidin-eFluor® 450.

Table 2.19 │ Multicolour fluorescent antibody panels to detect cells of myeloid, B- and T-lineages.

Antibody	Fluorochrome[1]			Dilution
	Panel A	**Panel B**	**Panel C**[2]	
anti-mouse CD4	Brilliant Violet 510™	Brilliant Violet 510™	Brilliant Violet 510™	1:250
anti-mouse CD8α	PE	PE	PE	1:250
anti-mouse CD19	APC	eFluor® 780	eFluor® 780	1:150
anti-mouse CD45.2	-	PE-Cy7	PE-Cy7	1:250
anti-mouse Gr-1	PE-Cy7	PerCP-Cy5.5	PerCP-Cy5.5	1:250
anti-mouse/human B220	PerCP-Cy5.5	APC	APC	1:250
anti-mouse/human CD11b	FITC	FITC	eFluor® 450	1:250

[1] Panel A was designed for non-transplant experiments. Panel B and C were designed for transplant experiments involved whole and transduced BM respectively.
[2] GFP expression was also measured as a marker for transduced donor cells.

Table 2.20 │ Multicolour fluorescent antibody panels to detect thymic subsets.

Antibody	Fluorochrome[1]				Dilution
	Panel A	**Panel B**	**Panel C**	**Panel D**	
anti-mouse CD11c anti-mouse Gr-1 anti-mouse NK1.1 anti-mouse Ter-119 anti-mouse/human B220	eFluor® 450	eFluor® 450	Biotin[2]	Biotin[2]	1:250
anti-mouse CD4	Brilliant Violet 510™	Brilliant Violet 510™	Biotin[2]	FITC	1:150[3] 1:250[4]
anti-mouse CD8α	PE	APC	Biotin[2]	APC	1:250
anti-mouse CD25	PE-Cy7	PE-Cy7	PE-Cy7	PE-Cy7	1:250
anti-mouse CD44	PerCP-Cy5.5	PerCP-Cy5.5	PerCP-Cy5.5	PerCP-Cy5.5	1:250
anti-mouse CD71	-	PE	-	-	1:250
anti-mouse c-Kit	APC-Cy7	APC-Cy7	APC-Cy7	APC-Cy7	1:150[5] 1:250[6]

[1] Panel A was designed for Annexin V (section 2.2.2), Ki-67 and phospho-p38 (section 2.2.10.3.3) staining. Panel B was designed to measure expression of CD71 for different thymic subsets. Panel C was designed for staining of cells in resting and cycling state (section 2.2.10.3.4), and for detection of incorporated bromodeoxyuridine (BrdU) (section 2.2.13). Panel D was designed for DNA staining of different thymic subsets (section 2.2.10.3.1).
[2] Biotinylated primary antibodies were revealed by streptavidin-PE.
[3] Antibody dilution used for panel A and B.
[4] Antibody dilution used for panel C and D.
[5] Antibody dilution used for panel C.
[6] Antibody dilution used for panel A, B and D.

Table 2.21 │ Multicolour fluorescent antibody panel to detect non-T-lineage cells present in the thymus.

Antibody	Fluorochrome	Dilution
anti-mouse CD11c	Biotin[†]	1:250
anti-mouse CD19	eFluor® 780	1:150
anti-mouse Gr-1	PE-Cy7	1:250
anti-mouse NK1.1	eFluor® 450	1:250
anti-mouse/human B220	APC	1:250
anti-mouse/human CD11b	FITC	1:250

[†] Biotinylated primary antibody was revealed by streptavidin-PerCP-Cy5.5.

Table 2.22 │ Multicolour fluorescent antibody panel used to monitor leukaemia development[†].

Antibody	Fluorochrome	Dilution
anti-mouse CD45.2	PE-Cy7	1:250
anti-mouse CD4	APC	1:250
anti-mouse Gr8	eFluor® 450	1:250

[†] GFP expression was also measured as a marker for transduced donor cells.

2.2.10.3 Intracellular staining

2.2.10.3.1 DNA staining for thymocytes

To enable identification of thymus subsets, cells were stained in 50 μL of antibody panel D from Table 2.20. Following that, cell suspension was centrifuged at 350 x g and at 4°C for 5 minutes. To fix and permeabilize the cells, BD Cytofix/Cytoperm™ Kit was used. 500 μL of BD Cytofix/Cytoperm solution was added to the cell pellet followed by pulse vortex and incubation on ice in the dark for 20 minutes. The fixed and permeabilized cells were washed twice in 500 μL of BD 1x Perm/Wash buffer followed by centrifugation at 350 x g and at 4°C for 5 minutes. To stain DNA, the cells were incubated with DNA selective Vybrant® DyeCycle Violet Stain (1:100 dilution), diluted in 100 μL of BD 1x Perm/Wash buffer, for 30 minutes on ice in the

dark. Finally, the cells were washed and resuspended in 500 μL of 2% FBS-supplemented PBS for flow cytometry analysis.

2.2.10.3.2 DNA staining for cell cycle synchronization

Cells were transferred to polystyrene tube (12 x 75 mm) and washed once in ice-cold PBS. The cells were centrifuged at 350 x g and at 4°C for 5 minutes. The cell pellet was resuspended in 300 µL of ice-cold PBS. 700 µL of ice-cold absolute ethanol was added to the cell suspension drop by drop while vortexing. The tube was sealed with parafilm and the sample was stored at -20°C. To prepare for DNA staining, the cells were centrifuged at 200 x g and at 4°C for 10 minutes. The cells were washed twice in ice cold PBS. Each wash involved centrifugation at 200 x g and at 4°C for 10 minutes. After the last wash, the cells were resuspended in 350 µL of BD Pharmingen™ PI/RNase Staining Buffer and incubated at room temperature in the dark for 15 minutes. The cells were ready for flow cytometry analysis.

2.2.10.3.3 Ki-67 and phospho-p38 staining

To enable identification of thymus subsets, cells were stained, as described in section 2.2.10.2, with antibody panel A from Table 2.20. Following that, cell suspension was centrifuged at 350 x g and at 4°C for 5 minutes. To fix the cells, 400 μL of 4% (wt/vol) paraformaldehyde solution was added to the cell pellet followed by pulse vortex and incubation at room temperature in the dark for 20 minutes. The fixed cells were centrifuged at 350 x g and at 4°C for 5 minutes. To permeabilize the cells, 400 μL of 0.1% (wt/vol) saponin solution was added to the cell pellet followed by pulse vortex and incubation at room temperature in the dark for 15 minutes. The fixed and permeabilized cells were centrifuged at 350 x g and at 4°C for 5 minutes. To stain the cells for Ki-67 and phospho-p38, 100 μL of antibody

cocktail (Table 2.23), diluted in 0.1% (wt/vol) saponin solution, was added to the cell pellet. This was followed by pulsed vortex and incubation on ice in the dark for 30 minutes. Finally, the cells were washed and resuspended in 500 μL of 2% FBS-supplemented PBS for flow cytometry analysis.

Table 2.23 │ Fluorescent antibody panel to stain Ki-67 and phospho-p38.

Antibody	Fluorochrome	Dilution
anti-mouse/human phosphor-p38 (T180/Y182)	APC	1:250
anti-mouse/rat Ki-67	FITC	1:250

2.2.10.3.4 Staining for cells in resting and cycling state

To enable identification of immature DN thymus subsets, cells were stained in 100 μL of antibody panel C from Table 2.20. Following that, cell suspension was centrifuged at 350 x g and at 4°C for 5 minutes. To fix and permeabilize the cells, 500 μL of BD Cytofix/Cytoperm Buffer was added to the cell pellet followed by pulse vortex and incubation on ice in the dark for 20 minutes. The fixed and permeabilized cells were washed twice in 500 μL of BD 1x Perm/Wash Buffer followed by centrifugation at 350 x g and at 4°C for 5 minutes. To distinguish resting (G_0) from cycling (G_1-S/G_2/M) cell cycle state, the cells were incubated with anti-Ki-67 FITC antibody (1:250 dilution) and Vybrant® DyeCycle Violet Stain (1:100 dilution), diluted in 100 μL of BD 1x Perm/Wash Buffer, for 30 minutes on ice in the dark. Finally, the cells were washed and resuspended in 500 μL of 2% FBS-supplemented PBS for flow cytometry analysis.

2.2.10.4 Data collection and analysis

UltraComp eBeads® was used to prepare single-color compensation controls in multicolor flow cytometry experiments. Flow cytometry was performed using BD FACSCanto II system (BD Biosciences), equipped with blue, red and violet lasers.

Aggregates were excluded by forward scatter (FSC) height versus area signals. The singlet population was then gated by FSC area versus side scatter area signals to exclude dead cells and debris. Whenever possible, dead cells were also excluded by DAPI (1:1000 dilution of 1 mg/mL stock solution) or PI (1:2000 dilution of 10 mg/mL stock solution) staining. In this case, the dye was added into cell suspension and mixed by pulsed vortex prior flow cytometry analysis. FlowJo (Tree Star, Ashland, OR, USA) was used to analyze flow cytometry data. Fluorescence Minus One (FMO) controls were used to facilitate gating as appropriate.

2.2.11 Gene set enrichment analysis (GSEA)

Gene expression profiles of T-ALL and healthy BM samples from GSE13159 data set (Haferlach et al., 2010) were downloaded from the Leukaemia Gene Atlas platform (Hebestreit et al., 2012). Based on 202478_at feature, *TRIB2* expression of low *TRIB2* T-ALL group ranged from 3.602 to 5.370 whereas high *TRIB2* T-ALL group ranged from 8.811 to 11.103. The mean value of *TRIB2* for healthy BM samples (n = 73) was 6.172. GSEA (Subramanian et al., 2005) was performed using the default settings. Gene sets from the Molecular Signatures Database v5.0 of GSEA (Broad Institute of MIT and Harvard, Cambridge, MA, USA) were used. These included the 1330 gene sets in C2: CP collection for canonical pathways and the 3 gene sets in C2: CGP collection (M4175, M2059 and M1007) for T-ALL molecular subtypes.

2.2.12 *In vivo* 5-FU treatment

On the drug administration day, mice were weighed to calculate the weight-adjusted dosage (150 or 250 mg/kg), as indicated in the related figure legends. 5-FU 50 mg/mL solution was diluted in PBS on the same day and was administered by intraperitoneal (i.p.) injection. For 150 mg/kg dosage, the diluted concentration of 5-

FU was 15 mg/mL whereas for 250 mg/kg dosage, it was 25 mg/mL. In this case, a mouse of 20 g received 0.2 mL of the diluted 5-FU.

2.2.13 *In vivo* BrdU pulsing and detection of incorporated BrdU

On day 14 post 5-FU treatment, mice were pulsed with 1 mg of BrdU Labelling Reagent, by i.p. injection, for one or four hours. Thymus was collected from euthanized mice and single cell suspension was prepared as described in section 2.2.10.1. To enable identification of immature DN thymus subsets, cells were stained in 100 μL of antibody panel C from Table 2.20. Following that, cell suspension was centrifuged at 350 x g and at 4°C for 5 minutes. To fix and permeabilize the cells, 250 μL of BD Cytofix/Cytoperm Buffer was added to the cell pellet followed by pulse vortex and incubation on ice in the dark for 30 minutes. The fixed and permeabilized cells were washed in 3% FBS-supplemented PBS, and were centrifuged at 350 x g and at 4°C for 5 minutes. To permeabilize the nuclear membrane further, 1 mL of 10% DMSO-supplemented FBS was added to the cell pellet followed by pulse vortex and incubation for overnight at -80°C. The cells were then thawed at 37°C, washed in 3% FBS-supplemented PBS, and incubated with 250 μL of BD Cytofix/Cytoperm Buffer for an additional 10 minutes on ice in the dark. Following incubation, the cells were washed in 3% FBS-supplemented PBS and treated in 100 μL of DNase I solution (30 μg per 1×10^6 cells diluted in PBS) for one hour at 37°C in the dark. The cells were washed once in BD 1x Perm/Wash Buffer before intracellular staining. The cells were incubated with anti-BrdU FITC antibody (1:50 dilution) and Vybrant® DyeCycle Violet Stain (1:100 dilution), diluted in BD Perm/Wash Buffer, for 30 minutes at room temperature in the dark. Finally, the cells were washed and resuspended in 500 μL of 3% FBS-supplemented PBS for flow cytometry analysis.

2.2.14 Making and staining a blood smear

Blood collected in EDTA-coated microvette was pulsed-vortexed. 3 µL of blood was transferred to one end of a clean glass slide. The blood was spread into a thin smear by using another clean slide to touch the blood drop and push carefully along the length of the first slide. The smear was allowed to air dry at room temperature before it was stained using Shandon™ Kwik-Diff™ Kit. The blood smear slide was dipped into Kwik-Diff Reagent 1 (Fixative) for 10 times, Reagent 2 (Eosin) for 10 times and into Reagent 3 (Methylene Blue) for 10 times. Each dip was about a second. After that, the slide was dipped into clean water for a few times to wash off the excess staining reagent. The stained blood smear was allowed to air dry at room temperature and DPX mountant was applied to preserve the stain.

2.2.15 Mycoplasma detection assay

Mycoplasma contamination in cultured cell lines was monitored using MycoAlert™ Mycoplasma Detection Kit (Lonza, Slough, UK). Aliquots of MycoAlert™ reagent and substrate (50 µL each), stored at -20°C, were thawed and allowed to equilibrate to room temperature. 50 µL of fresh supernatant of cultured cells was added to the reagent and incubated for 5 minutes before luminescence (reading A) was measured by GloMax® 20/20 Single Tube Luminometer (Promega, Southampton, UK). The substrate was subsequently added to the sample and incubated for 10 minutes before luminescence (reading B) was measured again. The results (ratio of reading B to reading A) were interpreted according to the manufacturer guidelines.

2.2.16 Plasmid construction

2.2.16.1 Sub-cloning to derive pCMV6-CDC25A/B-FLAG

pCMV6-CDC25A/CDC25B-MYC-FLAG and pCMV6-AC-FLAG (empty vector) plasmids were double-digested using MluI and AsiSI restriction enzymes. CDC25A and CDC25B inserts were extracted using QIAquick Gel Extraction Kit whereas the digested pCMV6-AC-FLAG was cleaned up using QIAquick PCR Purification Kit. CDC25A and CDC25B inserts were ligated individually with digested pCMV6-AC-FLAG using Sticky-end Ligase Master Mix with 1:3 molar ratio of vector to insert. Bacterial transformation was performed as described in section 2.2.3. Colonies were picked and screened by double digestion using MluI and AsiSI restriction enzymes.

2.2.16.2 Sub-cloning to derive pCMV6-CDC25C-FLAG

CDC25C (human/mouse) inserts were derived from pcDNA3-HisA-CDC25C (human) and pCMV6-CDC25C (mouse) plasmids. AsiSI and MluI cloning sites were appended to the 5' and 3' ends of the inserts respectively by PCR (Table 2.24) using Q5$^®$ Hot Start High-Fidelity DNA Polymerase. PCR products were cleaned up using QIAquick PCR Purification Kit. CDC25C inserts and pCMV6-AC-FLAG (empty vector) plasmids were double-digested using MluI and AsiSI restriction enzymes. The digested inserts and vector were cleaned up using QIAquick PCR Purification Kit. CDC25C (human/mouse) inserts were ligated individually with digested pCMV6-AC-FLAG using Sticky-end Ligase Master Mix. Bacterial transformation was performed as described in section 2.2.3. Colonies were picked and screened by double digestion using MluI and AsiSI restriction enzymes. Positive clones were verified further by DNA sequencing to ensure no mutation presents in the PCR-cloned inserts.

Table 2.24 │ PCR primers used to clone CDC25C inserts.

CDC25C	Forward primer (5'>3')[†]	Reverse primer (5'>3')[†]
mouse	gaggcgatcgccATGTCTACAGGACC TATCCCACC	gcgacgcgtTTGTGGGCTCGCA CCCTTCA
human	gaggcgatcgccATGTCTACGGAACT CTTCTCATC	gcgacgcgtTGGGCTCATGTCC TTCACC

[†] Letters in lower case contain the AsiSI and MluI cloning sites.

2.2.17 Plasmid purification

A sterile pipette tip was used to stab the frozen glycerol stock of transformed bacteria and placed in 5 mL of ampicillin-supplemented LB broth. The LB broth was incubated in a shaker at 37°C for approximate 8 hours. After that, the bacteria culture was transferred to a bigger flask containing 150 mL of fresh ampicillin-supplemented LB broth for overnight incubation in a shaker at 37°C. Plasmid DNA was purified from the overnight culture using PureYield[TM] Plasmid Midiprep System. The cells were centrifuged at 5,000 x g for 10 minutes. 6 mL of Cell Resuspension Solution was added to resuspend the cell pellet. 6 mL of Cell Lysis Solution was added and mixed by gently inverting the tube 3 times. The mixture was incubated for 3 minutes at room temperature. 10 mL of Neutralization Solution was added to the lysed cells and mixed by gently inverting the tube 3 times. The lysate was centrifuged at room temperature and at 15,000 x g for 15 minutes. The cleared lysate was transferred into the PureYield[TM] Clearing Column. Vacuum was applied so that the lysate passed through the Clearing and Binding Columns. 5 mL of Endotoxin Removal Wash and 20 mL of Column Wash Solution were added to the Binding Column sequentially and removed by the vacuum. The membrane was dried by applying a vacuum for 1 minute and the the tip of the column was tapped on a paper towel to remove excess ethanol. 400 µL of nuclease free water was added to elute the plasmid DNA by vacuum.

2.2.18 Protein BLAST

Basic Local Alignment Search Tool (BLAST) (Altschul et al., 1990) was used to align the amino acid sequence of human and mouse orthologs for CDC25B and CDC25C. The reference sequences for CDC25B were NP_075606.1 (mouse ortholog) and NP_068659.1 (human ortholog). The reference sequences for CDC25C were NP_033990.2 (mouse ortholog) and NP_001781.2 (human ortholog). Blastp (protein-protein BLAST) algorithm was executed with default parameters.

2.2.19 Quantitative RT-PCR

2.2.19.1 Analysis for *TRIB2* knockdown in U937 cells

High throughput quantitative RT-PCR analysis was performed on the Fluidigm 48.48 Dynamic Array Integrated Fluidic Circuits system (Biomark HD). Primer sequences are listed in Table 2.25. Specific target pre-amplification was carried out. Each target was measured in triplicate reactions. Expression levels of the target genes (*TRIB1* and *TRIB2*) were normalized relative to the mean of the reference genes (*ABL*, *B2M*, *ENOX2* and *RNF20*). Relative messenger ribonucleic acid (mRNA) levels were calculated using the $2^{-\Delta\Delta CT}$ method.

Table 2.25 │ Primers used for quantitative RT-PCR.

Gene	Forward primer (5'>3')	Reverse primer (5'>3')
TRIB1	CTTCAAGCAGATTGTCTCCGC	CTAAGCTGGGTTCTCTCCTCC
TRIB2	AGCCAGACTGTTCTACCAGA	GGCGTCTTCCAGGCTTTCCA
ABL	TGGAGATAACACTCTAAGCATAACTAAAGGT	GATGTAGTTGCTTGGGACCCA
β2M	TTGTCTTTCAGCAAGGACTGG	ATGCGGCATCTTCTAACCTCC
ENOX2	GAGCTGGAGGGAACCTGATTT	CACTGGCACTACCAAACTGCA
RNF20	GGTGTCTCTTCAACGGAGGAA	TAGTGAGGCATCATCAGTGGC

2.2.19.2 Analysis for cell cycle synchronization

Trib2 and β2m expressions were measured using Fast SYBR$^®$ Green Master Mix. Primer sequences are listed in Table 2.25. Each target was measured in triplicate reactions. Master mix (Table 2.26) was prepared on ice and 9 µL of the mix was aliquoted per well of a 384-well plate. 1 µL of cDNA was added into each well. The volume of a complete reaction was 10 µL. The plate was sealed and centrifuged briefly before loaded onto the Applied Biosystems 7900HT Fast Real-Time PCR system (Table 2.27). Expression of *Trib2* was normalized relative to *B2m*. Relative mRNA levels were calculated using the 2-ΔΔCT method.

Table 2.26 │ Master mix for quantitative RT-PCR.

Components	Volume per reaction (µL)
Fast SYBR$^®$ Green Master Mix	5
Forward primer (10 µM)	0.25
Reverse primer (10 µM)	0.25
Nuclease free water	3.5

Table 2.27 │ Thermal cycling conditons for quantitative RT-PCR.

Steps	Number of cycles	Temperature (°C)	Duration (seconds)
Activation	1	95	20
Melting		95	1
Annealing	40	60	20
Extending		50	120

2.2.20 RNA extraction and complementary DNA (cDNA) synthesis

Total ribonucleic acid (RNA) was extracted from cells using RNeasy$^®$ Mini Kit. Cells were washed once in ice-cold PBS and centrifuged at 350 x g and at 4°C for 5 minutes. Filtered tips were used during the whole procedure. 350 µL of Buffer RLT was added to the cell pellet. Cell lysis was aided by repeated pipetting. The lysate was transferred into a QIAshredder spin column placed in a 2 mL collection tube and centrifuged for 2 minutes at full speed and at room temperature. 350 µL of 70% ethanol was added to the homogenized lysate and mixed well by pipetting. The

sample was transferred to an RNeasy spin column placed in a 2 mL collection tube. The lid was closed gently and centrifuged for 15 seconds at 10,000 x g and at room temperature. The flow through was discarded. 700 µL of Buffer RW1 was added to the RNeasy spin column. The lid was closed gently and centrifuged for 15 seconds at 10,000 x g and at room temperature. The flow through was discarded. 500 µL of Buffer RPE was added to the RNeasy spin column. The lid was closed gently and centrifuged for 15 seconds at 10,000 x g and at room temperature. The flow through was discarded. Another 500 µL of Buffer RPE was added to the RNeasy spin column. The lid was closed gently and centrifuged for 2 minutes at 10,000 x g and at room temperature. The RNeasy spin column was placed in a new 2 mL collection tube, and centrifuged at full speed for 1 minute and at room temperature. The RNeasy spin column was placed in a new 1.5 mL microcentrifuge tube. 30 µL of nuclease free water was added directly to the spin column membrane. The lid was closed gently and centrifuged for 1 minute at 10,000 x g and at room temperature to elute the RNA. The RNA concentration was determined using NanoDrop® ND-1000 Spectrophotometer. All RNA samples were stored at -80°C.

cDNA was synthesized using High Capacity cDNA Reverse Transcription Kit. Master mix (Table 2.28) were prepared on ice and 6.8 µL of the master mix was aliquoted into individual PCR tube. 13.2 µL of sample containing up to 0.5 µg of RNA was added into each tube. The volume of a complete reaction was 20 µL. Tube was pulsed vortex and centrifuged briefly before loaded onto a PCR machine. The thermal cycling conditions were listed in Table 2.29. All cDNA samples were stored at -20°C.

Table 2.28 │ Master mix for cDNA synthesis.

Components	Volume per reaction (µL)
10x RT buffer	2
25x dNTP mix (100 mM)	0.8
10x RT Random Primers	2
MultiScribe Reverse Transcriptase (50 U/µL)	1
RNase inhibitor[†] (20 U/µL)	1

[†] RNase inhibitor was not included in the kit.

Table 2.29 │ PCR thermal cycling conditons for cDNA synthesis.

Steps	Temperature (°C)	Duration (minutes)
1	25	10
2	37	120
3	85	5
4	4	indefinite

2.2.21 Single thymidine block

RPMI-8402 cells were synchronized by single thymidine block. Cells were sub-cultured at 0.5×10^6 cells/mL the day before treatment with thymidine. The following day, the cells were plated at 0.5×10^6 cells/mL. Asynchronous samples (AS) were collected at this time point. The remaining cells were treated with 0.75 mM thymidine and cultured for 21 hours. At 21 hours post treatment, synchronous samples (S0) were collected. The remaining synchronous cells were released from thymidine block by washing for twice in PBS. Each wash involved centrifugation of cells at 350 x g and at room temperature for 5 minutes. After the final wash, the cells were resuspended in fresh complete culture medium and returned to tissue incubator. Samples were then collected at different time points (S12, S15, S17, S20, S22 and S24). At each time point, cells were collected for flow cytometry (Section 2.2.10.3.2), Western blotting (Section 2.2.28.4) and quantitative RT-PCR analyses (Section 2.2.19.2). Each analysis required 250×10^3 cells.

2.2.22 Statistics

GraphPad Prism (version 5.03; LA Jolla, CA, USA) was used for statistical analysis and graphing. An unpaired, two-tailed, Student's t-test was applied for comparison of two groups. For analysis of multiple groups between WT and $Trib2^{-/-}$ genotypes, two-way analysis of variance (ANOVA) with Bonferroni post-tests was applied. Log-rank test was applied for survival curve comparison. Pearson correlation test was applied to examine association between $TRIB2$ and $LYL1$ expressions of T-ALL samples from GSE33315 data set (Zhang et al., 2012c). This data set was downloaded from Gene Expression Omnibus and Robust Multichip Average method was used for data normalization. D'Agostino-Pearson omnibus test confirmed these samples had Normal distributions of $TRIB2$ and $LYL1$ values. Statistical significance of differences was attained when P value <0.05 and was indicated in the related graphs. Statistical analyses where P value ≥ 0.05 were not indicated in the graphs and deemed not significant.

2.2.23 Subcellular fractionation

Transfected cells were treated with DMSO (vehicle) or 10 μM of MG132 for 4 hours before being subcellular fractionated. Active Motif Nuclear Extract Kit was used to derive nuclear and cytoplasmic lysates. Cells were washed with 4 mL of ice-cold phosphatase inhibitors-supplemented PBS. Following that, the cells were harvested in 1 mL of ice-cold phosphatase-inhibitors supplemented PBS by using cell scrapper and the cell suspension was transferred to a pre-chilled microcentrifuge tube. The suspension was centrifuged for 4 minutes at 200 x g and at 4°C. The cell pellet was resuspended gently in 300 μL of 1x hypotonic solution and incubated on ice for 15 minutes. 25 μL of detergent was then added and the suspension was vortexed at the highest speed for exactly 10 seconds. The suspension was centrifuged for 30 seconds at 14,000 x g and at 4°C. The supernatant was the cytoplasmic lysate and transferred to a new microcentrifuge tube. The nuclear pellet

75

was resuspended in 25 μL of complete lysis buffer and vortexed at the highest speed for 1 minute. The nuclear suspension was incubated on a laboratory rocking mixer in a cold room for 30 minutes. The suspension was vortexed again at the highest speed for 30 seconds before being centrifuged for 10 minutes at 14,000 x g and at 4°C. The supernatant was the nuclear lysate and transferred to a new microcentrifuge tube. The concentration of nuclear and cytoplasmic lysates was determined by using Bio-Rad Protein Assay Dye Reagent Concentrate. All lysates were kept at -80°C until being analyzed as described in section 2.2.28.3.

2.2.24 Tissue culture

293T and 3T3 cell lines were cultured in DMEM complete medium whereas RPMI-8402 and HeLa cell lines were cultured in RPMI complete medium (Table 2.30). To maintain 293T, 3T3 and HeLa cell lines, cells were sub-cultured at 1:5 ratio in fresh medium every 2-3 days. Trypsin-EDTA solution was used to detach the cells from growth surface. To maintain RPMI-8402 cell line, cells were sub-cultured at 0.5×10^6 cells/mL in fresh medium every 2-3 days. To cryopreserve cells, cells were centrifuged at 350 x g and at room temperature for 5 minutes. Ice-cold cyopreservation medium (10% DMSO-supplemented FBS) was added to the cell pellet and cells were resuspended by gentle pipetting. 1 mL of cell suspension was aliquoted into each cryotube, and stored at -80°C for short term and in liquid nitrogen tank for long term. To resuscitate frozen cells, cryopreserved cells were thawed at 37°C and transferred to a 50 mL centrifuge tube. 10 mL of pre-warmed complete culture medium was added drop by drop to the cells and mixed by gentle shaking. The cells were centrifuged at 350 x g and at room temperature for 5 minutes. The cell pellet was resuspended in complete culture medium. The cell suspension was transferred to a culture flask and cultured at 37°C.

Table 2.30 │ Culture medium used to maintain cell lines.

Components	Final concentration
DMEM/RPMI	-
Penicillin/streptomycin	100 I.U.mL^{-1}/100 μgmL^{-1}
L-glutamine	2 mM
FBS	10%

2.2.25 Transient transfection

2.2.25.1 Examination of TRIB2 and CDC25A-C interactions

HeLa cells were transiently transfected with plasmid vectors using X-tremeGENE^{TM} HP DNA transfection reagent to express exogenous TRIB2, all human isoforms of CDC25 family and orthologs (human and mouse) for CDC25C. Cells were plated the day before transfection so that cells were at 90% confluency. Transfection reagent, plasmid DNA and serum free RPMI medium were allowed to equilibrate to room temperature and vortexed gently. 1:1 ratio of DNA (μg) to transfection reagent (μL) was used and was diluted in serum free medium followed by incubation at room temperature for 25 minutes. To transfect cells seeded in a culture dish of 150 x 20 mm, a total of 20 μg DNA was diluted in 2 mL of medium whereas for a culture dish of 100 x 20 mm, a total of 8 μg DNA was diluted in 1 mL of medium. For co-transfection, equal amount of plasmids were used. The transfection complex was added to the cells in a dropwise manner and the dish was swirled gently before being returned to tissue incubator. The cells were processed as described in section 2.2.7 after 24 hours of transfection.

2.2.25.2 Examination of CDC25C degradation

HeLa cells were plated in a culture dish of 100 x 20 mm the day before transfection so that cells were at 90% confluency for transfection. X-tremeGENE^{TM} HP DNA Transfection reagent, plasmid DNA and serum free RPMI medium were allowed to equilibrate to room temperature and vortexed gently. 1:1 ratio of DNA (μg) to

transfection reagent (µL) was used and was diluted in 1 mL of serum free medium followed by incubation at room temperature for 20 minutes. 6-8 µg of empty vector or pcDNA-FLAG-TRIB2 was used per transfection condition. The transfection complex was added to the cells in a dropwise manner and the dish was swirled gently before being returned to tissue incubator. The cells were processed as described in section 2.2.23 after 24 hours of transfection.

2.2.25.3 Examination of CDC25C ubiquitination.

HeLa cells were plated in a culture dish of 100 x 20 mm the day before transfection so that cells were at 90% confluency for transfection. X-tremeGENE™ HP DNA Transfection reagent, plasmid DNA and serum free RPMI medium were allowed to equilibrate to room temperature and vortexed gently. 1:1 ratio of DNA (µg) to transfection reagent (µL) was used and was diluted in 1 mL of serum free medium followed by incubation at room temperature for 25 minutes. Regardless of the transfection conditions, 3 µg of pcDNA3-Ub-HA, 3 µg of PHMA-MYC-(FL, dN, KD and dC)-TRIB2, 2 µg of pCMV6-human CDC25C-FLAG and 2 µg of pCMV6-mouse CDC25C-FLAG were used. The transfection complex was added to the cells in a dropwise manner and the dish was swirled gently before being returned to tissue incubator. The cells were processed as described in section 2.2.27 after 24 hours of transfection.

2.2.26 *Trib2* genotyping

2.2.26.1 DNA extraction

DNA was extracted from ear clips of weaned mice. 250 µL of Digestion Buffer 1 (Table 2.31) was added to a sample and boiled at 95°C for 15 minutes. During boiling, the sample was vortexed at an interval of 3 minutes. After boiling, 25 µL of

Digestion Buffer 2 (Table 2.31) was added and the sample was vortexed. All samples were stored at -20°C.

Table 2.31 │ DNA digestion buffers.

Buffer	Components	Final concentration
1	NaOH	50 mM
2	Tris buffer	1 M
	EDTA	10 mM

2.2.26.2 PCR amplification of *Trib2* WT and mutant alleles

Trib2 WT and mutant alleles were amplified by MangoMix™ PCR system using the primers listed in Table 2.32. All the reagents and DNA were thawed and kept on ice. 23 μL of master mix (Table 2.33) was aliquoted into individual PCR tubes. 2 μL of DNA was then added to the tubes. All tubes were pulsed vortexed and centrifuged briefly before loaded onto a PCR machine. The thermal cycling conditions were listed in Table 2.34. PCR products and 100 bp DNA ladder were separated on a 2% agarose gel, detected by SafeView Nucleic Acid Stain, and imaged using Bio-Rad ChemiDoc™ XRS system.

Table 2.32 │ PCR primers used for *Trib2* genotyping.

Primer	5'>3' sequence
1[†]	CACAATAGCGAGATATGGGAG
2	GCAATGCGACAAGTTCGGAG
Neo3A	GCAGCGCATCGCCTTCTATC

[†] Primer 1 anneals to genome sequence deleted in the disrupted region of *Trib2* exon1.

Table 2.33 │ PCR master mix for *Trib2* genotyping.

Components	volume per reaction (μL)	Final concentration
MangoMix™	12.5	-
Primer 1	0.5	2 µM
Primer 2	1.0	4 µM
Primer Neo3A	0.5	2 µM
Nuclease free water	8.5	-

Table 2.34 │ PCR thermal cycling conditions for *Trib2* genotyping.

Steps	Number of cycles	Duration	Temperature (°C)
Initial denaturation	1	5 minutes	94
Denaturation		30 seconds	94
Annealing	30	30 seconds	60
Elongation		1 minute	72
Final elongation	1	5 minutes	72
Cooling	unlimited	indefinite	4

2.2.27 Ubiquitination assay

Transfected cells were treated with 10 µM of MG132 or DMSO (vehicle control) and cultured at 37°C for 7 hours. After that, the cells were treated with 10 mM of NEM at room temperature for 30 seconds. The culture medium was removed and the cells were washed in 4 mL of ice-cold PBS containing 10 mM of NEM. The cells were harvested in 1 mL of ice-cold PBS containing 10 mM of NEM using cell scrapper and transferred to a microcentrifuge tube. The cell suspension was centrifuged at 11,000 x g at 4°C for 45 seconds. 100 µL of 1% (wt/vol) SDS was added to the cell pellet followed immediately by vortexing for 10 seconds and boiling at 95°C for 5 minutes. The crude cell lysate was sonicated using Soniprep 150 equipped with an exponential probe (MSE, London, UK), with 6 micron amplitude for 10 seconds to break down remaining DNA. The lysate was sonicated further if it was very viscous. The lysate was centrifuge at full speed and at 4°C for 10 minutes. The supernatant (cleared protein lysate) was transferred to a new microcentrifuge tube. 5 µL of the lysate was aliquoted as input and stored at -20°C. 900 µL of ice-cold protease inhibitors-supplemented Tris lysis buffer (Table 2.11) was added to the remaining lysate. Prior immunoprecipitation, the lysate was pre-cleared with addition of 20 µL of Protein G Agarose beads followed by incubation on a rotary tube mixer in a cold room for 30 minutes. The lysate was centrifuged at maximum speed and at 4°C for 2 minutes. The supernatant which was the pre-cleared lysate was transferred to a new microcentrifuge tube. 1 µg of antibody and 20 µL of Protein G Agarose beads

were added to the pre-cleared lysate followed by incubation on a rotary tube mixer in a cold room for overnight. The beads were washed in 1 mL of ice-cold Tris lysis buffer by inverting the tube repeatedly, and centrifugation at maximum speed and at 4°C for 30 seconds. The washing was repeated for three times. In the final wash, residual of supernatant was removed by 26 G needle. 25 µL of 2x Laemmli buffer containing 1.5% of fresh β-mercaptoethanol was added to the beads followed by boiling at 95°C for 5 minutes to elute immunoprecipitated proteins. The mixture was vortexed, and centrifuged at maximum speed and at 4°C for 2 minutes. 5 µL of 2x Laemmli buffer containing 1.5% of fresh β-mercaptoethanol was added to the inputs followed by boiling at 95°C for 5 minutes. The supernatant and input were analyzed as described in section 2.2.28.4.

2.2.28 Western blotting

Table 2.35 │ Solutions for preparing 5% stacking gel for SDS-PAGE.

Components	Volume required to cast a gel (5 mL)
Water	3.4
30% acrylamide mix	0.83
1.0 M Tris (pH 6.8)	0.63
10% SDS	0.05
10% ammonium persulfate	0.05
TEMED	0.005

Table 2.36 │ Solutions for preparing resolving gel for SDS-PAGE.

Components	Volume required to cast a gel (10 mL)	
	8%	12%
Water	4.6	3.3
30% acrylamide mix	2.7	4.0
1.5 M Tris (pH 8.8)	2.5	2.5
10% SDS	0.1	0.1
10% ammonium persulfate	0.1	0.1
TEMED	0.006	0.004

Table 2.37 │ Tris-glycine buffer for SDS-PAGE.

Components	Final concentration
Tris-Cl	25 mM
Glycine	192 mM
SDS	0.1% (wt/vol)

Table 2.38 │ Transfer buffer.

Components	Final concentration
Tris-Cl	25 mM
Glycine	192 mM
Methanol	20% (vol/vol)

2.2.28.1 Detection of MAPK signalling

Total BM cells collected from mice succumbed to leukaemia were lysed in protease inhibitors-supplemented RIPA buffer (Table 2.39). Crude cell lysates were centrifuged at maximum spend and at 4°C for 10 minutes after incubation for 30 minutes on ice with periodic pulse vortex. The supernatants which were cleared protein lysates were stored at -80°C. To prepare for gel electrophoresis, protein lysates were mixed with 4x Laemmli buffer (Table 2.40) containing 3% (vol/vol) fresh β-mercaptoethanol and boiled at 95°C for 5 minutes. Protein lysates and Precision Plus Protein™ Prestained Standards were resolved by SDS-polyacrylamide gel electrophoresis (PAGE) using 5% stacking (Table 2.35) and 12% resolving gels (Table 2.36). Electrophoresis was run at 100 volts using Tris-glycine buffer (Table 2.37) until the tracking dye diffused into the buffer. After electrophoresis, the separated proteins were wet-transferred (Table 2.38) from the gel to nitrocellulose membranes, with pore size of 0.45 μm, at 100 volts for 1 hour. The transfer efficiency was checked by Ponceau S staining. The membranes were blocked with PBS supplemented with 5% (wt/vol) milk and 0.01% (vol/vol) Tween 20, at room temperature for 1 hour. Triplicate membranes were incubated with primary antibodies (Table 2.41), to detect activation of p38, p44/42 and JNK separately, on a roller mixer in a cold room for overnight. The following day, the

membranes were washed thrice in PBS supplemented with 5% (wt/vol) milk and 0.01% (vol/vol) Tween 20. Each time the incubation was 5 minutes. The membranes were incubated with horseradish peroxidise-conjugated secondary antibodies (Table 2.41) on a roller mixer at room temperature for 1 hour. The membranes were washed thrice and each time the incubation was 10 minutes. The signals were detected by chemiluminescence method using SuperSignal™ West Pico and Femto Substrates, and were developed onto CL-XPosure™ radiography films. For each membrane, Restore™ stripping buffer was used for secondary probing to detect total level of MAPK and for tertiary probing to detect β-actin.

Table 2.39 │ Protease inhibitors-supplemented RIPA buffer.

Components	Final concentration
Tris buffer [pH 7.4]	50 mM
NaCl	150 mM
IGEPAL® CA-630	0.5%
Sodium deoxycholate	0.25%
EDTA	1 mM
PMSF[†]	1 mM
Aprotinin[†]	2 μg/mL
Leupeptin[†]	5 μg/mL
Pepstastin[†]	1 μg/mL
Na$_3$VO$_4$[†]	1 mM
NaF[†]	5 mM

[†] Fresh protease inhibitors were added to RIPA buffer prior cell lysis.

Table 2.40 │ 4x Laemmli buffer.

Components	Final concentration
Tris buffer [pH6.8]	250 mM
SDS	8% (wt/vol)
Glycerol	40% (vol/vol)
Bromophenol blue	0.005% (wt/vol)

Table 2.41 │ Antibodies used to detect MAPK signalling.

Primary antibody[†]	Dilution	Dilution for secondary antibody[†]
anti-β-actin	1:5000	1:5000
anti-JNK1	1:1000	1:1000
anti-p38	1:2000	1:4000
anti-p44/42	1:2000	1:2000
anti-phospho-JNK (T183/Y185)	1:1000	1:1000
anti-phospho-p38 (T180/Y182)	1:3000	1:3000
anti-phospho-p44/42 (T202/Y204)	1:2000	1:2000

[†] Anti-β-actin and secondary antibodies were diluted in PBS supplemented with 5% (wt/vol) milk and 0.01% (vol/vol) Tween 20. The rest were diluted in Tris-buffered saline (TBS) containing 20 mM Tris and 150 mM NaCl, and supplemented with 5% (wt/vol) BSA and 0.01% (vol/vol) Tween 20.

2.2.28.2 Detection of co-immunoprecipitated proteins

Inputs, eluates and Precision Plus Protein™ Prestained Standards were resolved by SDS-PAGE using 5% stacking (Table 2.35) and 12% resolving (Table 2.36) gels. Electrophoresis, wet transfer, membrane blocking, antibody incubation (Table 2.42), membrane washing and signal detection were performed as described in section 2.2.28.1. Restore™ stripping buffer was used for repeated probing as appropriate.

Table 2.42 │ Antibodies used to analyze co-immunoprecipitation assay.

Primary antibody[†]	Dilution	Dilution for secondary antibody[†]
anti-β-actin	1:5000	1:5000
anti-CDC25C	1:500	1:1000
anti-FLAG	1:1000	1:1000
anti-MYC	1:1000	1:1000

[†] All antibodies were diluted in PBS supplemented with 5% (wt/vol) milk and 0.01% (vol/vol) Tween 20.

2.2.28.3 Detection of nuclear and cytoplasmic proteins

2x Laemmli buffer containing 1.5 % of fresh β-mercaptoethanol was added to the nuclear and cytoplasmic lysates and were boiled at 95°C for 5 minutes. The lysates were resolved by SDS-PAGE using 5% stacking (Table 2.35) and 12% resolving (Table 2.36) gels. Unless stated otherwise, electrophoresis, wet transfer, membrane blocking, antibody incubation (Table 2.43), membrane washing and signal detection

were performed as described in section 2.2.28.1. Restore^{TM} stripping buffer was used for repeated probing as appropriate.

Table 2.43 │ Antibodies used to analyze subcellular fractions.

Primary antibody[†]	Dilution	Dilution for secondary antibody[†]
anti-α-tubulin	1:2000	1:1000
anti-CDC25C	1:500	1:1000
anti-FLAG	1:1000	1:1000
anti-HDAC1	1:1000	1:1000

[†] All antibodies were diluted in PBS supplemented with 5% (wt/vol) milk and 0.01% (vol/vol) Tween 20.

2.2.28.4 Detection of ubiquitination

Inputs and eluates were resolved by SDS-PAGE using 12% and 8% resolving gels respectively (Table 2.36). Unless stated otherwise, electrophoresis, wet transfer, membrane blocking, antibody incubation (Table 2.44), membrane washing and signal detection were performed as described in section 2.2.28.1. For eluates, the electrophoresis was run till the 50 kDa marker of Precision Plus Protein^{TM} Prestained Standards reached the bottom of the gel. Restore^{TM} stripping buffer was used for repeated probing as appropriate.

Table 2.44 │ Antibodies used to analyze ubiquitination assay.

Primary antibody[†]	Dilution	Dilution for secondary antibody[†]
anti-β-actin	1:5000	1:5000
anti-CDC25C	1:500	1:1000
anti-FLAG	1:1000	1:1000
anti-MYC	1:1000	1:1000
anti-HA	1:1000	1:1000
anti-K48-Ub	1:1000	1:1000

[†] All antibodies were diluted in PBS supplemented with 5% (wt/vol) milk and 0.01% (vol/vol) Tween 20.

2.2.28.5 Detection of TRIB2 during cell cycle progression

Cells were washed once in ice-cold PBS and centrifuged at 350 x g and at 4°C for 5 minutes. 25 µL of 2x Laemmli buffer containing 1.5 % of fresh β-mercaptoethanol was added directly to the cell pellet followed by vortexing and boiling at 95°C for 5 minutes. The lysate was stored at -80°C. Sample was thawed at room temperature and boiled again at 95°C for 5 minutes prior SDS-PAGE. Lysate and Precision Plus Protein™ Prestained Standards were resolved by SDS-PAGE using 5% stacking (Table 2.35) and 12% resolving (Table 2.36) gels. Electrophoresis, wet transfer, membrane blocking, antibody incubation (Table 2.45), membrane washing and signal detection were performed as described in section 2.2.28.1. Restore™ stripping buffer was used for repeated probing as appropriate.

Table 2.45 │ Antibodies used to analyze cell cycle synchronization.

Primary antibody[†]	Dilution	Dilution for secondary antibody[†]
anti-β-actin	1:5000	1:5000
anti-CDC25C	1:500	1:1000
anti-phospho-Histone H3 (Ser10)	1:1000	1:1000
anti-TRIB2	1:200	1:1000

[†] All antibodies were diluted in PBS supplemented with 5% (wt/vol) milk and 0.01% (vol/vol) Tween 20 except anti-phospho-Histone H3 which was diluted in TBS supplemented with 5% (wt/vol) BSA and 0.01 (vol/vol) Tween 20.

2.2.29 Whole bone marrow transplantation

BM cells were harvested from WT and $Trib2^{-/-}$ mice. After lysis of red blood cells, cell counting (Section 2.2.6) was performed. 8×10^6 unfractionated cells were injected intravenously into lethally irradiated (2 x 4.25 grays fractionated doses were given with three hours apart) recipients. The recipients were kept in individually ventilated cages and treated with Baytril antibiotic, administered in the drinking water at a concentration of 80 mg/L, daily for 10 days post transplantation. The recipients were monitored by periodic tail vein bleedings 4 weeks post transplantation. The collected blood was used for flow cytometry analysis with

antibody panel B from Table 2.19. All the recipients were euthanized at 17 weeks post transplantation where blood and BM were collected. Blood cell counts were determined as described in section 2.2.4. The blood was also analyzed by flow cytometry using antibody panel B from Table 2.19. Cell counting (Section 2.2.6) was performed to determine the cellularity of the BM. To immunophenotype HSPCs, the BM was also analyzed by flow cytometry using antibody panels listed in Table 2.17 and 2.18.

CHAPTER 3: EXAMINATION OF THE ROLE OF TRIB2 IN
STEADY STATE HAMATOPOIESIS

3.1 Introduction

Studies focused on the pathological role of TRIB2 in various disease states including haematological malignancy, solid tumours, autoimmune and inflammatory diseases have identified TRIB2 as a critical signalling modulator and mediator (Yokoyama and Nakamura, 2011). However, it is unclear if this is true in a physiological context where regulation of diverse signalling pathways is cell type and developmental stage dependent. Studies of Tribbles orthologues in *Xenopus* (Saka and Smith, 2004) and *Drosophila* (Grosshans and Wieschaus, 2000, Mata et al., 2000, Seher and Leptin, 2000) highlight an evolutionary conserved role for Tribbles in the regulation of normal cellular proliferation. In these organisms, Tribbles coordinates cell division and morphogenesis to ensure proper organ development. In *Drosophila*, Tribbles ensures mitosis occurs in a timely manner by regulating String turnover at the protein level (Grosshans and Wieschaus, 2000, Mata et al., 2000, Seher and Leptin, 2000). Takasato and colleagues generated a *Trib2* knockout mouse model (*Trib2^{tm1Ryn}*) where the exon 1 of *Trib2* is disrupted with the insertion of a *LacZ-Neo* cassette, to investigate the role of TRIB2 in kidney development (Takasato et al., 2008). However, microscopic examinations of WT and *Trib2^{tm1Ryn}* mutant embryos at 14.5 days post coitum showed no phenotypic defects in organs (heart, eye, testis, thymus and kidney) where *Trib2* is abundantly expressed (Takasato et al., 2008). These data suggest TRIB2 function is required for proper cellular behaviour rather than tissue organization.

In Chapter One, literature review of previous TRIB2 studies allowed us to speculate the possible roles of TRIB2 in normal haematopoiesis. TRIB2 could be important in the development and differentiation of erythroid/megakaryocyte

lineages, and intrathymic T-cell development. Elucidation of the role of TRIB2 in normal haematopoiesis is crucial because TRIB2 has been implicated in both AML and T-ALL which are malignant haematopoiesis (Section 1.7). This could improve our understanding of how dysregulation of *Trib2* in normal haematopoiesis contributes to leukaemogensis. Hence, we aimed to investigate the impact of *Trib2* ablation in adult BM haematopoiesis and intrathymic T-cell development using a commercially available *Trib2* knockout mouse model (129S5-*Trib2*^{tm1Lex}, referred as *Trib2*$^{-/-}$ hereafter). Similar to *Trib2*^{tm1Ryn} (Takasato et al., 2008), exon 1 of *Trib2* in *Trib2*^{tm1Lex} is disrupted (Lexicon Phenotypic Analysis Database: LEXKO-1136). A third *Trib2* knockout mouse model (*Trib2*^{tm1Myam}) was generated by Satoh and colleagues, where exon 2 of *Trib2* is replaced with neomycin-resistance gene, to study tissue-resident macrophages in the spleen (Satoh et al., 2013). In all the three *Trib2* knockout mouse models, characterization of BM haematopoiesis and intrathymic T-cell development has not been reported.

3.2 Results

3.2.1 TRIB2 is dispensable for murine bone marrow haematopoiesis.

The coding and non-coding regions of exon 1 of *Trib2* in *Trib2*$^{-/-}$ mice were disrupted and thus enabled *Trib2* genotyping by PCR analysis (Figure 3.1). Compared to WT mice, *Trib2*$^{-/-}$ mice had similar RBC and WBC differential (neutrophil, lymphocyte, monocyte, eosinophil and basophil) counts, except for the platelet count which was significantly higher but within the normal physiological range (Figure 3.2A and 3.2B). In addition, no difference was found between WT and *Trib2*$^{-/-}$ mice in the distribution of mature myeloid, B and T cells in the blood (Figure 3.2C). These data indicate loss of TRIB2 does not affect terminal differentiation and production of mature blood cells of different lineages. We next studied the BM, the primary site of adult haematopoiesis, to determine if TRIB2 influences

hematopoietic cell fate choice at an earlier stage of differentiation. $Trib2^{-/-}$ mice had similar BM cellularity compared to WT mice (Figure 3.2D) as determined by cell counting. No difference was found in the peripheral blood for the frequency of circulating $CD4^+$ and $CD8^+$ T cells, lineage committed $Gr-1^+/CD11b^+$ myeloid cells and $CD19^+/B220^+$ B-lymphoid cells (Figure 3.2E). Moving up the hematopoietic hierarchy, $Trib2^{-/-}$ mice had similar frequencies of HSPCs, including HSCs, MPPs, CMPs, GMPs, MEPs and CLPs compared to WT mice (Figure 3.2F and 3.2G). Hence, TRIB2 is not essential for hematopoietic cell fate choice since loss of TRIB2 did not lead to skewing of hematopoietic cell differentiation. Thus, at steady state, $Trib2$ ablation does not affect the hierarchical organization of the murine haematopoietic system.
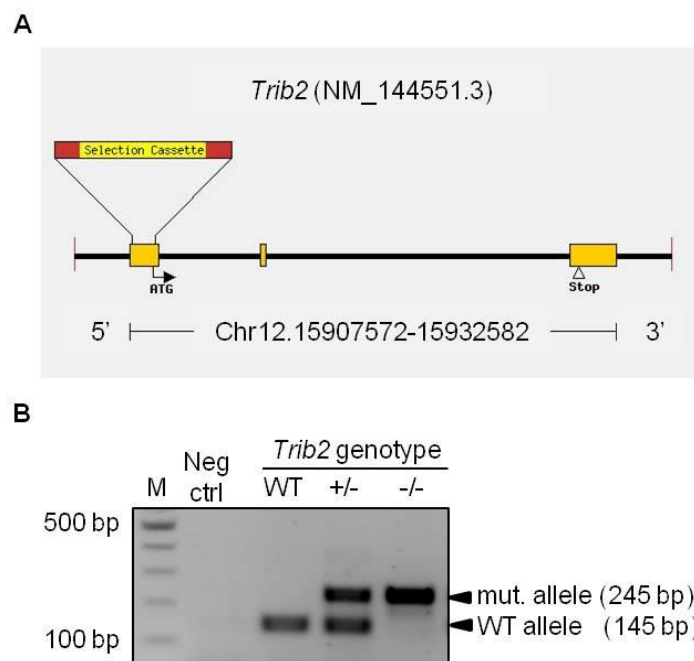
Figure 3.1 │ Genotyping of *Trib2* by genomic DNA PCR. (A) Exon 1 of *Trib2* in *Trib2^tm1Lex^* is disrupted by insertion of LacZ/Neo selection cassette. Modified from Lexicon Phenotypic Analysis Database: LEXKO-1136. **(B)** A representative gel electrophoresis image showing resolution of PCR products amplified from WT, *Trib2^+/-^* and *Trib2^-/-^* mice using primers listed in Appendix D: Table 1. M, marker; Neg ctrl, no template negative control; mut, mutant.
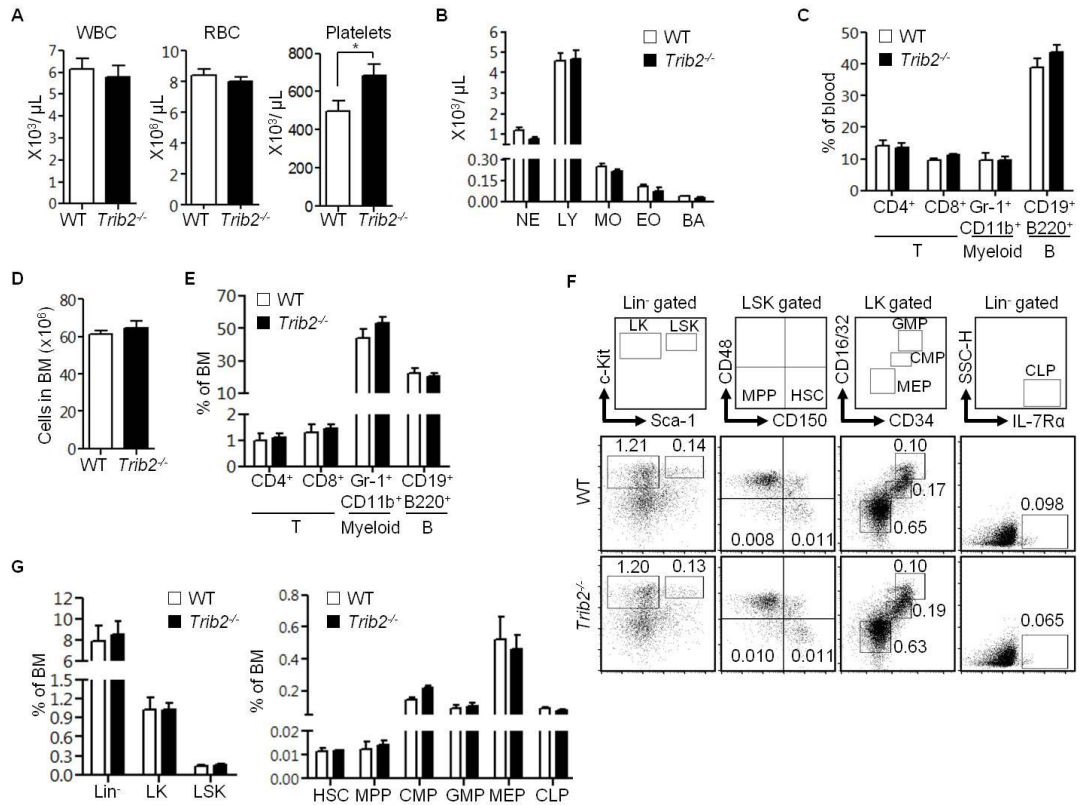
Figure 3.2 | TRIB2 loss does not affect murine haematopoiesis in BM.
Complete blood counts **(A)** and WBC differential counts **(B)** of WT (n = 13) and
$Trib2^{-/-}$ (n = 22) mice were determined by haematology analyzer. NE, neutrophils;
LY, lymphocytes; MO, monocytes; EO, eosinophils; BA, basophils. **(C)** The
distribution of mature myeloid, B and T cells in the blood of WT (n = 3) and $Trib2^{-/-}$
(n = 10) mice were measured by flow cytometry using the indicated lineage specific
cell surface markers. **(D)** BM cellularity (n=5-7 per genotype) was counted by trypan
blue exclusion after RBC lysis of the cell suspension harvested from two pelvises,
femurs and tibias. **(E)** The distribution of myeloid, B and circulating T cells in the BM
of WT (n = 3) and $Trib2^{-/-}$ (n = 9) mice. **(F)** Immunophenotyping of HSPCs
populations (HSC, MPP, CMP, GMP, MEP and CLP) in BM. Each sub-population is
indicated in the outlined areas (top row). The corresponding values in the
representative staining profile of WT (middle row) and $Trib2^{-/-}$ (bottom row) mice (n =
3 per genotype) are frequency of BM and graphed in **(G)**. Lin, lineage; LK, Lin⁻c-Kit⁺
cells; LSK, Lin⁻Sca-1⁺c-Kit⁺ cells; HSC: LSK CD150⁺CD48⁻; MPP: LSK CD150⁻
CD48⁻; CMP: LK CD34⁺CD16/32ˡᵒ; GMP: LK CD34⁺CD16/32ʰⁱ; MEP: LK CD34⁻
CD16/32⁻; CLP: Lin⁻IL-7Rα⁺; SSC-H, side scatter-height. For **A**, unpaired Student's
t-test was used for statistical analysis. *P<0.05, all quantified data are presented as
mean and SEM.

We next assessed the repopulating capability and multi lineage differentiation potential of *Trib2*$^{-/-}$ HSPCs by transplantation of CD45.2$^+$ whole BM nucleated cells (WT or *Trib2*$^{-/-}$ donor) into lethally irradiated CD45.1$^+$ mice (recipients). At 17 weeks post transplantation, recipients transplanted with cells from both genotypes had similar expression of donor marker, CD45.2 (Figure 3.3A). This indicates TRIB2 loss did not affect long-term engraftment of donor cells. In the absence of TRIB2, HSPCs retain their capability to fully reconstitute the blood system of recipients as the recipients had no measurable difference of RBC, platetet and WBC (total and differential) counts compared to the control group (Figure 3.3B and 3.3C). Analysis of blood collected periodically at 6, 10, 14 and 17 weeks post transplantation from recipients showed no skewing of differentiation into myeloid and lymphoid lineages in the absence of TRIB2 during hematopoietic reconstitution (Figure 3.3D). No significant difference was found in the HSPCs in recipients transplanted with either genotype (Figure 3.3E and 3.3F). We conclude that TRIB2 is dispensable for the maintenance of the hematopoietic system through differentiating HSPCs that reside in the BM.
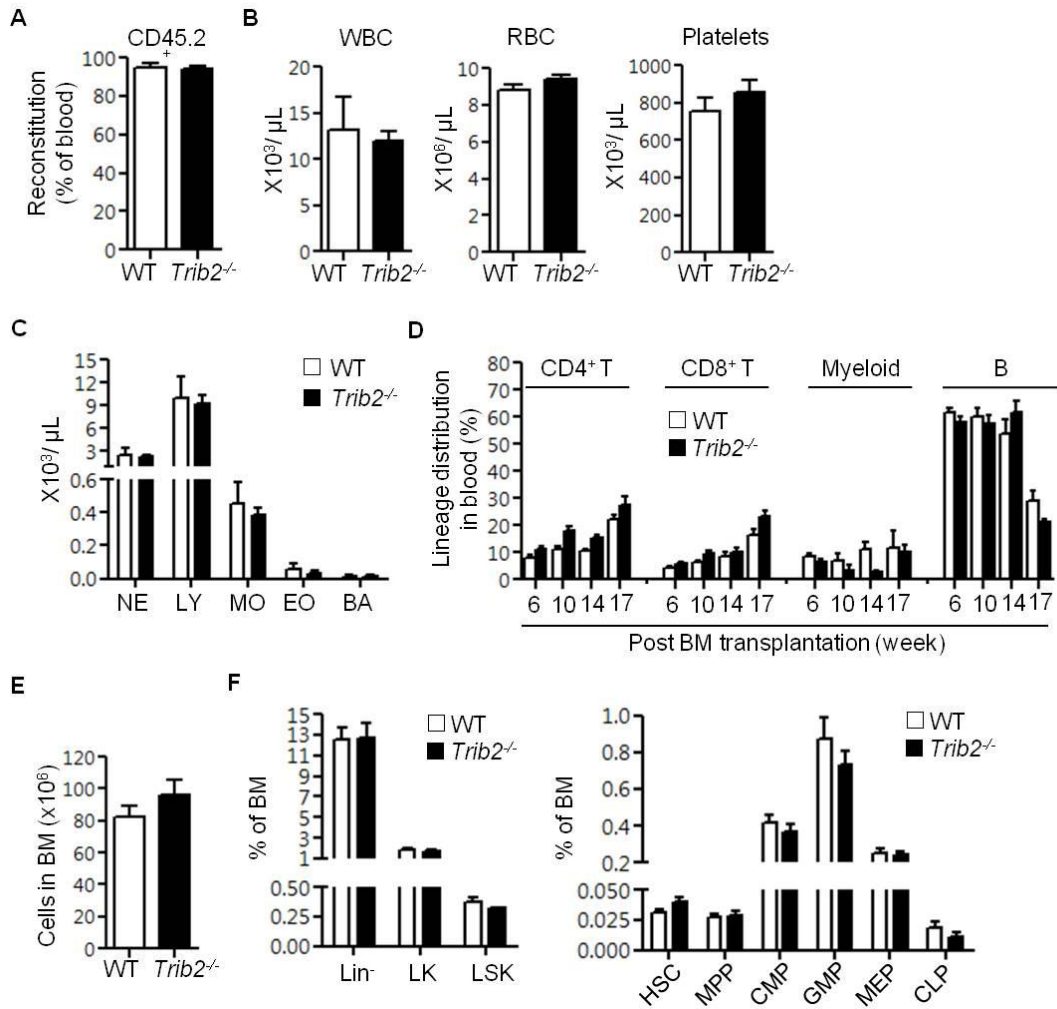
Figure 3.3 │ TRIB2 loss does not affect the repopulation capability of BM HSPCs. Lethally irradiated CD45.1[+] mice were transplanted with CD45.2[+] WT (*n* = 5) or *Trib2*^{-/-} (*n* = 5) whole BM cells, and sacrificed after 17 weeks of transplantation. **(A)** Engraftment of donor cells was determined by measurement of CD45.2 expression in the blood of transplanted mice. Complete blood counts **(B)** and WBC differential counts **(C)** of these two groups of mice were determined by hematology analyzer. NE, neutrophils; LY, lymphocytes; MO, monocytes; EO, eosinophils; BA, basophils. **(D)** The distribution of donor derived mature myeloid, B and T cells in the blood of these mice was measured by flow cytometry. **(E)** BM cellularity was counted by trypan blue exclusion. **(F)** Immunophenotyping and quantification of donor derived HSPCs in BM. All quantified data are presented as mean and SEM.

3.2.2 TRIB2 regulates the proliferation of developing thymocytes.

At steady state, we found that *Trib2^{-/-}* mice had statistically significant higher thymic cellularity compared to WT mice (Figure 3.4A). This suggests dysregulation of thymopoiesis in the absence of TRIB2. We further examined thymic subsets along the $\alpha\beta$ T lineage developmental pathway by immunophenotyping. Non-T lineage markers (CD11c, Gr-1, B220, Ter119 and NK1.1) were included in all the experimental analysis to exclude cells of other lineages present in thymus. Gating for lineage markers, including CD4 and CD8, were adjusted so as not to exclude c-Kit$^+$ thymic progenitors that express low cell surface levels of lineage markers when defining immature DN thymocytes (Bhandoola and Sambandam, 2006) (Figure 3.4B). For gating of thymic subsets, DN3 thymocytes (Lin^{lo}CD44$^-$CD25$^+$) were divided further into DN3$_E$ (expected: FSC^{lo}) and DN3$_L$ (larger: FSC^{hi}) subsets, based on cell size (Hoffman et al., 1996). This is equivalent to characterization of DN3 into DN3a and DN3b subsets, based on CD27 marker, that are corresponded to pre- and post β selection (Taghon et al., 2006). Similarly, DP thymocytes were divided further into DP$_{sm}$ (small resting: FSC^{lo}) and DP$_{bl}$ (blasts: FSC^{hi}) subsets (Mingueneau et al., 2013). To validate the thymic subsets identified by our gating strategy, we assessed their cell cycle profile and proliferation status by DNA staining and measurement of CD71 expression respectively. In accordance with previous studies (Hoffman et al., 1996, Seitan et al., 2011, Brekelmans et al., 1994), we found that WT DN3$_E$ and DP$_{sm}$ subsets were not proliferative as >99% were in G$_0$/G$_1$ phase and only 10-20% were CD71$^+$ (Figure 3.5A-C). In contrast, WT DN3$_L$ and DP$_{bl}$ subsets were actively cycling as 60-70% were in S-G$_2$/M phases and 90% were CD71$^+$ (Figure 3.5A-C). In comparison of WT and *Trib2^{-/-}* thymic subsets, no measurable difference was found in their cell cycle profile and expression of CD71 (Figure 3.5A-C).
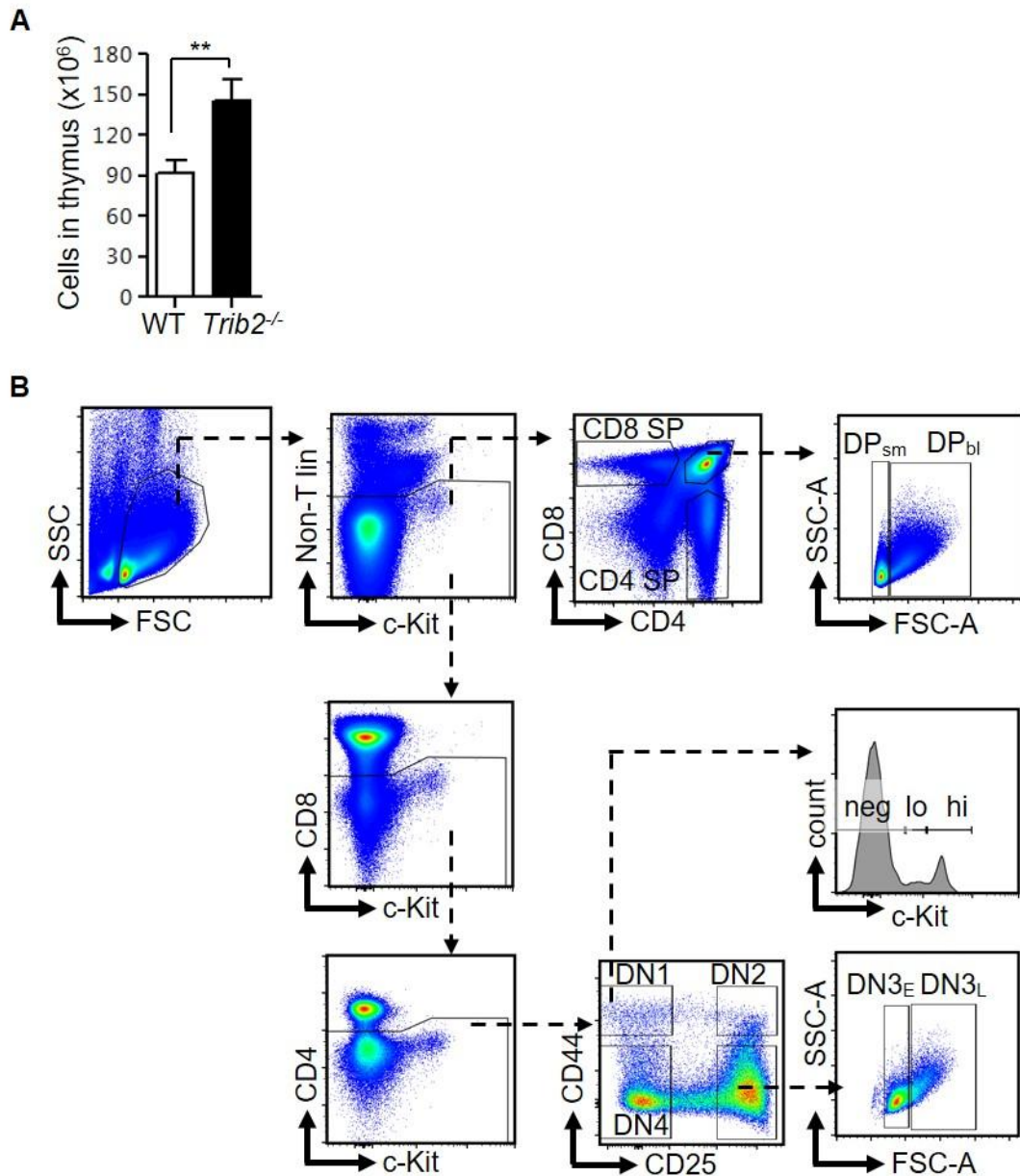
Figure 3.4 │ TRIB2 loss causes increased thymic cellularity. (A) Thymic cellularity of WT (n = 31) and *Trib2*$^{-/-}$ (n = 21) mice was counted by trypan blue exclusion after RBC lysis. **(B)** Gating strategy to identify thymic subsets. FSC-A, forward scatter-area; SSC-A, side scatter-area; DN1: Lin^{lo}CD44$^+$CD25$^-$; DN2: Lin^{lo}CD44$^+$CD25$^+$; DN3$_E$: Lin^{lo}CD44$^-$CD25$^+$FSC^{lo}; DN3$_L$: Lin^{lo}CD44$^-$CD25$^+$FSC^{hi}; DN4: Lin^{lo}CD44$^-$CD25$^-$; DP$_{bl}$: CD4$^+$CD8$^+$FSC^{hi}; DP$_{sm}$: CD4$^+$CD8$^+$FSC^{lo}; CD4 SP: CD4$^+$CD8$^-$; CD8 SP: CD4$^-$CD8$^+$. For statistical analyses, unpaired Student's t-test was used for **A**. $^{**}P$<0.01, all quantified data are presented as mean and SEM.

Figure 3.5 │ TRIB2 loss does not affect cell cycle phase progression and CD71 expression of thymocytes. Overlay of a representative cell cycle profile **(A)** of WT and *Trib2*^{-/-} thymic subsets and the fractions of cell cycle phases were graphed in **(B)**. Norm, normalized. **(C)** Quantification of CD71 expression of each thymic subset. For **A-C**, n = 3 per genotype. All quantified data are presented as mean and SEM.

We next analysed the impact of TRIB2 loss on the frequency and cellularity of each thymic subset despite no change in cell cycle progression with TRIB2 loss. At steady state, our analysis of the thymic subsets showed that, in general, *Trib2*^{-/-} mice had a lower frequency of immature DN1-4 subsets, but the mature DP and SP subsets were unaffected compared to WT mice (Figure 3.6A and 3.6B). The higher cellularity of *Trib2*^{-/-} thymus was due to the significant increase of mature subsets (DP$_{sm}$ and CD4 SP) but not the immature DN1-4 subsets (Figure 3.6C). The DN1 (Lin^{lo}CD44^{+}CD25^{-}) subset is heterogeneous and divided into DN1a-e subsets based on CD24 and c-Kit surface expression (Porritt et al., 2004). Here, the DN1 subset was divided broadly into c-Kit^{hi} (DN1a/b), c-Kit^{lo} (DN1c) and c-Kit^{-} (DN1d/e) subsets (Figure 3.6D). At steady state, *Trib2*^{-/-} c-Kit^{-} DN1 progenitors were present at a significantly lower frequency but had similar cell numbers compared to WT mice (Figure 3.6E and 3.6F). To rule out the possibility that lower frequency of *Trib2*^{-/-} of DN1-4 subsets were due to increased apoptosis, we measured Annexin V

expression and showed no difference between the two genotypes (Figure 3.6G). Since $Trib2^{-/-}$ mice had higher numbers of mature subsets which must be derived from immature subsets, we hypothesized that immature thymocytes were cycling faster and gave rise to more mature differentiated thymocytes in the absence of TRIB2. Ki-67 is a proliferation marker, expressed by cells in active cell cycle (G_1-S-G_2/M) but not by resting cells in G_0 (Byeon et al., 2005). Indeed, intracellular staining of Ki-67 showed $Trib2^{-/-}$ DN1, DN2 and $DN3_E$ subsets had significantly higher levels of Ki-67 compared to WT thymic subsets (Figure 3.6H), indicating more $Trib2^{-/-}$ developing thymocytes are in cycling state. This does not result in T cell accumulation outside the thymus however because there was no difference in the distribution of WT and $Trib2^{-/-}$ T-cells in the spleen (Figure 3.7). This is possible as TRIB2 loss could affect the later stages of T-cell development which we explain in the discussion. Satoh and colleagues also found that TRIB2 loss does not alter the populations of CD4$^+$ and CD8$^+$ splenic T-cells in a different $Trib2$ knockout mouse model ($Trib2^{tm1Myam}$) although they did not studied the thymus (Satoh et al., 2013).
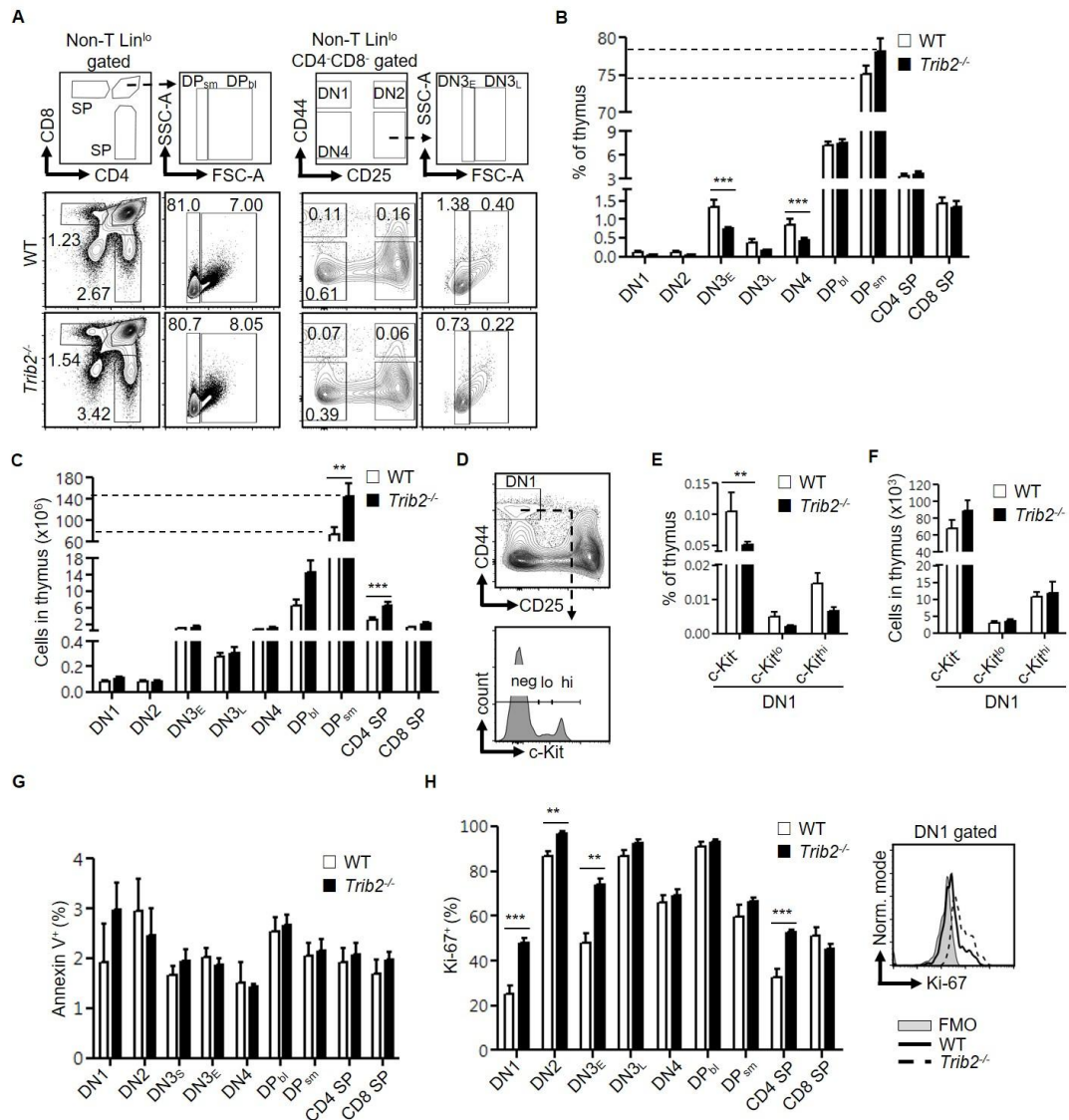
Figure 3.6 │ TRIB2 regulates the homeostasis of intrathymic T-cell development. (A) Flow cytometry of thymic subsets. The complete gating strategy is provided in Fig. 4. Each subset is indicated in the outlined areas (top row). The corresponded values in the representative staining profile of WT (middle row) and *Trib2⁻/⁻* (bottom row) mice are frequency of thymus and graphed in **(B)**. FSC-A, forward scatter-area; SSC-A, side scatter-area; DN1: $Lin^{lo}CD44^{+}CD25^{-}$; DN2: $Lin^{lo}CD44^{+}CD25^{+}$; DN3$_E$: $Lin^{lo}CD44^{-}CD25^{+}FSC^{lo}$; DN3$_L$: $Lin^{lo}CD44^{-}CD25^{+}FSC^{hi}$; DN4: $Lin^{lo}CD44^{-}CD25^{-}$; DP$_{bl}$: $CD4^{+}CD8^{+}FSC^{hi}$; DP$_{sm}$: $CD4^{+}CD8^{+}FSC^{lo}$; CD4 SP: $CD4^{+}CD8^{-}$; CD8 SP: $CD4^{-}CD8^{+}$. **(C)** Number of cells for each subset. **(D)** Further characterization of DN1 cells based on c-Kit surface expression. Neg, negative; lo, low; hi, high. DN1 subsets were graphed in frequency of thymus **(E)** and cell number **(F)**. For **B**, **C**, **E** and **F**, $n = 7$-8 per genotype. **(G)** Basal level of apoptosis of each thymic subset ($n = 3$ per genotype) was determined by the surface expression of Annexin V after exclusion of DAPI-stained dead cells. **(H)** Intracellular level of Ki-67 across thymic subsets ($n = 4$-5 per genotype) was measured by flow cytometry (left). An overlap of histogram (right) showed *Trib2⁻/⁻* DN1 cells had higher level of Ki-67 compared to that of WT. Norm, normalized; FMO, Fluorescence Minus One. For statistical analyses, unpaired Student's t-test was used for **H**, and two-way ANOVA was used for **B**, **C** and **E**. $^{**}P<0.01$; $^{***}P<0.001$, all quantified data are presented as mean and SEM.
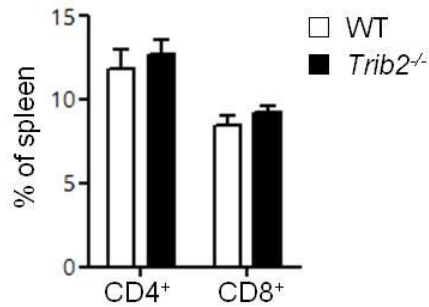
Figure 3.7 │ TRIB2 loss does not affect the distribution of splenic T cells.
Distribution of CD4^{+} and CD8^{+} T cells in the spleen of WT ($n = 4$) and $Trib2^{-/-}$ ($n = 5$) mice at steady state. All quantified data are presented as mean and SEM.

Cell cycle regulation is crucial for proper T cell development. DN3 thymocytes must be briefly arrested ($DN3_E$) at the G_0/G_1 cell cycle phases to allow V(D)J recombination to take place at the *Tcrb* locus, initiated by the RAG proteins (Li et al., 1996, Lin and Desiderio, 1994). Functional *Tcrb* rearrangements lead to formation of pre-TCR where the signals drive the subsequent development of thymocytes to early DP stage. Given that $Trib2^{-/-}$ developing thymocytes proliferate faster, we determined if loss of TRIB2 affects the cell cycle status of these subsets and *Tcrb* rearrangements. DNA staining showed $Trib2^{-/-}$ thymocytes at each stage of the T-cell development had a similar cell cycle profile compared to WT mice (Figure 3.5A and 3.5B). This suggests TRIB2 does not regulate the cell cycle phase progression and that the increased cycling of $Trib2^{-/-}$ developing thymocytes is likely due to changes in cell division kinetics at the steady state. Importantly, $Trib2^{-/-}$ $DN3_E$ thymocytes were arrested at G_0/G_1 phases like WT $DN3_E$ thymocytes. As such, analysis of *Tcrb* rearrangement involving the Jβ2.1 to Jβ2.7 gene segments demonstrated that $Trib2^{-/-}$ thymocytes contain polyclonal *Tcrb* rearrangements similar to WT thymocytes (Figure 3.8). This indicates that proper *Tcrb* rearrangements take place and TRIB2 loss doesn't affect β-selection, a key checkpoint of early T-cell development.
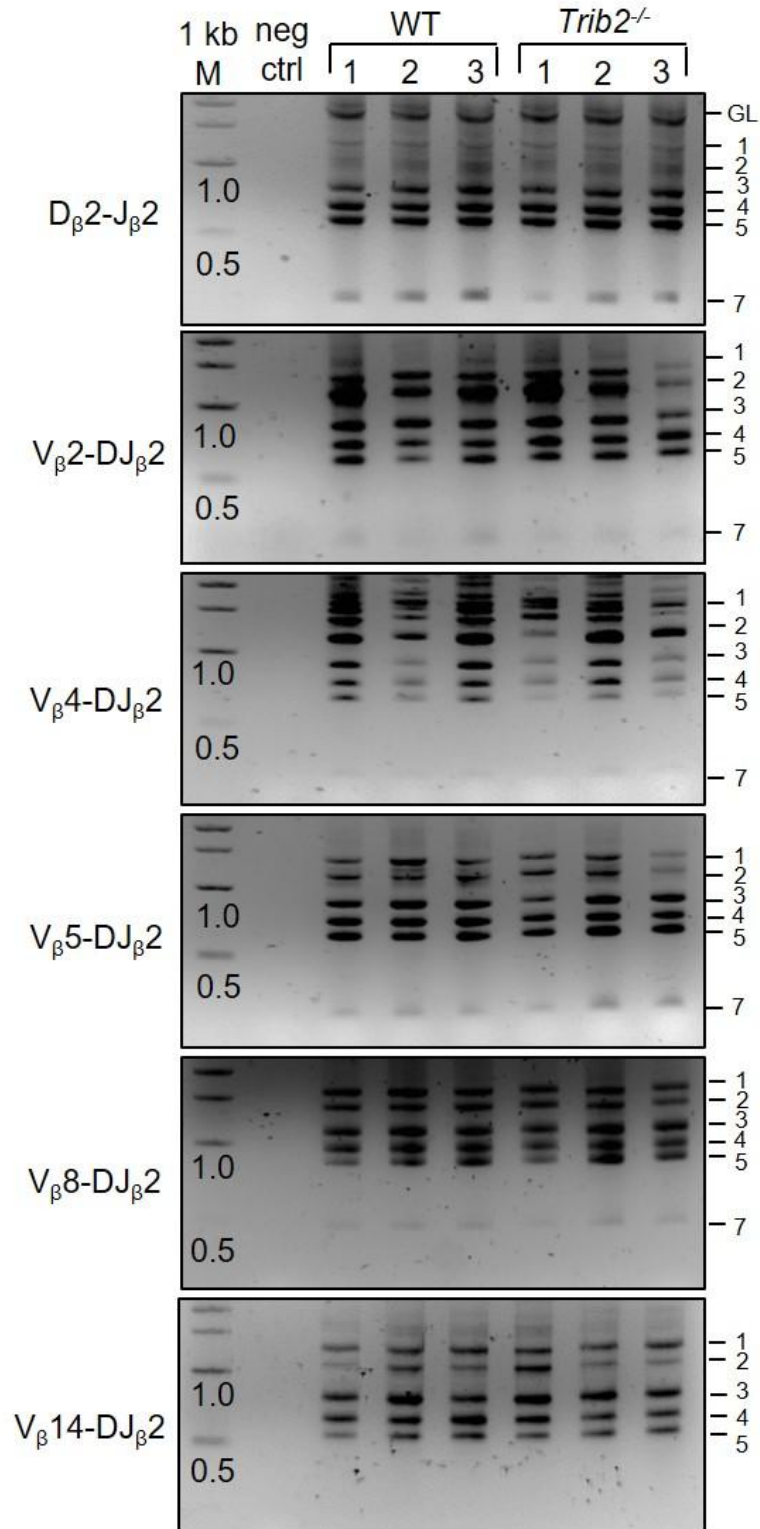
Figure 3.8 │ Polyclonal *Tcrb* rearrangements in *Trib2*^{-/-} thymocytes. Endogenous *Tcrb* rearrangements of WT and *Trib2*^{-/-} total thymocytes were analyzed by genomic DNA PCR. GL denotes the position of the germline PCR product and number indicates the different rearrangements involving the $J_\beta 2.1$ to $J_\beta 2.7$ gene segments. 1 kb M, 1 kb DNA marker; neg ctrl, no template negative control.

3.3 Discussion

Here, we show TRIB2 as the first member of the mammalian Tribbles family to play an anti-proliferative role in the context of developing thymocytes during T cell development. TRIB1 was reported previously to negatively regulate proliferation of human aortic smooth muscle cells *in vitro* via interaction with MAPK kinase 4 (MKK4) (Sung et al., 2007). TRIB2 regulates cell division kinetics of developing thymocytes. We found that the dysregulated proliferation of $Trib2^{-/-}$ developing thymocytes does not affect *Tcrb* rearrangement, a key event in early T cell differentiation. Furthermore, loss of TRIB2 did not affect terminal maturation of developing thymocytes. Intriguingly, the increased proliferation of developing thymocytes, in the absence of TRIB2, does not affect the percentage of peripheral T cells. Previous literature has showed that mice overexpressing CD69 have increased thymic SP subsets but a reduction in the number of T cells in the peripheral lymphoid organs (Nakayama et al., 2002). Our data suggests that TRIB2 may impact on thymic selection (DPsm to CD69$^+$ DP transition) or thymic T cell export. It is also likely that TRIB2 has a distinct role in mature T cell biology and function because *Trib2* expression distinguishes CD4$^+$ from CD8$^+$ peripheral T cells (Mingueneau et al., 2013). This could be further explored using appropriate infection and immunization models.

Previous literature suggests a role of TRIB2 in the development of megakaryocyte/erythroid lineage (Mancini et al., 2012). We did not detect any difference in the frequency of MEP populations in the BM but we found a significant increase of platelets (but not RBC counts) in the blood in the absence of TRIB2. Hence, the increase of platelets could have arisen from another source. Recent studies showed that platelets could be derived directly from stem cell-like megakaryocyte progenitors within the HSC compartment (Yamamoto et al., 2013,

Haas et al., 2015). Hence, our study did not rule of the role of TRIB2 in the development of platelets and characterization should be focused on the upper primitive populations that commit to megakaryocyte lineage.

Analysis of haematopoietic system at steady state allowed us to establish a role for TRIB2 in negatively regulating the proliferation of developing thymocytes. In the absence of TRIB2, more immature thymocytes are in the active cycling state. However, the thymic phenotype we found in *Trib2*^{-/-} mouse at steady state appears to be modest and have little impact on the development of peripheral T-cells in the blood as well as in the spleen. We speculate that TRIB2 function is more critical in perturbed T-cell development where the cellular proliferation is a key determinant of developing thymocyte response to stress inflicted on the thymopoietic system.

CHAPTER FOUR: EXAMINATION OF THE ROLE OF TRIB2 IN
5-FU INDUCED STRESSED HAEMATOPOIESIS

4.1 Introduction

5-FU is a standard chemotherapeutic drug widely used to treat cancers since it targets rapidly cycling cells. Misincorporation of 5-FU metabolite into DNA during DNA replication initiates futile cycles of DNA excision, repair, and further misincorporation that eventually lead to DNA strand breaks and cell death (Longley et al., 2003). Due to its mechanism of action, 5-FU has been widely used experimentally as a BM haematopoietic stress inducer. In this context, 5-FU targets cycling haematopoietic cells and this depletes the supply of mature blood cells. Hence, 5-FU treatment creates a proliferative stress to HSCs which are relatively quiescent at steady state to enter cell cycle, undergo extensive self renewal and differentiation to meet increased haematopoietic demands (Randall and Weissman, 1997, Wilson et al., 2008, Harrison and Lerner, 1991). Hence, application of 5-FU in research not only allows study of the acute response of haematopoietic system to a genotoxic agent but also the dynamic cellular changes that occur from steady state to stressed BM haematopoiesis during recovery. Importantly, proliferative stress inflicted on HSCs by 5-FU is a universal feature in stressed haematopoiesis which can be caused by other conditions such ageing and irradiation (Section 1.6). Beerman and colleagues showed that induced proliferation of HSCs by repeated exposure to 5-FU leads to functional decline and DNA methylation changes that closely mimic physiological HSC aging observed in old (25 months old) mice (Beerman et al., 2013). Hence, 5-FU appears to be a useful experimental tool to model stressed BM haematopoiesis and to study haematopoietic regeneration.

Clinically, 5-FU chemotherapy affects BM haematopoiesis and also disrupts T cell development in the thymus, depletes T cell repertoire, and impairs T cell immunity of patients. At steady state, human T cell repertoire is established during early childhood (Spits, 2002). Hence, thymopoietic recovery is critical to replenish the T cell repertoire in order to reconstitute cellular immunity of patients. However, unlike stressed BM haematopoiesis which has been studied and characterized in depth (Brenet et al., 2013), thymopoietic restoration following experimental 5-FU mediated thymic injury is poorly understood. Previous studies focused on the acute response of thymus to 5-FU treatment and were limited to morphological and biochemical descriptions (Eichhorst et al., 2001, Aquino Esperanza et al., 2008). Treatments are available to counteract the clinical 5-FU induced myelosuppresion such as blood and platelet transfusions, and injection of granulocyte colony-stimulating growth factors to promote granulocytic regeneration. However, no clinical therapy is available yet to improve thymopoietic recovery in order to restore cellular immunity of patients (Awong et al., 2010).

In the previous chapter, we showed that ablation of *Trib2* does not affect steady state haematopoiesis in the BM. However, TRIB2 appears to regulate the proliferation of developing thymocytes and hence thymopoietic homeostasis. On account of the mechanism of 5-FU action, it was of primary interest in this chapter to use 5-FU as an experimental tool to test our hypothesis that $Trib2^{-/-}$ developing thymocytes which are highly proliferative would be more sensitive to 5-FU compared to WT thymocytes. As 5-FU is a haematopoietic stress inducer in the BM and thymopoiesis in the thymus, we also aimed to examine if TRIB2 plays a role in the regeneration of these two biologic systems following genotoxic insult mediated by 5-FU.

4.2 Results

4.2.1 *Trib2^{-/-}* thymocytes are hypersensitive to 5-FU induced cell death.

To address our hypothesis, we performed a time course study of *in vivo* 5-FU treatment. *Trib2$^{-/-}$* mice had significantly higher total thymic cellularity at steady state (Figure 3.6), however this significant difference was lost at 16 and 24 hours post treatment (Figure 4.1A). Significant increase of cell death (late apoptotic) was found in *Trib2$^{-/-}$* thymic cells at 24 hours post treatment (Figure 4.1B and 4.1C). Notably, we demonstrated that $DN3_L$ and DP_{bl} subsets, which are known to be proliferative (Figure 3.5), were significantly reduced in *Trib2$^{-/-}$* mice 16 hours post treatment. $DN3_E$ and DP_{sm} subsets which are in resting state were unaffected in treated WT and *Trib2$^{-/-}$* mice. Unexpectedly, *Trib2$^{-/-}$* c-Kit^{hi} DN1 thymic progenitors were also significantly reduced after 16 hours of exposure to 5-FU whereas *Trib2$^{-/-}$* c-Kit^{-} and c-Kit^{lo} DN1 progenitors were unaffected like WT mice (Figure 4.1D and 4.1E). c-Kit^{hi} DN1 progenitors were shown previously to exclusively exhibit a proliferative burst capacity by OP9-DL1 co-culture system compared to c-Kit^{-} and c-Kit^{lo} DN1 progenitors (Porritt et al., 2004). Interestingly, 5-FU was shown recently to preferentially induce apoptosis in c-Kit^{hi} HSCs that have rapid cell division kinetics compared to c-Kit^{lo} HSCs *in vitro* (Shin et al., 2014). Overall, these data showed that the thymic subsets that are most sensitive to apoptosis following 5-FU treatment are the subsets with increased cycling kinetics due to loss of TRIB2. This confirmed a role for TRIB2 in controlling the cell division kinetics of thymocytes and hence their enhanced sensitivity to 5-FU genotoxic drug.
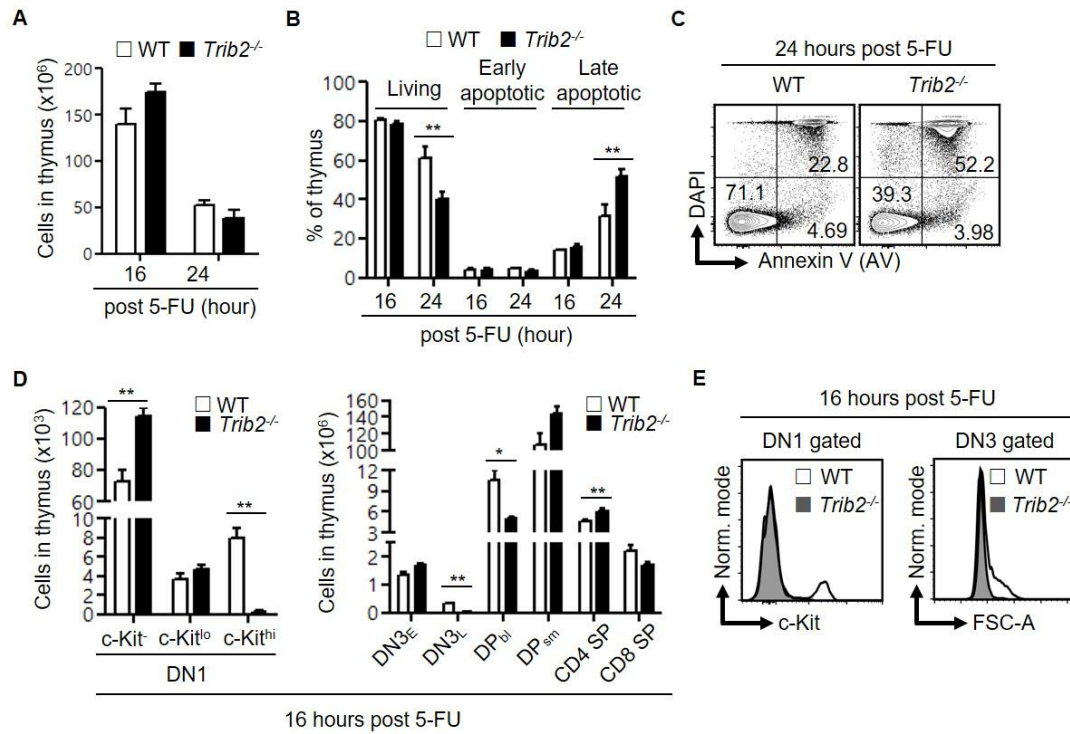
Figure 4.1 │ *Trib2⁻ᐟ⁻* thymocytes are more susceptible to 5-FU induced cell death. (A) Mice were treated with 5-FU (250 mg/kg, i.p.) and sacrificed after 16 and 24 hours to determine the thymic cellularity. **(B)** Apoptosis assays were performed to determine the fraction of living, early and late apoptotic cells in thymus at 16 and 24 hours post treatment. **(C)** A representative staining profile **(B)** of 5-FU treated WT and *Trib2⁻ᐟ⁻* thymus. Living: DAPI⁻AV⁻; early apoptotic: DAPI⁻AV⁺; late apoptotic: DAPI⁺AV⁺. The values indicated in the outlined areas are frequency of thymus. **(D)** The cellularity of thymic subsets at 16 hours post treatment. **(E)** Overlay of the histograms of DN1 and DN3 cells for c-Kit expression and FSC-A signals respectively showed loss of *Trib2⁻ᐟ⁻* DN1 c-Kit⁺ and DN3$_L$ cells at 16 hours post treatment. For **A,B** and **D**, *n* = 5 per genotype per studied time point. For statistical analyses, unpaired Student's t-test was used for **A**, and two-way ANOVA was used for **B** and **D**. $^*P<0.05$; $^{**}P<0.01$, all quantified data are presented as mean and SEM.

4.2.2 Acceleration of thymopoietic recovery in the absence of TRIB2 after genotoxic insult.

Previous studies on the response of thymus organ and thymocytes to 5-FU mediated genotoxic insult have showed that 5-FU induces apoptosis of thymocytes, thymic weight loss and damages to thymic architecture which are crucial for T-cell development (Aquino Esperanza et al., 2008, Anderson and Takahama, 2012). Thymic inner architecture exhibited morphological recovery on day 7 and was back to normal on day 10 post 5-FU injury in previously published data (Aquino Esperanza et al., 2008). We compared thymopoietic recovery of WT and $Trib2^{-/-}$ mice 4 and 14 days after a single dose of 5-FU administration. $Trib2^{-/-}$ mice had higher thymic cellularity compared to WT mice at 4 and 14 days post treatment and the thymus was relatively bigger 14 days post treatment (Figure 4.2A and 4.2B), despite the observed earlier increase in apoptosis (Figure 4.1B and 4.1C). Importantly, the higher cell count was due to increase of T cells, natural killer cells and dendritic cells but not myeloid and B cells which do not normally develop in thymus (Figure 4.2C and 4.2D). Although WT and $Trib2^{-/-}$ mice both had the hierarchy of thymic subsets restored to normal at day 14 compared to day 4 post 5-FU treatment (Figure 4.3), $Trib2^{-/-}$ mice had significantly higher numbers of DN1 progenitors and the subsequent mature subsets at day 14 post 5-FU treatment (Figure 4.2D). This indicates that $Trib2^{-/-}$ mice had accelerated thymopoietic recovery. At steady state, thymopoiesis is sustained mainly by c-Kit^{hi} DN1 progenitors (Benz et al., 2008). However, these progenitors were absent in WT and $Trib2^{-/-}$ thymus from day 1 to day 14 post 5-FU treatment (Figure 4.2F). Instead, we found a significant increase of c-Kit^{-} DN1 progenitors in $Trib2^{-/-}$ thymus suggesting expansion of these progenitors drives the accelerated recovery (Figure 4.2E).
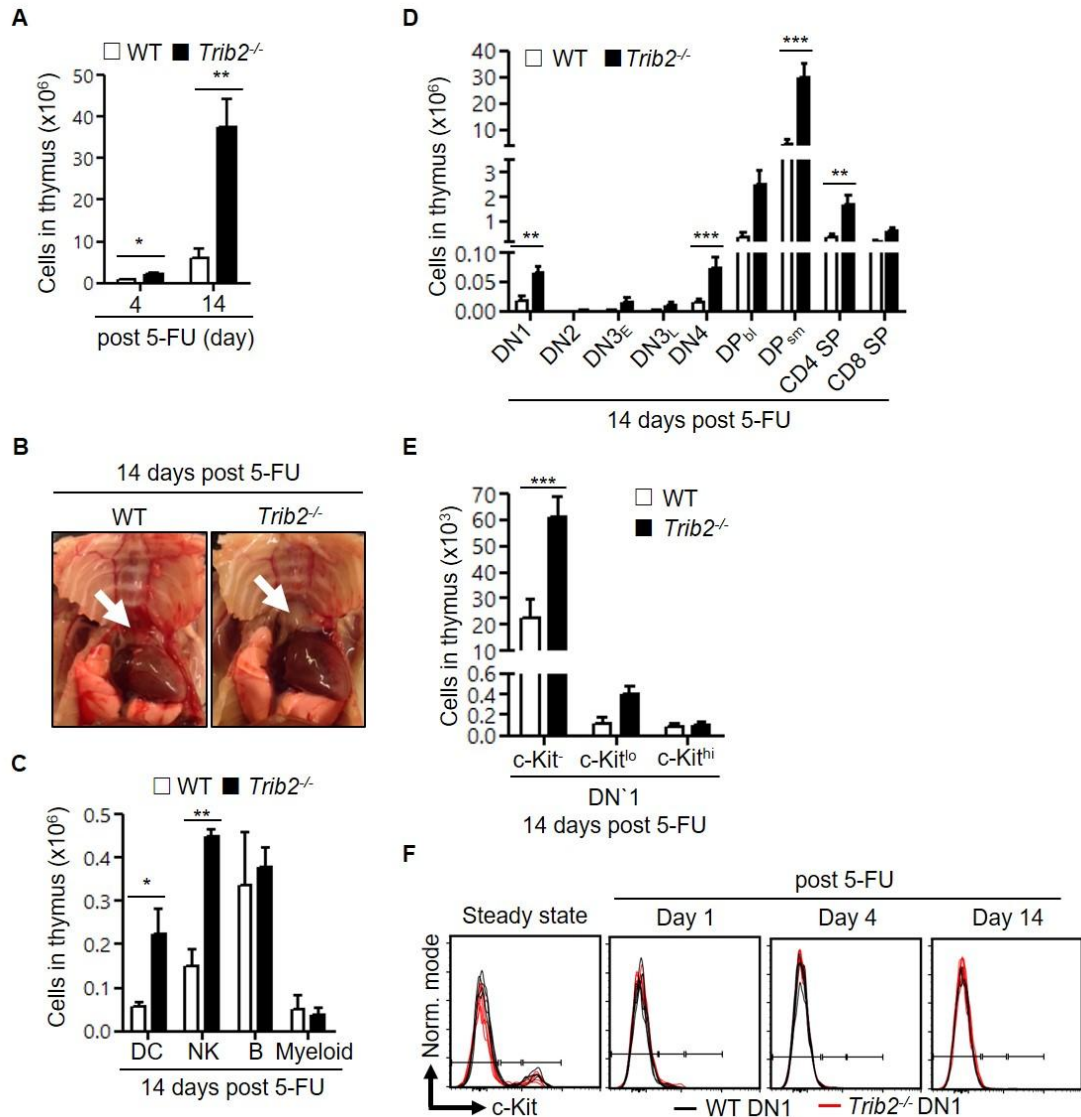
Figure 4.2 | Expansion of c-Kit⁻ DN1 progenitors, in the absence of TRIB2, drives the accelerated thymopoietic recovery after genotoxic stress. (A) Thymic cellularity of mice after 4 and 14 days of 5-FU treatment. **(B)** The white arrow indicates representative thymus of the dissected WT and *Trib2⁻/⁻* mice. **(C)** The cellularity of non-T lineage cells (DC: $CD11c^+$; NK cells: $Nk1.1^+$; B: $CD19^+B220^+$; Myeloid: $Gr-1^+CD11b^+$) in thymus (n = 3 per genotype) were determined by flow cytometry. Cellularity for thymic subsets **(D)** and DN1 subsets **(E)**. **(F)** c-Kit expression of WT and *Trib2⁻/⁻* DN1 thymocytes at steady state (n = 7-8 per genotype) and after 5-FU treatment (n = 4-6 per genotype per studied time point) were shown in overlaid histograms. For **A,D** and **E**, n = 9 per genotype per studied time point. 5-FU dosage for **A-F** was 250 mg/kg. For statistical analyses, unpaired Student's t-test was used for **A**, and two-way ANOVA was used for **C**, **D** and **E**. *P<0.05; **P<0.01; ***P<0.001, all quantified data are presented as mean and SEM.
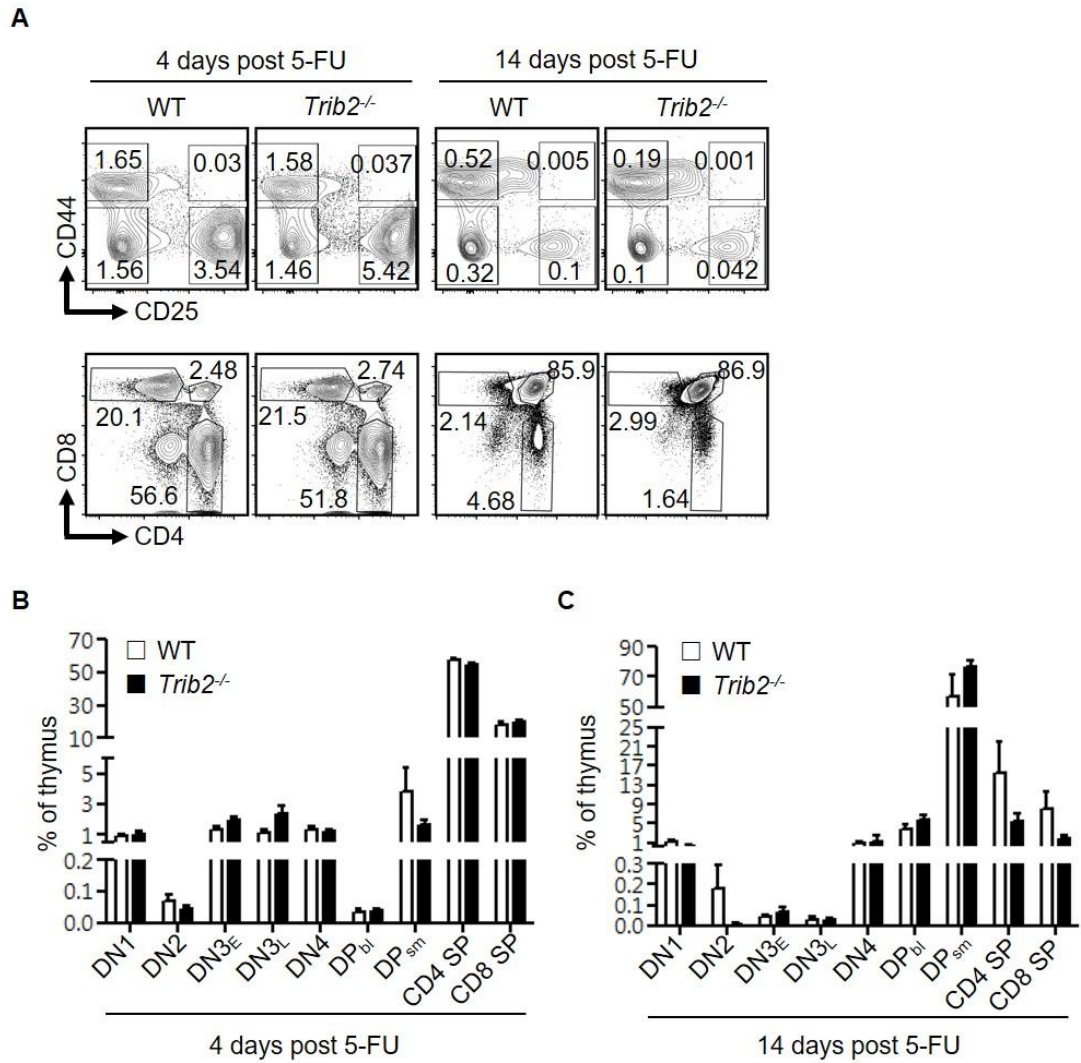
Figure 4.3 │ Hierarchical organization of thymopoietic system restored to normal at 14 days after genotoxic insult. (A) A representative staining profile of WT and *Trib2⁻/⁻* thymus (*n* = 9 per genotype per studied time point) after 4 and 14 days of 5-FU treatment (250 mg/kg, i.p.) were shown here. The values indicated in the outlined areas are frequency of each thymic subset, and graphed in **(B)** and **(C)**. All quantified data are presented as mean and SEM.

We postulated that the acceleration of thymopoietic recovery in the absence of TRIB2 is due to the intrinsic highly proliferative nature of $Trib2^{-/-}$ thymocytes. In developing thymocytes, proliferation and differentiation are tightly linked. Analysis of $Tcrb$ rearrangements for the joining of Dβ2 to Jβ2 gene segments showed less immature thymocytes that haven't undergo $Tcrb$ rearrangements (Germline (GL) band) present in $Trib2^{-/-}$ thymus compared to WT thymus 14 days post 5-FU treatment (Figure 4.4A). Importantly, we showed in the previous chapter that, at steady state, there is no difference in the GL band for the $Tcrb$ rearrangement analysis between WT and $Trib2^{-/-}$ total thymoctes (Figure 3.8). Hence, the 5-FU induced stress exacerbated the impact of loss of TRIB2 function in regulation of thymocyte proliferation. This supports our finding that thymopoiesis was more active in treated $Trib2^{-/-}$ mice. We further assessed the quiescent state of DN thymocytes through dual staining of DNA and Ki-67. Compared to WT DN thymocytes, significantly less $Trib2^{-/-}$ thymocytes in DN1 and DN4 subsets were resting (G_0) and correspondingly more $Trib2^{-/-}$ thymocytes in these subsets were in cycling state (G_1-S/G_2-M) following 5-FU treatment at day 14 (Figure 4.4B and 4.4C). This indicates TRIB2 regulates the cell cycle entry of thymocytes. To expand beyond a static assessment of proliferation, we did time course experiments of in $vivo$ BrdU pulsing in WT and $Trib2^{-/-}$ mice. DN3 thymocytes of both genotypes had similar uptake of BrdU after 1 hour of pulsing, however BrdU$^+$ $Trib2^{-/-}$ DN3 thymocytes were significantly increased after 4 hours of pulsing (Figure 4.4D and 4.4E). This demonstrated that $Trib2^{-/-}$ developing thymocytes had higher cell division kinetics and more DN3 thymocytes were available to uptake BrdU while replicating their DNA.
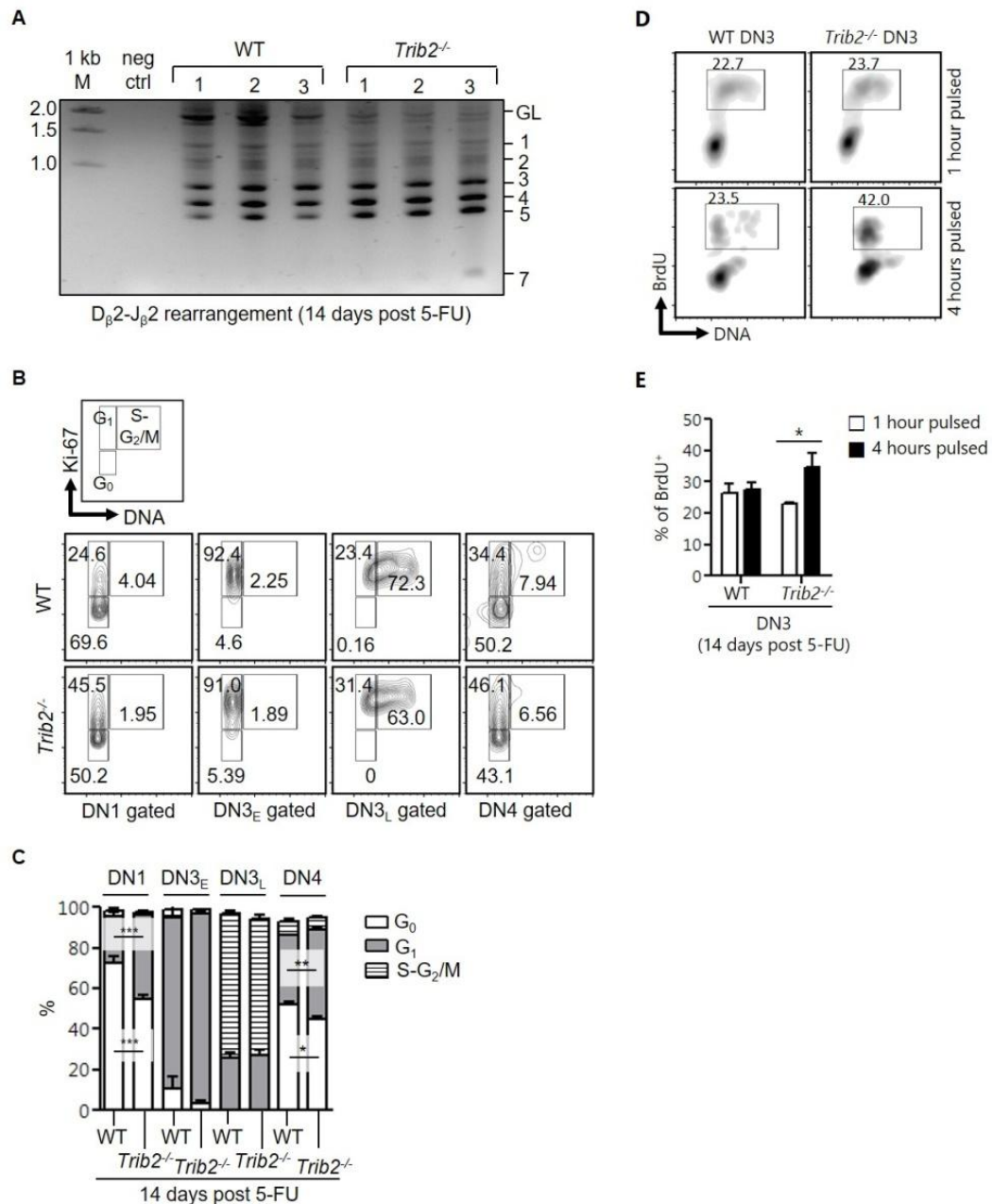
Figure 4.4 │ Higher cell division kinetics of *Trib2-/-* developing thymocytes accelerates the thymopoietic recovery after genotoxic stress. (A) PCR analysis (*n* = 3 per genotype) of *Tcrb* rearrangement involving the $D_\beta 2$ to $J_\beta 2$ gene segments. GL denotes the position of the germline PCR product and number indicates the different rearrangements. 1 kb M, 1 kb DNA marker; neg ctrl, no template negative control. **(B)** Flow cytometry to determine the fraction of developing thymocytes in resting (G_0) and active (G_1-S/G_2/M) cell cycle. Each phase is indicated in the outlined areas (top row). The corresponding values in the representative staining profile of WT (middle row) and *Trib2-/-* (bottom row) mice (*n* = 2-3 per genotype) are frequency of each phase and graphed in **(C)**. **(D)** The frequency of BrdU uptake by DN3 thymocytes after 1 and 4 hours of pulsing. A representative staining profile of WT and *Trib2-/-* mice (*n* = 3 per genotype per studied time point) is shown here. The values indicated in the outlined areas are the frequencies of BrdU+ DN3 thymocytes and graphed in **(E)**. 5-FU dosage for **A-E** was 200 mg/kg. For statistical analyses,

111

two-way ANOVA was used for **C** and **E**. $^{*}P<0.05$; $^{**}P<0.01$; $^{***}P<0.001$, all quantified data are presented as mean and SEM.

It is noteworthy that TRIB2 loss only affected thymopoietic recovery but not hematopoietic regeneration in BM following 5-FU induced genotoxic stress. On day 14 post 5-FU treatment, blood cell counts of WT and $Trib2^{-/-}$ mice were restored to normal with no measurable differences detected (Figure 4.5A and 4.5B). However, more CD4^{+} and CD8^{+} T cells were present in the blood of $Trib2^{-/-}$ mice though these were not statistically significant (Figure 4.5C). Both genotypes had similar BM cellularity and HSPC populations including CLPs that are lymphoid restricted progenitors (Kondo et al., 1997) (Figure 4D-F). Hence, our immunophenotyping analyses showed that haematopoietic regeneration in BM is not impeded in the absence of TRIB2. Nevertheless, we did not investigate if TRIB2 loss affects the functionality of the reconstituted HSPC populations. Our finding was confirmed in another experiment where we examined the long-term (9 weeks) restoration of haematopoietic homeostasis following 5-FU treatment (Figure 4.6). Similar to what we found at 14 days post treatment, no measurable differences detected in blood cell counts (Figure 4.6A), BM cellularity (Figure 4.6C) and HSPC populations (Figure 4.6D) of the treated WT and $Trib2^{-/-}$ mice. However, the $Trib2^{-/-}$ mice had significantly higher number of CD4 SP subset (Figure 4.6F). This was in accordance with $Trib2^{-/-}$ mice have increased number of mature thymocyte subsets at steady state (Figure 3.6).
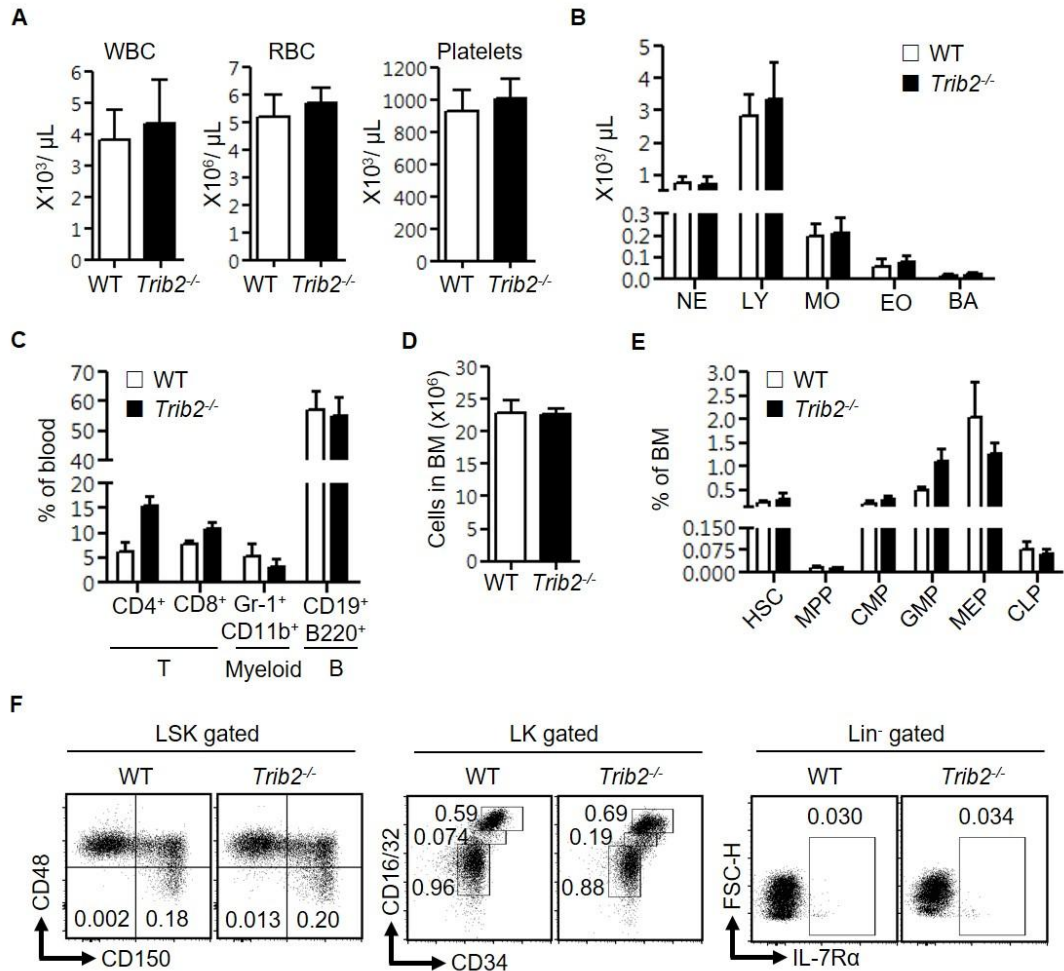
Figure 4.5 │ TRIB2 loss does not affect the recovery of haematopoietic system after 5-FU genotoxic insult. Mice were sacrificed for analysis after 14 days of 5-FU treatment (250 mg/kg, i.p.). Complete blood counts **(A)** and WBC differential counts **(B)** of treated WT and *Trib2$^{-/-}$* mice (*n* = 8-9 per genotype) were determined by haematology analyzer. **(C)** The distribution of mature myeloid, B and T cells in the blood of treated WT and *Trib2$^{-/-}$* mice (*n* = 4-5 per genotype) were measured by flow cytometry. **(D)** BM cellularity was counted by trypan blue exclusion after RBC lysis of the cell suspension harvested from two pelvises, femurs and tibias. **(E)** Distribution of HSPC populations in BM of treated WT and *Trib2$^{-/-}$* mice. **(F)** A representative staining profile of the HSPC populations measured in WT and *Trib2$^{-/-}$* mice is shown here. For **D-F**, *n* = 3 per genotype. All quantified data are presented as mean and SEM.
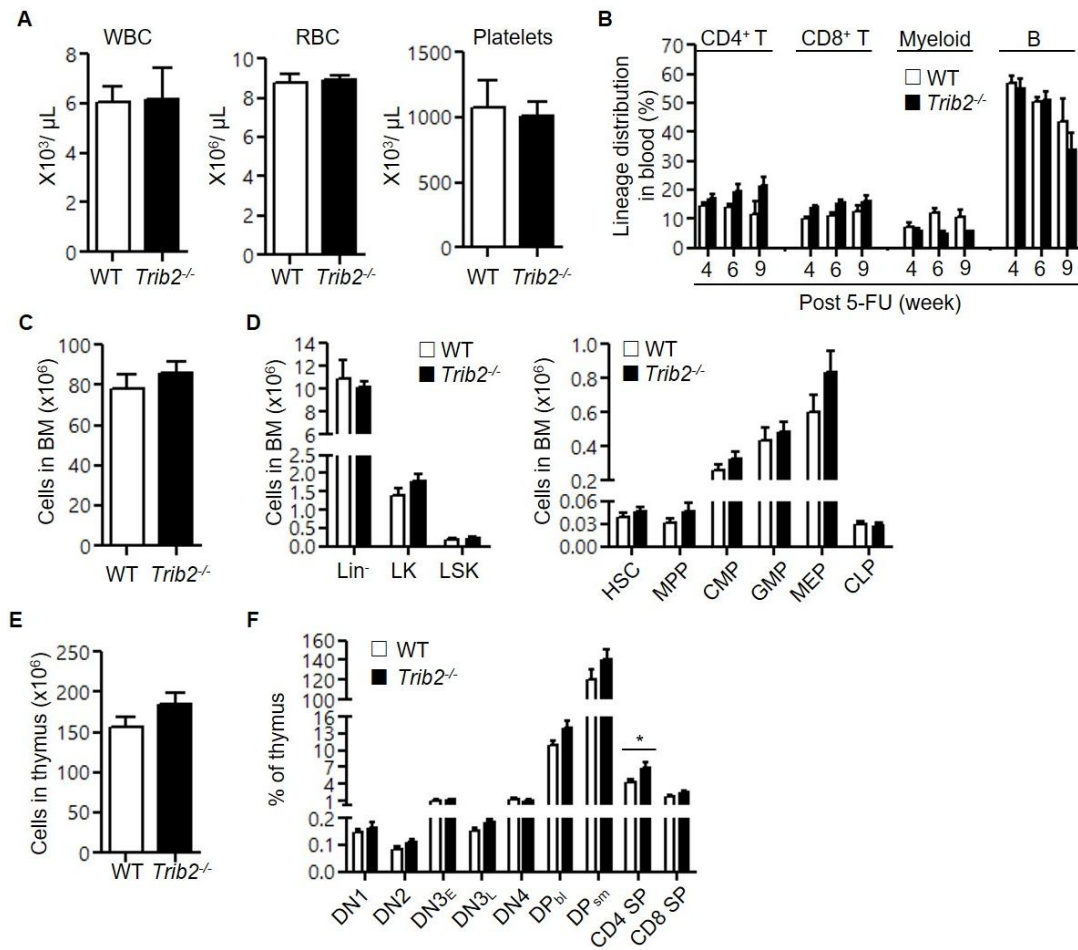
Figure 4.6 │ TRIB2 loss does not affect the restoration of haematopoietic homeostasis after 5-FU genotoxic insult. WT and *Trib2*^{-/-} mice (*n* = 4-5 per genotype) were sacrificed at 9 weeks post 5-FU treatment (150 mg/kg, i.p.). Complete blood counts **(A)** and lineage distribution of blood cells **(B)** were measured by haematology analyzer and flow cytometry respectively. Cellularity of BM **(C)** and thymus **(E)** was determined by trypan blue exclusion after RBC lysis of the cell suspension. Immunophenotyping and quantification of HSPCs residing in the BM **(D)** and thymus subsets **(F)**. For statistical analyses, two-way ANOVA was used for **A**. *$P<0.05$, all quantified data are presented as mean and SEM.

4.2.3 A single case of partial block in T-cell developmental in the absence of TRIB2 during thymopoietic recovery.

While studying the impact of TRIB2 loss on thymopoietic recovery following 5-FU treatment at day 14, a *Trib2*^{-/-} mouse (#381) treated with 5-FU showed abnormal thymic cellular phenotypes. Hence, analysis of this mouse was interpreted and presented separately. #381 had more than 2 fold increase of thymic cellularity compared to the other 5-FU treated *Trib2*^{-/-} mice (Figure 4.7A) indicating an exaggerated rate of thympoietic recovery in the absence of TRIB2. However, unlike the treated WT and the other *Trib2*^{-/-} mice, #381 had a partial block in T-cell developmental at the DP stage because subsequent mature CD4 and CD8 SP subsets were detected but their frequency in the thymus was much lower (Figure 4.7B bottom row). The DP population of #381 had varying expression levels of CD4 and CD8 compared to the other treated WT and *Trib2*^{-/-} mice (Figure 4.7B bottom row). Hence, direct comparison of the frequency of DP subset with the same gating was not possible. The absolute number of CD4 and CD8 SP subsets did not increased proportionally although #381 had a much higher thymic cellularity compared to the other treated *Trib2*^{-/-} mice (Figure 4.7C). Cytospin of #381 thymic cells followed by Romanosky staining also revealed that some of these cells were relatively bigger compared to the treated WT and the other *Trib2*^{-/-} which had similar even cellular size (Figure 4.7B top row). We did not investigate further the reason underlying the partial block in T-cell developmental in this context as it was a single case observed. However, it suggests that TRIB2 is required to limit excessive proliferation of developing thymocytes during stress to ensure proper recovery of thymopoiesis.
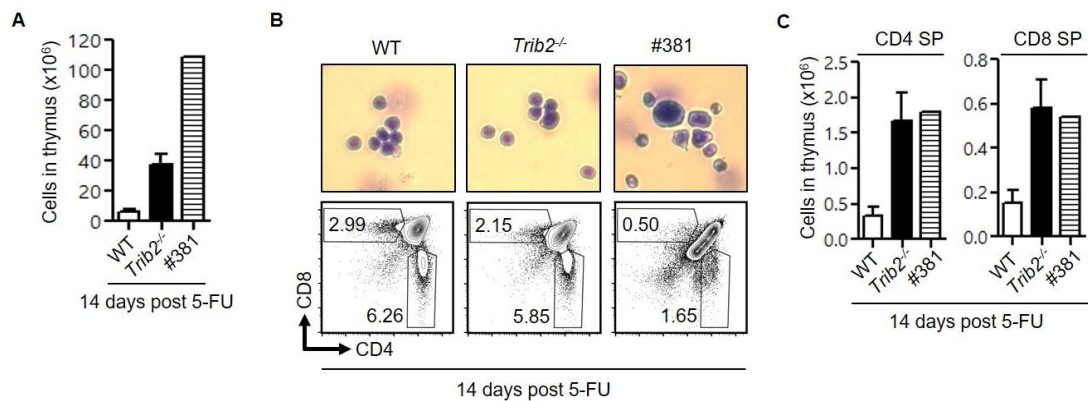
Figure 4.7 │ A 5-FU treated *Trib2*^{-/-} mouse (#381) had partial block of T-cell development during recovery. (A) Thymic cellularity after 14 days of 5-FU treatment (250 mg/kg, i.p.). **(B)** Romanowsky stained cytospin (top row) and flow cytometry (bottom row) profiles of #381 thymocytes. Representative profiles from treated WT (*n* = 9) and *Trib2*^{-/-} mice (*n* = 9) were included for comparison. The values in the indicated areas (bottom row) are frequency of CD4 and CD8 SP subsets in the thymus and their absolute numbers were graphed in **(C)**. For **A** and **C**, the data for WT and *Trib2*^{-/-} mice was derived from Figure 4.2A and 4.2D respectively, and presented as mean and SEM.

4.3 Discussion

We examined the thymic response to 5-FU through a series of *in vivo* experiments with different study end points, and showed that TRIB2 loss has an impact on the susceptibility of thymocytes to genotoxic insult and on the thymopoietic restoration. In the absence of TRIB2, DN1, DN2 and DN3 thymocytes have increased cell division kinetics, and c-kit^{hi} DN1, DN3$_L$ and DP$_{bl}$ had heightened sensitivity to 5-FU induced cell death. Following 5-FU mediated thymic injury, c-Kit$^-$ DN1 progenitors expanded in the absence of TRIB2 and the intrinsic highly proliferative nature of *Trib2*^{-/-} developing thymocytes (DN1, DN3 and DN4 subsets) accelerate the recovery of thymopoiesis. Hence, our study showed TRIB2 limits the thymopoietic recovery after 5-FU injury.

In the past, BM haematopoietic and thymopoietic recoveries following 5-FU injury have been generally studied separately. It has not been clearly established when the import of BM progenitors into thymus and thymopoietic homeostasis is re-

116

established after 5-FU injury. Our study suggest this occurs after the restoration of haematopoiesis in BM since CLPs were detected in the WT and $Trib2^{-/-}$ BM 14 days post 5-FU treatment but c-Kit$^+$ DN1 progenitors, which are derived from BM progenitors including CLP (Benz and Bleul, 2005, Gounari et al., 2002, Schlenner et al., 2010), were barely detected throughout the studied end points. Importantly, c-Kit$^-$ DN1 progenitors were detected and remained resident in the thymus throughout this period. The origin of c-Kit$^-$ DN1 progenitors is currently unknown. Using the OP9-DL1 co-culture system, Poritt and colleagues showed that this subset of DN1 has lower proliferative capacity but faster kinetics of T cell differentiation compared to c-Kit$^+$ DN1 subset (Porritt et al., 2004). However, using a lineage tracing approach, Benz and colleagues showed that thymopoiesis at steady state is sustained by c-Kit$^+$ instead of c-Kit$^-$ progenitors (Benz et al., 2008). Hence, the contribution of c-Kit$^-$ DN1 progenitors to *in vivo* T cell development is unclear. Our study demonstrated, in the absence of c-Kit$^+$ DN1 progenitors, c-Kit$^-$ DN1 progenitors remaining resident in $Trib2^{-/-}$ thymus expand and drive the thymopoietic recovery. Although a recent study showed c-Kit$^-$ DN1 progenitors are transcriptionally primed for dendritic cell development (Moore et al., 2012), we found expansion of c-Kit$^-$ DN1 progenitors led to an increase of T cells, dendritic cells as well as natural killer cells in the thymus of the treated $Trib2^{-/-}$ mice. Our findings suggest that TRIB2 regulates c-Kit$^-$ DN1 progenitor proliferative capacity as we have shown these cells have an important role in the initiation of the first wave of thymopoiesis during recovery which is modulated by the loss of TRIB2.

T cell development in the thymus is maintained by continual input from BM progenitors. It is generally accepted that all thymocyte subpopulations have short life spans and cannot self renew. The notion is based on evidence from thymus transplants where the grafted thymic pool of donor cells is replaced completely within 4 weeks by cells originated from the host BM (Berzins et al., 1998). Other

studies also showed that when WT thymus are transplanted into severe combined immunodeficiency or *Rag2*^{-/-} hosts, the competent WT thymocyte populations from the graft are rapidly replaced by the incompetent BM-derived precursors (arrested at DN3 stage) from the host and additional T cell production stops (Frey et al., 1992, Takeda et al., 1996). However, the long standing dogma that the thymus lacks self renewing progenitors is overturned by recent studies that showed autonomous T cell development in WT thymus engrafted in hosts that are devoid of (*Rag2*^{-/-}γ_c[-/-] *Kit*[W/Wv] (Martins et al., 2012)) or have incompetent BM-derived precursors (*Rag2*^{-/-} *Il7r*^{-/-} (Peaudecerf et al., 2012): arrested at DN2 stage). The capability of resident progenitors to self renew was not recognised previously because, under normal conditions, they are continuously replaced by the import of fresh BM progenitors. A later study showed that natural cell competition between 'young' BM-derived and 'old' thymus-resident progenitors is crucial to suppress T cell leukaemic transformation and development of T-ALL (Martins et al., 2014).

In our study, 5-FU mediated genotoxic insult stressed the haematopoietic system and led to deprivation of the thymus from BM progenitors as c-Kit[+] DN1 progenitors were barely detected during recovery. We observed that c-Kit[-] DN1 progenitors remain residing in the thymus after 5-FU injury and expand in the absence of TRIB2. Hence, the accelerated thymopoiesis found in *Trib2*^{-/-} mice could be autonomous. Further studies are warranted to examine thymic autonomous T cell development under stress conditions.

CHAPTER FIVE: EXAMINATION OF THE ROLE OF TRIB2 IN
T-CELL LEUKAEMOGENESIS

5.1 Introduction

T-ALL is an aggressive haematological malignancy arising from the transformation of thymic progenitors. In paediatric leukaemia 80-85% of cases are ALL, of which 10-15% are T-ALL (Sallan, 2006). In adults, ALL incidence is only 15% of leukaemia cases, of which 20-25% are T-ALL (Sallan, 2006). Hence, T-ALL is mainly a childhood leukaemia. Currently, high dose multi-agent chemotherapeutic regimen is the standard frontline therapy for paediatric T-ALL patients. Despite its high efficacy with patients achieving a five-year event-free survival (EFS) rate of 75-80%, the regimen is aggressive and often associated with severe acute toxicities and long term adverse effects. Compared to the superior outcomes of paediatric T-ALL patients, only 45-55% of adults achieve long term EFS after being diagnosed (Sallan, 2006). Although salvage chemotherapy such as Nelarabine and allogeneic stem cell transplantation treatments are available for relapsed or refractory patients, their clinical outcomes remain very poor (Litzow and Ferrando, 2015, Durinck et al., 2015). Unlike other types of leukaemia, there is no clinically approved targeted therapy for T-ALL yet (Durinck et al., 2015, Freireich et al., 2014). Thus, further understanding of the biology of T-ALL disease is crucial to improve patient risk stratification to current therapy, and to enable development of effective targeted therapies.

The understanding of the biology of T-ALL disease begun in the early 1990s where cytogenetic studies of T-ALL cases revealed genomic alterations (Table 5.1) that include rearrangements involving *TCR* genes, translocations resulting in formation of fusion genes, and cryptic deletions. These genomic alterations lead to

the constitutive activation of developmentally important transcription factor genes (Table 5.1), including *TLX1*, *TLX3*, *HOXA* cluster, *TAL1*, *TAL2*, *LYL1*, *MYC*, *LMO1* and *LMO2* and their aberrant expression in thymic progenitors has been associated with leukaemic transformation. However, genomic abnormalities in T-ALL are rare as 80% of paediatric T-ALLs do not have *TCR* translocations which are the most common alterations (Grabher et al., 2006). Nevertheless, the discovery of these genomic abnormalities has far more impact in human T-ALL pathogenesis than their incidence suggests. Later studies showed that overexpression of the oncogenic transcription factors, identified by previous cytogenetic studies, can be detected in up to 80% of T-ALLs. This can occur in the absence of chromosomal locus specific abnormalities due to loss of upstream transcriptional regulations (Ferrando et al., 2004, Bash et al., 1995). Another classic example is *NOTCH1*, a T-cell oncogene, which was discovered in 1991 in three cases of T-ALL (less than 1%) where a truncated, activated form of *NOTCH1* is translocated to the *TCRB* locus (Table 5.1) (Ellisen et al., 1991). A role of NOTCH1 in human T-ALL was not recognized widely until 1996 when enforced expression of the truncated *NOTCH1* was shown to induce T-ALL in a BM transplant murine model (Pear et al., 1996). The significance of activated NOTCH1 in T-ALL was solidified in 2004 when Weng and colleagues showed somatic activating mutations of *NOTCH1* occur in more than 50% of all T-ALL cases (Weng et al., 2004).

With the advance of microarray technology in gene expression profiling, oncogenic pathways involved in T-ALL pathogenesis begun to be unravelled in the 2000s. In 2002, a landmark study defined three distinct gene expression signatures of T-ALL that represent leukaemic arrest at different stages of T-cell development: LYL1$^+$ signature (pro-T), TLX1$^+$ signature (early cortical thymocyte) and TAL1$^+$ signature (late cortical thymocte) (Ferrando et al., 2002). This formed the basis for classification of T-ALL into different molecular subtypes (Figure 5.1). Both TLX1$^+$

and TAL1^{+} mature T-ALLs are associated with favourable outcome whereas the prognosis of LYL1^{+} immature T-ALLs is currently unknown (Van Vlierberghe and Ferrando, 2012).
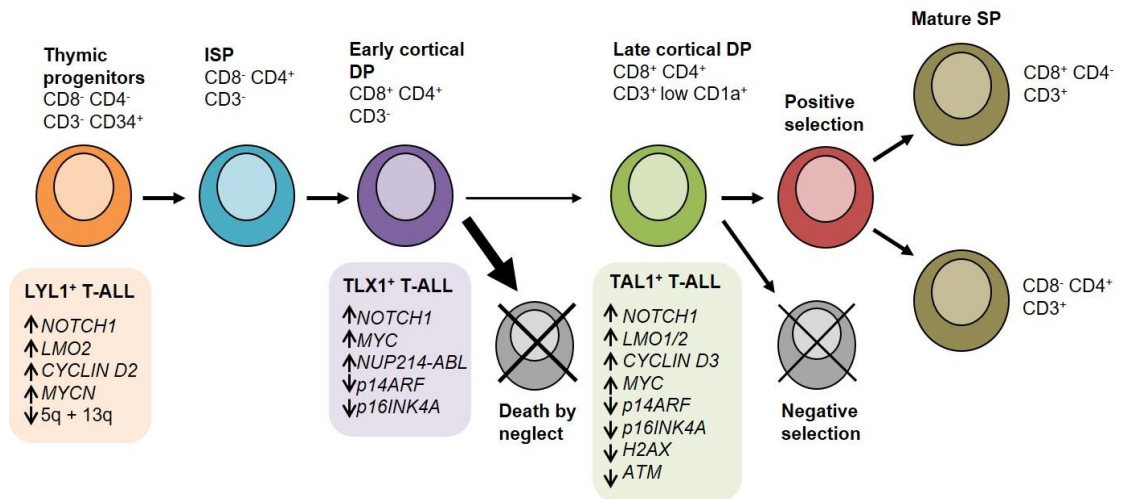
Figure 5.1 │ Correlation between different molecular subtypes of T-ALL and stage of thymocyte differentiation along the αβ T-cell lineage. LYL1^{+} T-ALL shows an expression profile indicating maturation arrest at the immature stage. Leukaemic cells from TLX1^{+} T-ALL are arrested at the early cortical DP stage, whereas TAL1^{+} T-ALL cases are arrested at the late cortical DP stage. Each molecular subtype has distinct gene expression profile except the upregulation of *NOTCH1*, which is the unifying feature. MLL[+] T-ALL which is of γδ lineage is not included. Modified from (Grabher et al., 2006).

Regardless of the molecular subtypes of human T-ALL, abbrerant activation of NOTCH1 signalling is the unifying feature (Grabher et al., 2006). Indeed, as mentioned above, overexpression of a constitutively activated intracellular NOTCH1 (ICN1) in BM cells is capable to induce T-ALL in mice where they are transplanted into (Pear et al., 1996). However, this orginal model only results T-ALL in 30-50% of BM-reconstituted mice (Pear et al., 1996). The BM transplant model was refined by Aster and colleagues to enable induction of NOTCH1-dependent T-ALL in 100% of mice (Aster et al., 2000). Since then, the refined BM transplant model has been widely used to study the molecular pathogenesis of T-ALL (Aster et al., 2011, Chiang et al., 2006, Li et al., 2008). BM cells that overexpress ICN1 undergo DN stages but are blocked at DP stage of extrathymic T-cell development. Li and

colleagues showed that *ICN1*-transduced BM cells generate polyclonal non-tumourigenic DP cells at 2 weeks post transplantation and leukaemic transformation occur later in immature intermediate CD8^{+} single positive cells (Li et al., 2008).

In normal human (Casero et al., 2015) and murine (Mingueneau et al., 2013) T-cell development, *TRIB2* expression is higher in the early uncommitted thymic progenitors compared to other DN thymic subsets but increases as cells develop into DP and SP stages. In T-ALL, *TRIB2* was identified as a target gene of oncogenic NOTCH1 (Wouters et al., 2007), PITX1 (Nagel et al., 2011) and TAL1 (Sanda et al., 2012). However, *TRIB2* mRNA and TRIB2 protein levels have not been examined in cell lines or primary samples representing different molecular subtypes of T-ALL. Although TRIB2 was shown to be essential for the maintenance of TAL1^{+} T-ALL (Sanda et al., 2012), it remains unclear the role of TRIB2 in the initiation of T-ALL. Yokoyama and colleagues showed that activation of ERK signalling is essential for TRIB1–induced leukaemogenesis as well as cooperation with HOXA9 and MEIS1 to initiate murine AML (Yokoyama et al., 2010). A separate study showed that TRIB1 mutant accelerates the initiation of murine AML through enhanced ERK signalling (Yokoyama et al., 2012). In contrast to AML, activation of p38 and ERK signalling were found in dormant instead of aggressive T-ALL xenografts (Masiero et al., 2011). Although TRIB2 is known to modulate MAPK signalling, as explained in Section 1.3.5, its implications in T-ALL has not been studied.

In the previous chapter, we showed that TRIB2 negatively regulates the proliferation of developing thymocytes and limits thymopoietic recovery following genotoxic insult. Tight regulation of thymopoietic restoration has been proposed to prevent adverse consequences such as leukaemic transformation of T cells and autoimmunity (Boehm and Swann, 2013). The observation of a *Trib2^{-/-}* mouse that

developed a block in T cell development at DP stage following 5-FU treatment suggests TRIB2 could be important in T cell leukemogenesis. Hence, in this chapter, we aimed to investigate the role of TRIB2 in the initiation of T-ALL.

Table 5.1 │ Genomic alterations in T-ALL[†].

T-ALL oncogene	Type of protein	Chromosomal alterations	Normal developmental role	Frequency of T-ALL (%)		References
				Children	**Adults**	
Rearrangements involving *TCR* genes (*TCRA/D* on 14q11 and *TCRB* on 7q34)						
TLX1	Homeodomain	t(7;10)(q34;q24) t(10;14)(q24;q11)	Spleen development	4-7	14	(Dube et al., 1991, Hatano et al., 1991, Kennedy et al., 1991, Lu et al., 1991, Bergeron et al., 2007)
TLX3	Homeodomain	t(5;14)(q35;q32) t(5;14)(q35;q11)	Central nervous system (CNS) development	22	13	(Hansen-Hagge et al., 2002, Berger et al., 2003)
HOXA cluster	Homeodomain	Inv(7)(p15q34) t(7;7)(p15;q34)	Axial patterning	3.3		(Speleman et al., 2005, Soulier et al., 2005, Cauwelier et al., 2007)

TAL1	bHLH	t(1;14)(p32;q11) t(1;7)(p32;q34)	Embryonic HSC development	3	(Begley et al., 1989, Chen et al., 1990, Carroll et al., 1990)
TAL2	bHLH	t(7;9)(q34;q32)	CNS development	Two cases	(Xia et al., 1991, Smith et al., 1988)
LYL1	bHLH	t(7;19)(q34;p13)	Haematopoiesis	Two cases	(Mellentin et al., 1989, Cleary et al., 1988, Homminga et al., 2012)
BHLHB1	bHLH	t(14;21)(q11.2;q22)	CNS development	Single case	(Wang et al., 2000)
MYC	bHLH/Lzip	t(8;14)(q24;q11)	Cell growth and apoptosis	2	(Finger et al., 1986, McKeithan et al., 1986, Shima et al., 1986, Erikson et al., 1986)
LMO1	LIM domain	t(11;14)(p15;q11)	Hindbrain patterning	2	(Greenberg et al., 1990, McGuire et

					al., 1989)
LMO2	LIM domain	t(11;14)(p13;q11) t(7;11)(q35;p13)	Embryonic HSC development	7	(Van Vlierberghe et al., 2006)
LCK	Tyrosine kinase	t(1;7)(p34;q34)	TCR signalling	Two cases	(Tycko et al., 1991)
NOTCH1	Notch receptor	t(7;9)(q34;q34.3)	T-cell fate specification	Three cases	(Ellisen et al., 1991)
CCND2	D-type cyclin	t(7;12)(q34;p13) t(12;14)(p13;q11)	Cell cycle	3	(Clappier et al., 2006)
Formation of fusion genes					
NUP214-ABL1	Nucleoporin/ Tyrosine kinase	t(9;9)(q34;q34) (episomal)	Nuclear transport-nuclear signalling	6	(Graux et al., 2004, Cimino et al., 2001)
NUP98-RAP1GDS1	Nucleoporin/ GEF	t(4;11)(q21;p15)	Nuclear transport-Ras activation	5	(Hussey et al., 1999)
EML1-ABL1	CC domain/ Tyrosine kinase	t(9;14)(q34;q32) (cryptic)	Cytoskeleton-nuclear signalling	Single case	(De Keersmaecker et al., 2005, Hagemeijer and Graux, 2010)
ETV6-JAK2	ETS domain/ Tyrosine kinase	t(9;12)(p24;p13)	Haematopoiesis-immune response	3	(Zhou et al., 2012,

126

					Lacronique et al., 1997)
ETV6-ABL1	ETS domain/ Tyrosine kinase	t(9;12)(q34;p13)	Haematopoiesis-nuclear signalling	Single case	(Zuna et al., 2010, Van Limbergen et al., 2001)
CALM-AF10	ENTH domain AT-hook	t(10;11)(p13;q21)	Clathrin assembly-transcriptional factor	10	(Carlson et al., 2000, Asnafi et al., 2003)
MLL-ENL	Methyltransferase Nuclear targeting sequence containing	t(11;19)(q23;p13)	Transcriptional regulator-super elongation complex	8 (all MLL)	(Graux et al., 2006)
MLL-AF6	Methyltransferase GLGF motif containing	t(6;11)(q27;q23)	Transcriptional regulator-organization of cell junctions	8 (all MLL)	(Graux et al., 2006)
MLL-AF10	Methyltransferase AT-hook	t(10;11)(p13;q23)	Transcriptional regulator-transcriptional factor	8 (all MLL)	(Graux et al., 2006)
MLL-AFX1	Methyltransferase Forkhead family	t(X;11)(q13;q23)	Transcriptional regulator-cell cycle regulation	8 (all MLL)	(Graux et al., 2006)
MLL-AF4	Methyltransferase Nuclear targeting sequence containing	t(4;11)(q21;q23)	Transcriptional regulator-transcriptional activator	8 (all MLL)	(Graux et al., 2006)
Others					

LMO2	LIM domain	del(11)(p12p13)	Embryonic HSC development	4	unknown	(Van Vlierberghe et al., 2006)
SIL-TAL1	Proline rich extension/ bHLH	del(1p) (cryptic)	Mitotic spindle checkpoint Embryonic HSC development	16	11	(Brown et al., 1990, Asnafi et al., 2005, D'Angio et al., 2015)

[†] Modified from REF. (Grabher et al., 2006, Graux et al., 2006).*CALM-AF10* and *MLL* fusion genes are restricted to γδ lineage T-ALL subtype.

5.2 Results

5.2.1 TRIB2 loss accelerates murine T-ALL via defective MAPK signalling.

We examined the role of TRIB2 in T-cell leukaemogenesis using a NOTCH1 induced T-ALL BMT mouse model (Aster et al., 2000). WT and $Trib2^{-/-}$ total BM cells were transduced with an empty vector control (MigR1) or a retroviral vector encoding an intracellular $Notch1$ transgene (ICN1). This transgene is known to induce T-ALL with a $CD4^+/CD8^+$ phenotype with a latency of 7-12 weeks in the BM transplantation model (Aster et al., 2000, Pui et al., 1999, Aster et al., 2011, Chiang et al., 2006, Allman et al., 2001). The cells, which were $CD45.2^+$, were then transplanted into lethally irradiated $CD45.1^+$ recipient mice to monitor the development of T-ALL. All experimental groups were verified by $Trib2$ genotyping analysis of the transplanted moribund mice (Figure 5.2).
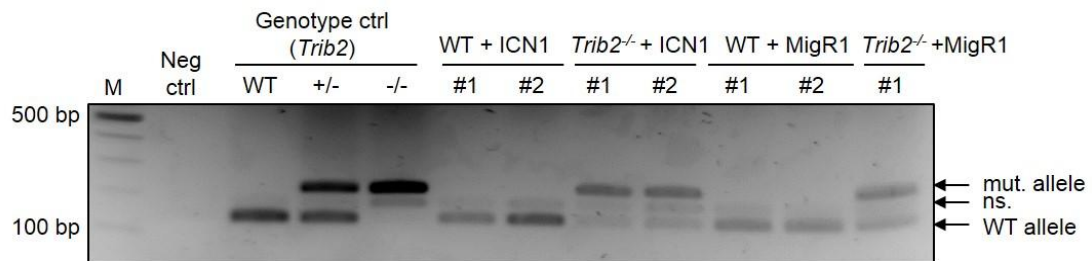
Figure 5.2 │ Transplant experimental groups were verified by *Trib2* genotyping analysis. Splenic total genomic DNA was extracted from the moribund mice. PCR analysis of representative samples from different groups is shown here. M, marker; neg ctrl, no template negative control; ctrl, control; mut, mutant; ns, non specific.

Mice transplanted with ICN1-transduced $Trib2^{-/-}$ donor cells succumbed to T-ALL disease with a shorter latency (median survival of 43.5 days) whereas mice transplanted with ICN1-transduced WT donor cells had a median survival of 63.5 days. Kaplan Meier survival analysis for these two groups was significantly different (Figure 5.3A) indicating T-ALL onset driven by NOTCH1 overexpression was accelerated in the absence of TRIB2. GFP expression was used as a marker for transduced donor cells and analysis showed similar engraftment levels of transduced WT and $Trib2^{-/-}$ donor cells in the recipients from all groups across different organs post mortem (Figure 5.3B). Importantly, the difference in disease latencies in mice from WT and $Trib2^{-/-}$ expressing ICN1 was not due to differences in engraftment levels of transduced donor cells post-transplant. Similar engraftment levels of transduced cells were present upon sequential analysis post transplant until the mice succumbed to disease (Figure 5.3C). Analysis of BM showed engrafted MigR1-transduced donor cells developed normally into lineage committed Gr-1$^+$/CD11b$^+$ myeloid cells and CD19$^+$/B220$^+$ B-lymphoid cells whereas ICN1-transduced donor cells displayed CD4$^+$/CD8$^+$ T-ALL leukaemic cell profile (Figure 5.3D). TRIB2 loss did not alter the immunophenotype (Figure 5.3D) and histological morphology (Figure 5.3E) of NOTCH1-induced T-ALL. Compared to mice from control groups (WT+MigR1 and $Trib2^{-/-}$+MigR1), mice that succumbed to T-ALL disease had leukocytosis, anaemia and thrombocytopenia (Figure 5.4A). Despite a difference of 20 days for disease onset, mice that succumbed earlier to $Trib2^{-/-}$ T-ALL had a similar degree of leukaemic burden (Figure 5.4B and 5.4C) but exhibited a trend of higher organ infiltration of leukaemic cells (Figure 5.4D) compared to mice that succumbed to WT T-ALL. We have ruled out that the accelerated T-ALL phenotype is not due to an increase in $TRIB1$ expression, as $TRIB1$ expression levels do not change upon knockdown of $TRIB2$ in T-ALL or AML cell lines (Figure 5.5). To understand how TRIB2 loss accelerated the initiation of T-ALL, we compared MAPK signalling between WT and $Trib2^{-/-}$ T-ALL as Tribbles family

(TRIB1-3) is known to be associated with MAPK signalling and required for the activation of ERK, JNK and p38 (Yokoyama et al., 2010, Wang et al., 2013c, Wei et al., 2012, Izrailit et al., 2013). Western blotting for MAPK signals in leukaemic infiltrated BM samples showed impaired activation of ERK, JNK and p38 in *Trib2^{-/-}* T-ALL compared to WT T-ALL (Figure 5.4E). We also confirmed reduced activation of p38 signalling in normal developing DN2 and $DN3_L$ thymic subsets (Diehl et al., 2000) in the absence of TRIB2 (Figure 5.6). These imply that modulation of MAPK signalling by TRIB2 may influence the phenotype of T-ALL.
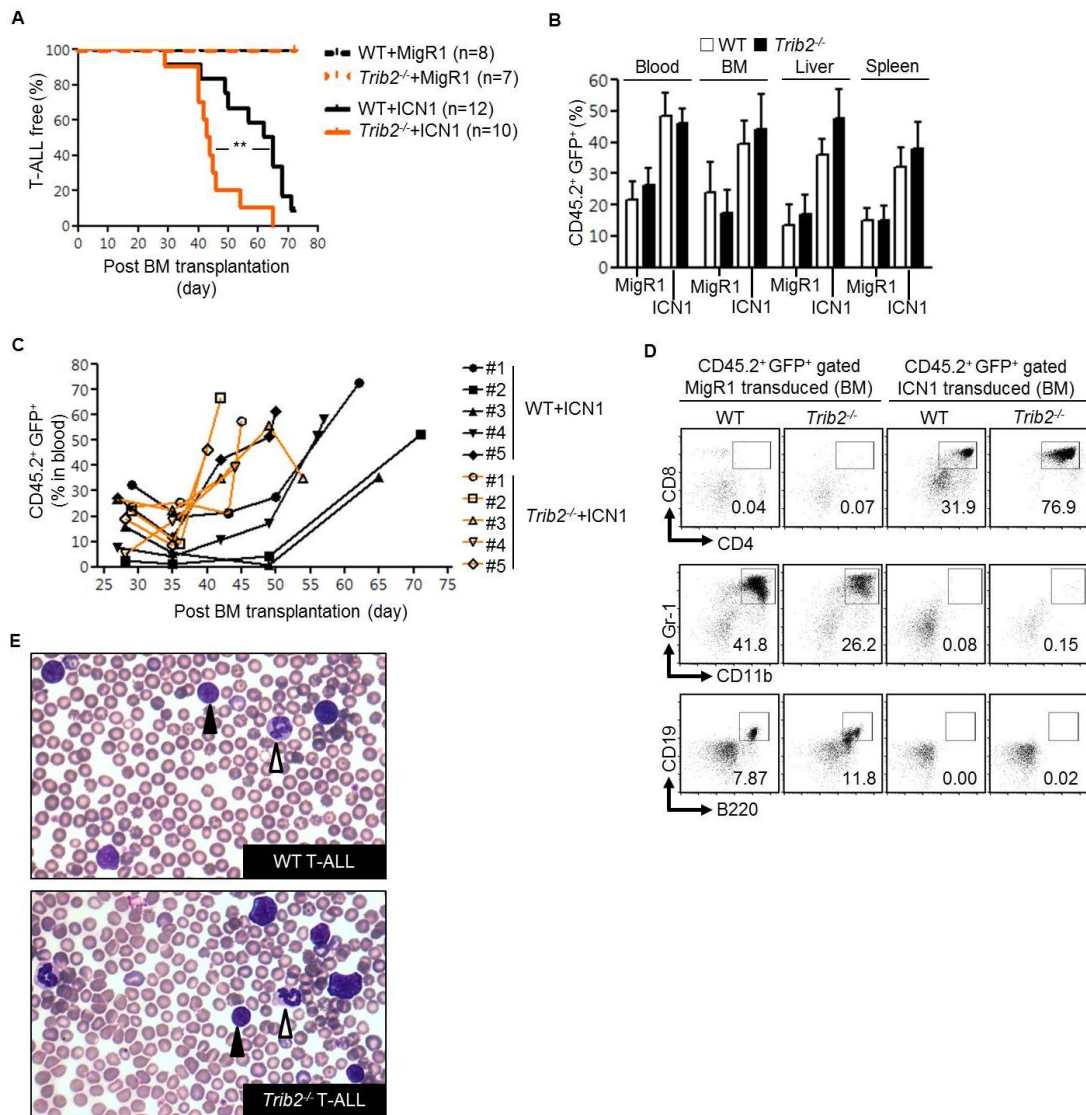
Figure 5.3 │ Loss of TRIB2 accelerates the onset of NOTCH1-induced T-ALL.
(A) Kaplan-Meier survival analysis of the lethally irradiated recipient (CD45.1$^+$) mice transplanted with 5-FU enriched WT or *Trib2$^{-/-}$* BM cells (donor: CD45.2$^+$) transduced with either MigR1 control or ICN1 transgene. The number (*n*) of mice analysed was from three independent experiments. T-ALL, T-cell acute lymphoblastic leukaemia. **(B)** Engraftment of donor cells in all experimental groups across different organs were determined based on GFP expression post mortem. **(C)** Evolvement of transduced donor cells in test groups (WT and *Trib2$^{-/-}$*+ICN1) after transplantation and till morbidity. Five mice from each group were shown here. **(D)** Development of T-ALL leukaemia was verified by immunophenotyping analysis of transduced donor cells for surface expression of different lineage markers. The values in the outlined areas are frequency of leukaemic cells (top row: CD4$^+$/CD8$^+$), lineage committed myeloid cells (middle row: Gr-1$^+$/CD11b$^+$) or B-lymphoid cells (bottom row: CD19$^+$/B220$^+$) in the BM of moribund mice. **(E)** Romanowsky staining of representative blood smears of moribund mice from test groups. Filled arrow head indicates a lymphoblast (WT and *Trib2$^{-/-}$* T-ALL) and unfilled arrow head indicates a normal neutrophil. For **A**, Log-rank test was used to compare the survival curves. $^{**}P$ = 0.0053, all quantified data are presented as mean and SEM.
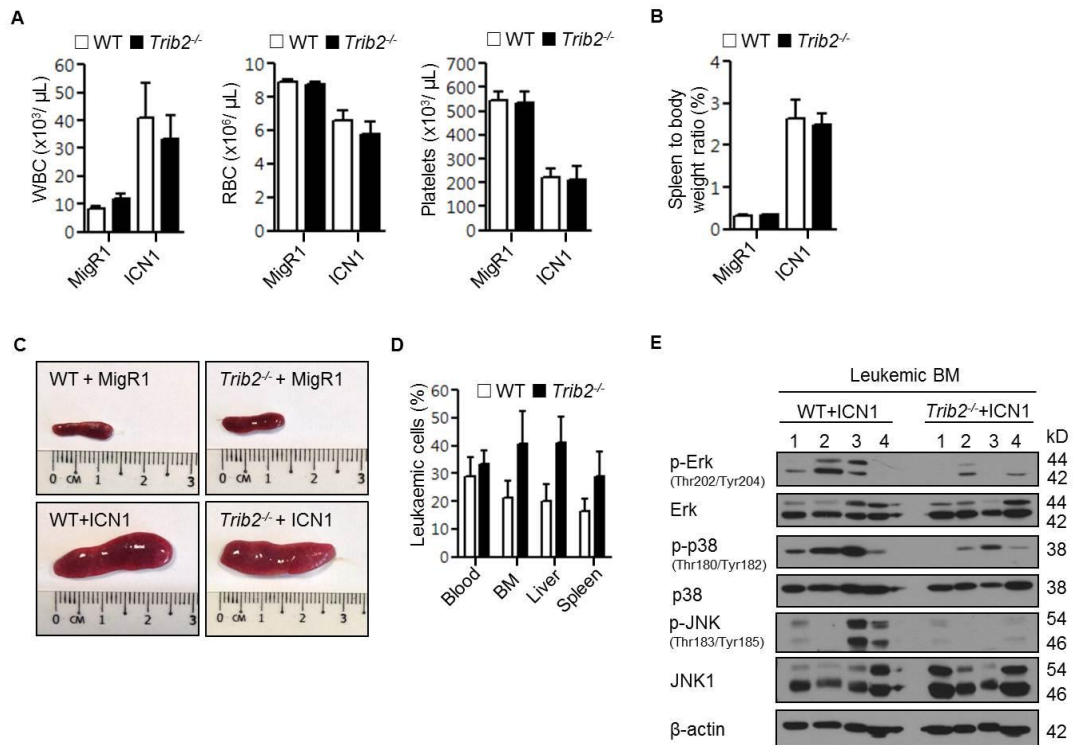
Figure 5.4 │ *Trib2^(-/-)* T-ALL is more aggressive and has defective MAPK signalling compared to WT T-ALL. (A) Health of the moribund mice was assessed by WBC, RBC and platelet counts. **(B)** Leukaemic burden was determined by spleen to body weight ratio. **(C)** Representatives of a spleen from each experimental group. **(D)** Leukaemic infiltration was assessed by measurement of the frequency of leukaemic cells in various organs of moribund mice. **(E)** Activation of MAPK signalling in T-ALL was determined by western blotting for p-Erk, total Erk, p-p38, total p38, p-JNK, JNK1 and β-actin signals in the leukaemic BM (n = 4 per group). Signals shown were developed from triplicate immunoblots. For **A**, **B** and **D**, the number (n) of mice analysed was stated in Figure 5.3A. All quantified data are presented as mean and SEM.

133
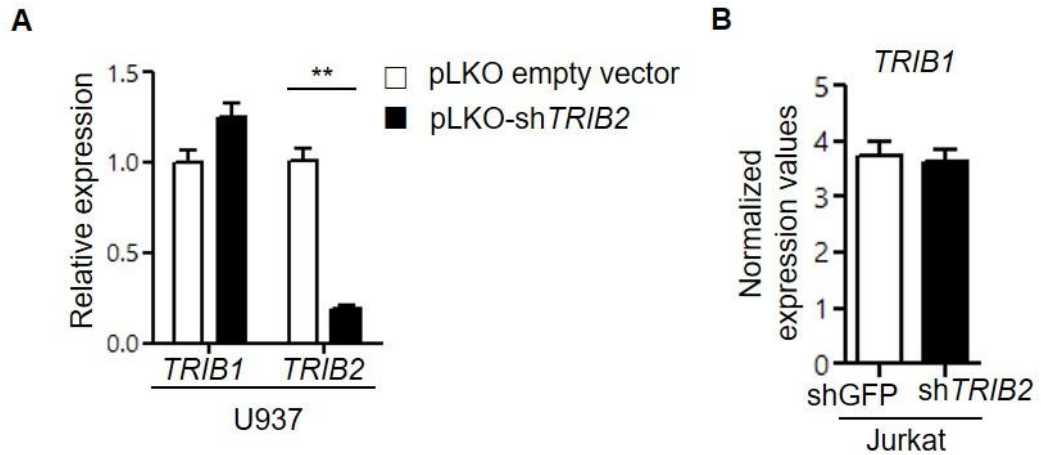
Figure 5.5 │ *TRIB1* expression remained unchanged following *TRIB2* knockdown. (A) Expression of *TRIB1* and *TRIB2* in GFP-sorted U937 cells was measured by quantitative RT-PCR after 48 hours of transduction with pLKO empty vector or pLKO-sh*TRIB2*. **(B)** Normalized expression values of *TRIB1* (average of 202241_at, 235641_at and 239818_x_at) in Jurkat cells following *TRIB2* knockdown were derived from GSE66013 dataset (Tan et al., 2015). For statistical analyses, unpaired Student's t-test was used for **A** and **B**. $^{**}P<0.01$, all quantified data are presented as mean and SEM.
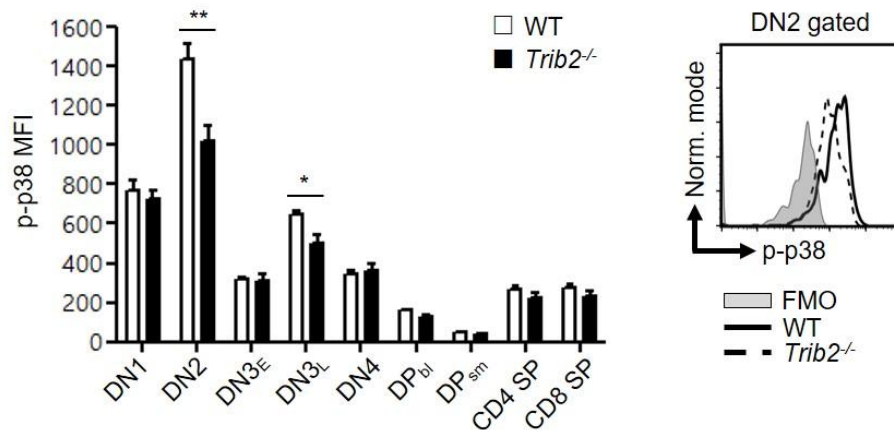
Figure 5.6 │ Reduced activation of p38 in *Trib2*$^{-/-}$ DN2 and DN3$_L$ thymic subsets. Intracellular level of p-p38 across thymic subsets ($n = 4$ for *Trib2*$^{-/-}$ and $n = 5$ for WT), indicated by the mean fluorescence intensity (MFI), was measured by flow cytometry (left). MFI of each subset was presented after deduction of the MFI of the corresponded FMO control. An overlap of histogram (right) showed *Trib2*$^{-/-}$ DN2 cells had lower level of p-p38 compared to that of WT. Norm, normalized; FMO, Fluorescence Minus One. For statistical analyses, unpaired Student's t-test was used. $^{*}P<0.05$; $^{**}P<0.01$, all quantified data are presented as mean and SEM.

5.2.2 *TRIB2* expression levels distinguish molecular subtypes of human T-ALL and correlate with MAPK signalling.

Since TRIB2 loss accelerated T-ALL onset in our experimental model, we performed GSEA analysis to compare gene expression profiles of low and high *TRIB2* expression (Table 5.2) from a database (GSE13159) derived from 174 T-ALL patient samples (Haferlach et al., 2010) (Figure 5.7A). GSEA analysis showed these two groups, defined by *TRIB2* expression, were of distinct molecular subtypes of T-ALL (Figure 5.7B). Low *TRIB2* expressing T-ALL group was enriched with gene set associated with TLX1$^+$ T-ALL (early cortical mature T-ALL) whereas high *TRIB2* expressing T-ALL group had upregulation of LYL1$^+$ T-ALL (immature T-ALL) gene set (Table 5.3) (Ferrando et al., 2002). TAL1$^+$ T-ALL (late cortical mature T-ALL) gene set was not enriched in either group. A significant positive correlation between *TRIB2* and *LYL1* expression was confirmed in an independent T-ALL dataset (GSE33315) (Zhang et al., 2012c) (Figure 5.7C). As shown in Fgure 5.4E in our experimental model, *Trib2*$^{-/-}$ T-ALL leukaemic cells exhibited deficiencies in MAPK signalling. In accordance with this, using GSEA analysis of low and high *Trib2* expressed human T-ALL groups, MAPK signalling was found to be upregulated in the high *Trib2* expressing T-ALL group (Figure 5.7D). Hence, impaired activation of MAPK signalling in the absence of TRIB2 contributed to the increased aggressiveness of NOTCH1 induced murine T-ALL disease which recapitulated the immunophenotypes of human cortical mature T-ALL. Our analysis suggests TRIB2 possesses tumour suppressive functions important for T-ALL.

Table 5.2 │ Low and high *TRIB2* expressed human T-ALLs (GSE13159 dataset).

T-ALL ID	202478_at	*TRIB2* level
sample_347	3.602	low
sample_736	3.890	low
sample_1573	3.966	low
sample_1557	4.191	low
sample_348	4.244	low
sample_1267	4.292	low
sample_790	4.432	low
sample_2216	4.501	low
sample_2118	4.745	low
sample_824	4.788	low
sample_809	4.805	low
sample_1682	4.914	low
sample_845	4.919	low
sample_907	4.970	low
sample_1631	4.973	low
sample_1335	4.987	low
sample_1664	5.006	low
sample_551	5.014	low
sample_2099	5.024	low
sample_2166	5.041	low
sample_1955	5.111	low
sample_2156	5.220	low
sample_1699	5.248	low
sample_810	5.259	low
sample_1807	5.314	low
sample_974	5.370	low
sample_2125	8.811	high
sample_616	8.887	high
sample_2089	8.913	high
sample_615	8.998	high
sample_470	9.032	high
sample_565	9.037	high
sample_771	9.132	high
sample_313	9.305	high
sample_1337	9.355	high
sample_1090	9.489	high
sample_1851	9.491	high
sample_2081	9.509	high
sample_2132	9.557	high
sample_1829	9.610	high
sample_334	9.653	high
sample_1076	9.680	high
sample_500	9.683	high
sample_2138	9.767	high
sample_1568	9.910	high
sample_1969	10.034	high
sample_867	10.092	high
sample_1354	10.107	high
sample_2073	10.124	high
sample_1189	10.134	high
sample_2204	10.528	high
sample_552	11.103	high
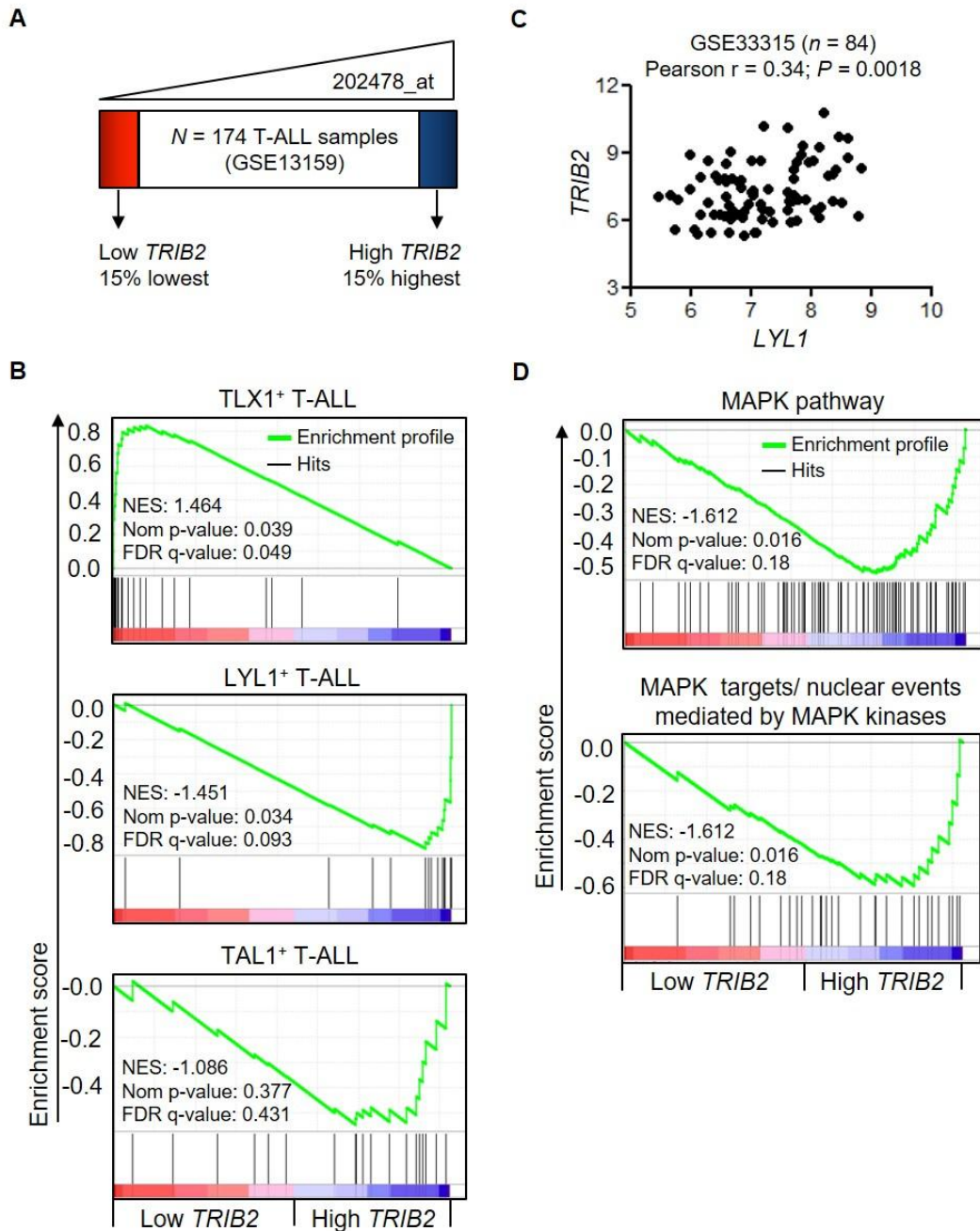
Figure 5.7 │ *TRIB2* levels distinguish molecular subtypes of human T-ALL and associate with MAPK signalling. (A) GSEA was performed to compare human T-ALL samples from GSE13159 dataset (Haferlach et al., 2010) that expressed low and high *TRIB2* (*n* = 26 per group) for enrichment of human T-ALL molecular subtypes **(B)** and canonical pathways **(D)**. NES, normalized enrichment score; Nom, nominal; FDR, false discovery rate. **(C)** Correlation between *TRIB2* (average of 202478_at and 202479_s_at) and *LYL1* (210044_s_at) expressions were examined in 84 human T-ALL samples from GSE33315 dataset (Zhang et al., 2012c). For **C**, Pearson correlation test was used to examination association between *TRIB2* and *LYL1* expressions.

Table 5.3 | Core enrichment genes upregulated in low and high *TRIB2* T-ALLs.

Gene set (systematic name)	Upregulated in	Size of gene set	Core enrichment genes
TLX1[+] T-ALL (M2059)	Low *TRIB2* T-ALL	23	*ADA; CCNA2; CD1A; CD1B; CD1C; CD1D; CD1E; DNTT; MCM4; MME; PTPRF; TK1; TLX1; TOP2A; TYMS; UNG*
LYL1[+] T-ALL (M4175)	High *TRIB2* T-ALL	15	*CCND2; CD34; FES; HHEX; LGALS9; LMO2; MYCN; SELL; TNFRSf1A; ZBTB16*
MAPK pathway (M13863)	High *TRIB2* T-ALL	85	*ARAF; CEBPA; CHUK; CREB1; DAXX; IKBKB; MAP2K1; MAP2K2; MAP2K4; MAP2K6; MAP2K7; MAP3K1; MAP3K11; MAP3K3; MAP3K7; MAP3K8; MAP4K1; MAP4K2; MAP4K4; MAPK13; MAPK14; MAPK6; MAPK7; MAPK8; MAPKAPK2; MAPKAPK3; MAX; MEF2C; NFKB1; NFKBIA; RELA; RIPK1; RPS6KA1; RPS6KA3; RPS6KB2; STAT1; TGFB1; TGFBR1; TRADD*
MAPK targets (M15195)	High *TRIB2* T-ALL	30	*ATF1; CREB1; DUSP4; DUSP6; MAPK14; MAPK7; MAPK8; MAPKAPK2; MEF2C; PPP2CB; PPP2R1A; RPS6KA1; RPS6KA3*

5.3 Discussion

We showed TRIB2 is required to suppress T cell leukaemogenesis induced by NOTCH1 overexpression. A role for TRIB2 in T-ALL maintenance was demonstrated by Sanda and colleagues (Sanda et al., 2012) as knockdown of *Trib2* in a panel of TAL1 positive human T-ALL cell lines induced apoptosis and inhibited cell growth. This appears to be consistent with the role of TRIB2 in other solid (Zanella et al., 2010, Grandinetti et al., 2011, Wang et al., 2013a) and haematological (Rishi et al., 2014) malignancies that overexpression of TRIB2 confers growth and survival advantages to tumour cells. However, we provide strong evidence that TRIB2 has opposing roles in the initiation and potency of T-ALL. In the absence of TRIB2, the latency of NOTCH1-induced T-ALL was shortened significantly. The tumour suppressive role of TRIB2 in the initiation of NOTCH1-induced T-ALL was verified by another independent study where similar experiments were performed using a different *Trib2* knockout mouse model generated by the authors (Stein et al., 2016). As a cell signalling modulator and mediator, it is likely that TRIB2 function, whether tumour promoting or suppressing, is dependent on the cellular state in which it is activated, similar to what has been described for p53 (Kruiswijk et al., 2015). In leukaemic initiation, signalling networks in normal cells are perturbed by driver mutations to enable leukaemic transformation. However, in leukaemic maintenance, signalling networks in transformed cells are governed by both driver and passenger mutations to cope with increasing metabolic and genomic stresses. Hence, the differing roles of TRIB2 in T-ALL initiation and maintenance could be due to alterations in signalling networks during and after leukaemic transformation.

We previously reported elevated *TRIB2* levels in a cohort of paediatric T-ALLs that contain *Notch1*/*Fbxw7* mutations compared to wild type T-ALLs and this was

important in the profile and phenotype of mutant NOTCH1 T-ALL (Hannon et al., 2012). However, mutant NOTCH1 does not cluster into the aforementioned LYL1^{+}, TLX1^{+} and TAL1^{+} T-ALL. Instead, aberrant NOTCH1 signalling is the unifying feature in all the subtypes. Hence, we performed GSEA analysis in this study to show *TRIB2* is highly expressed in immature (LYL1^{+}) T-ALLs that are arrested at the DN stage of early thymocyte development and transcriptionally related to HSCs and myeloid progenitors (Zhang et al., 2012c, Van Vlierberghe et al., 2013). Further studies of this subset of T-ALL, reviewed by Yui and Rothenberg (Yui and Rothenberg, 2014), indicate that leukaemic transformation is due to failure of uncommitted thymic progenitors to repress a 'legacy' stem and progenitor cell gene network that is inherited from multipotent precursors. These genes include but are not limited to *MEIS1*, *HOXA9*, *LYL1*, *LMO2*, *HHEX* and *MYCN* that are normally expressed only in DN1 and/or DN2a cells, and are functionally implicated as proto-oncogenes. Furthermore, a high prevalence of AML mutations (*FLT3*, *NRAS*, *DNMT3A*, *IDH1* and *IDH2*) (Van Vlierberghe et al., 2013) in immature (LYL1^{+}) T-ALLs suggests contribution of myeloid oncogenes to leukaemogenesis of this subset of T-ALL. In turn, *TRIB2* expression is suppressed in TLX1^{+} human T-ALLs which have a mature cortical DP phenotype where the transformed cells have committed to the T cell lineage (Ferrando et al., 2002). We propose the role of TRIB2 in different subtypes of human T-ALL depends on the stage at which thymic progenitors undergo malignant transformation and if they have committed to T cell lineage. In immature T-ALL, we speculate that the oncogenic property of TRIB2 in myeloid leukaemia is 'inherited' in transformed uncommitted thymic progenitors. We further speculate that TRIB2 is tumour suppressing in mature T-ALL as TRIB2 exerts its physiological role in normal T-cell development. As such, targeting of TRIB2 could be beneficial in the treatment of LYL1^{+} instead of TLX1^{+} T-ALLs.

There is a strong correlation with *TRIB2* and MAPK signalling in human T-ALL as shown by GSEA analysis. Previously, the activation of ERK and p38 were shown to inversely correlate with aggressiveness of T-ALL in a model of T-ALL cell dormancy (Masiero et al., 2011). Furthermore, drug treatment of established human T-ALL cell lines was shown to induce cell death via activation of p38 and JNK (Liu et al., 2014, Ge et al., 2013, Jiang et al., 2013). Thus, activation of MAPK signalling appears to be a limiting factor, at least, in the context of T-ALL. TRIB family members acts as scaffold proteins for the binding of MAPK signalling complexes and hence modulates their activity. All TRIB family members have the conserved MEK1 binding motif and have been shown to interact with MEK1 (Yokoyama et al., 2010). In human T-ALLs, upregulation of ERK1/2 signalling was found in 38% of T-ALL patients (Gregorj et al., 2007) and MEK/ERK can be activated due to RAS mutations, found in about 10% of T-ALL patients (Kindler et al., 2008). Targeting of MEK/ERK signalling by MEK inhibition was shown to be effective in treating KRAS-mutated T-ALL in a murine model (Dail et al., 2010). The upregulation of MAPK signalling in specific subtypes of T-ALL has not been studied and remains unclear. Here we show *TRIB2* expression is high in LYL1^{+} immature T-ALLs enriched with MAPK signalling and our experimental data show defective MAPK signalling in the absence of TRIB2. Thus, it appears that TRIB2 functions to control T-ALL via MAPK modulation.

We and others (Dedhia et al., 2010, Keeshan et al., 2006) have shown that *Trib2* is a myeloid oncogene when overexpressed in a murine BM transplant model. Here, loss of TRIB2 potentiated murine T-ALL induced by a T cell oncogene. Given that *TRIB2* is expressed highest in normal T cells (Liang et al., 2013), it is not surprising that overexpression of *Trib2* does not drive T-ALL in the BMT model, and our data would suggest that TRIB2 functions to suppress T-ALL. Our data provide insight into the understanding of the opposing leukaemogenic roles of TRIB2 in

myeloid and lymphoid leukaemia. However, the mechanisms that underlie whether TRIB2 acts as an oncogene or tumour suppressor are not well understood. It may be linked to its function in cell proliferation and MAPK pathway modulation, which could be cell context specific. Anti- and pro-proliferative effects connected with MAPK signalling and TRIB1 have been previously demonstrated in different cell contexts. In vascular smooth muscle cells, TRIB1 was shown to interact with MKK4 which led to inhibition of JNK pathway and decreased proliferation (Sung et al., 2007). In murine BM cells, TRIB1 was shown to interact with MEK1 which led to increased activation of ERK pathway and increased proliferation (Yokoyama et al., 2010).

This work is a paradigm shift in the definition of TRIB2 function in malignant haematopoiesis. TRIB2 is capable of driving myeloid leukaemogenesis and this tumour promoting function is likely to be retained in leukaemogenesis of immature T-ALL where the transforming thymic progenitors have not terminated properly the previously established legacy stem and progenitor cell transcriptional networks. However, in leukaemogenesis of mature T-ALL, TRIB2 is tumour suppressing owing to its physiological role in normal T-cell development.

6.1 Introduction
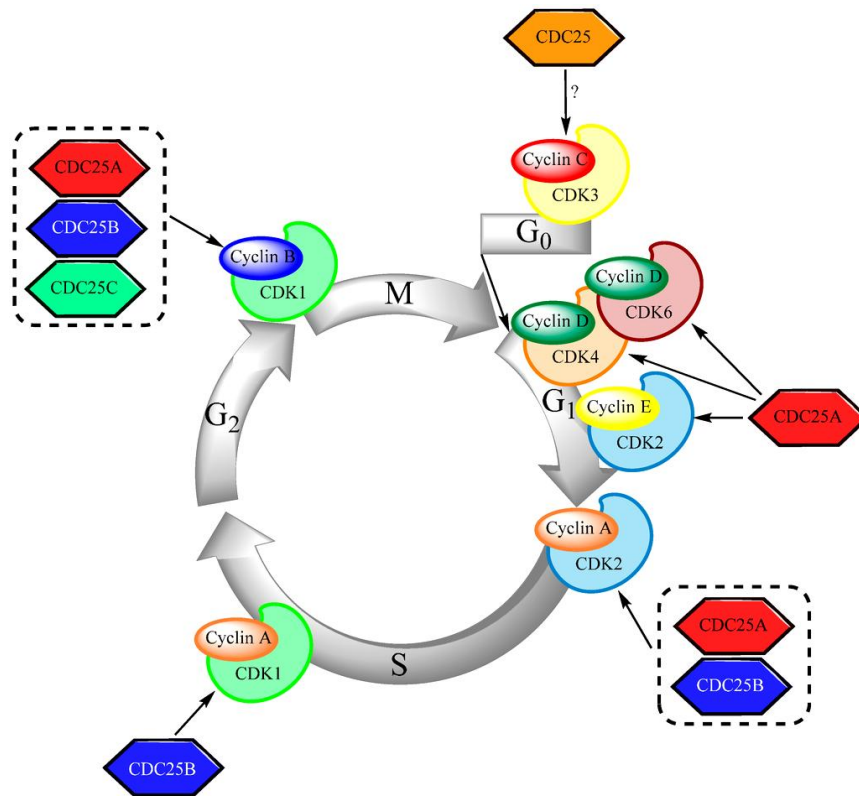
Figure 6.1 │ CDC25 family regulates cell cycle transitions. Each phase of cell cycle is controlled by different CDK-Cyclin complexes which are held inactive by the phosphorylation of two residues (for example Threonine 14 and Tyrosine 15 of CDK1) within the ATP binding loop. CDC25 proteins promote cell cycle progression by dephosphorylating these two residues. Adapted from (Brenner et al., 2014).

The CDC25 family of proteins are cell cycle regulators that act as phosphatases. They activate cyclin-dependent kinase (CDK) complexes by dephosphorylation, which in turn promote cell cycle phase progression (Figure 6.1) (Brenner et al., 2014). The functions of the CDC25 family are highly conserved across species. In *Drosophila*, String is the ortholog of CDC25 family (Edgar and O'Farrell, 1990). In mammalians, CDC25 family exists in three isoforms: CDC25A, CDC25B and CDC25C (Boutros et al., 2007). CDC25A mainly promotes G_1 to S phase transition

by activating the CDK2-Cyclin E and CDK2-Cyclin A complexes (Blomberg and Hoffmann, 1999, Hoffmann et al., 1994) whereas CDC25B/C promote G_2 to M phase transition primarily (Millar et al., 1991, Gabrielli et al., 1996). Nevertheless, CDC25A has also been shown to regulate G_2/M phase progression (Mailand et al., 2002) and this is supported by studies that found no apparent cell cycle phenotype in *Cdc25b* single (Lincoln et al., 2002), *Cdc25C* single (Chen et al., 2001) and *Cdc25b/c* double (Ferguson et al., 2005) knockout mouse models. CDC25 family might have a role in regulation of cell cycle entry/exit (G_0 to G_1 transition) as a recently discovered CDC25 inhibitor (NSC 119915) was found to arrest cells in the G_0/G_1 and G_2/M phase transitions of the cell cycle (Lavecchia et al., 2012). Furthermore, regulation of *Cdc25* expression has been implicated in quiescence (G_0) maintenance and exit in naïve and activated T-cells respectively (Yusuf and Fruman, 2003). However, it is currently unknown if CDC25 family regulates CDK3-Cyclin C complex which was found to be required for quiescence exit (Ren and Rollins, 2004).

In the previous chapters, we provide evidence that TRIB2 negatively regulates the proliferation of immature developing thymocytes during thymopoiesis at steady state and under stress conditions. However, the mechanism underlying the anti-proliferative role of TRIB2 is unknown. In *Drosophila*, Tribbles was shown to promote the proteasomal dependent degradation of String in order to coordinate cell division and morphogenesis during embryonic development (Grosshans and Wieschaus, 2000, Seher and Leptin, 2000, Mata et al., 2000). Furthermore, TRIB3 was found to interact with CDC25A and regulate its expression (Sakai et al., 2010). Hence, we aimed to determine if the function of *Drosophila* Tribbles-mediated degradation of String is conserved in TRIB2.

6.2 Results

6.2.1 TRIB2 binds to CDC25B/C but not CDC25A.

To examine the interaction of TRIB2 with all three isoforms of CDC25 family, we overexpressed tagged versions of the proteins in HeLa cells and performed co-immunoprecitation binding assays. Upon immunoprecipitation with anti-FLAG antibody and western blotting with anti-MYC antibody, we found that TRIB2 co-immunoprecipitated with human CDC25B and CDC25C but not CDC25A (Figure 6.2A). Hence, TRIB2 interaction with CDC25 family is selective and, in contrast to TRIB3, does not interact with CDC25A. Alignment of amino acid sequences of CDC25B/C between human and mouse orthologs showed that amino acid residues from 206 to 254 from the human CDC25C ortholog were absent in mouse (Figure 6.2B). Nevertheless, we found that TRIB2 bound to both human and mouse CDC25C orthologs (Figure 6.2C). This suggests TRIB2 and CDC25C interaction is conserved in mouse, and rules out the region containing the 206-254 amino acid residues of human CDC25C as the binding site for TRIB2. Lastly, overexpressed TRIB2 was found to bind to the endogenously expressed CDC25C in HeLa cells (Figure 6.2D), showing that endogenously and exogenously expressed CDC25C interact with TRIB2.
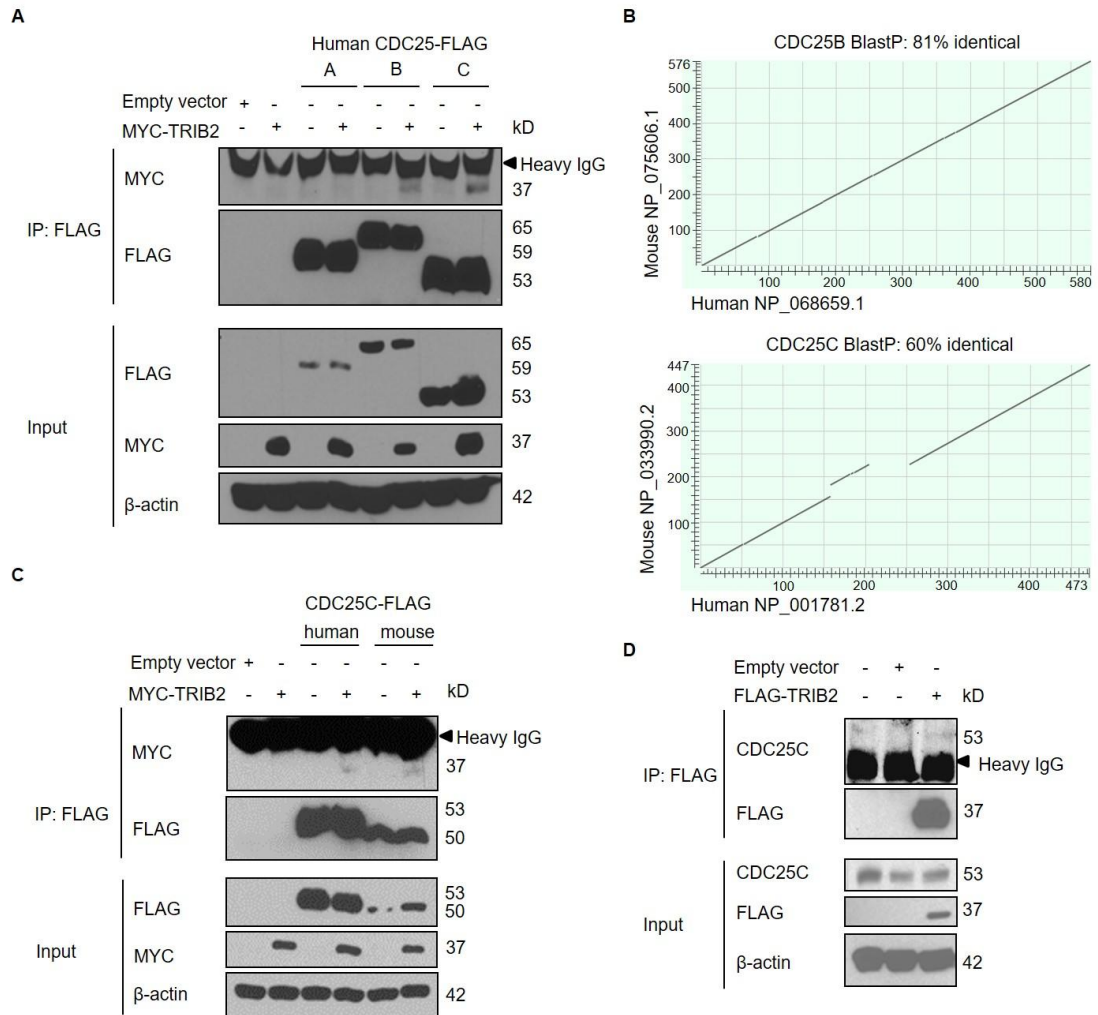
Figure 6.2 │ TRIB2 interacts with isoform B and C of CDC25 family. (A) Interaction of MYC-tagged TRIB2 with different isoforms of FLAG-tagged CDC25 family was examined by co-immunoprecipitation (co-IP). IP, immunoprecipitation. **(B)** Similarity of amino acid sequences of different orthologs (human and mouse) for CDC25B and CDC25C was examined by BlastP program and presented as dot matrix views. **(C)** Interaction of MYC-tagged TRIB2 with human and mouse orthologs of FLAG-tagged CDC25C was examined by co-IP. **(D)** Interaction of FLAG-tagged TRIB2 with endogenous CDC25C was examined by co-IP. For **A**, **C** and **D**, HeLa cells were used for the experiments. Panel **C** and **D** are representatives of two independent experiments.

146

6.2.2 TRIB2 promotes ubiquitination and proteasomal dependent degradation of CDC25C.

To determine if TRIB2 regulates CDC25C in a similar way demonstrated in *Drosophila* (Mata et al., 2000, Seher and Leptin, 2000, Grosshans and Wieschaus, 2000), we examined the impact of TRIB2 overexpression on CDC25C protein expression levels. In HeLa cells, overexpression of TRIB2 led to a decrease in endogenous CDC25C protein expression (Figure 6.3A) indicating TRIB2 regulates CDC25C turnover. In contrast to CDC25A which is primarily a nuclear protein, CDC25B/C are held inactive in the cytoplasm and only translocate to the nucleus when they are activated in order to promote cell cycle progression (Brenner et al., 2014).On account of that, we used MG132, a proteasome inhibitor to assess degradation of endogenous CDC25C in both cellular compartments in the presence of ectopic TRIB2. Subcellular fractionation showed that endogenous CDC25C was located primarily in the cytoplasm consistent with the literature (Figure 6.3B). In vehicle-treated cells, overexpression of TRIB2 did not affect nuclear translocation of CDC25C as the expression of CDC25C protein in the nucleus remained similar compared to empty vector-transfected cells (Figure 6.3B). However, in MG132-treated cells where proteasome was inhibited, overexpression of TRIB2 led to increase level of nuclear CDC25C protein (Figure 6.3B). Shabbeer and colleagues showed that, in response to DNA damage, breast cancer type 1 susceptibility protein (BRCA1) which is an E3 ubiquitin ligase polyubiquitinates CDC25C protein to promote its degradation (Shabbeer et al., 2013). BRCA1-mediated CDC25C degradation was suggested via nuclear proteasome because, upon inhibition of protein degradation by MG132, overexpression of BRCA1 caused stabilized CDC25C to retain in the nucleus (Shabbeer et al., 2013). As such, our data suggests that TRIB2 may regulate the turnover of CDC25C in the nucleus. Intriguingly, our data also suggests that TRIB2 itself is regulated in a similar fashion (Figure 6.3B).
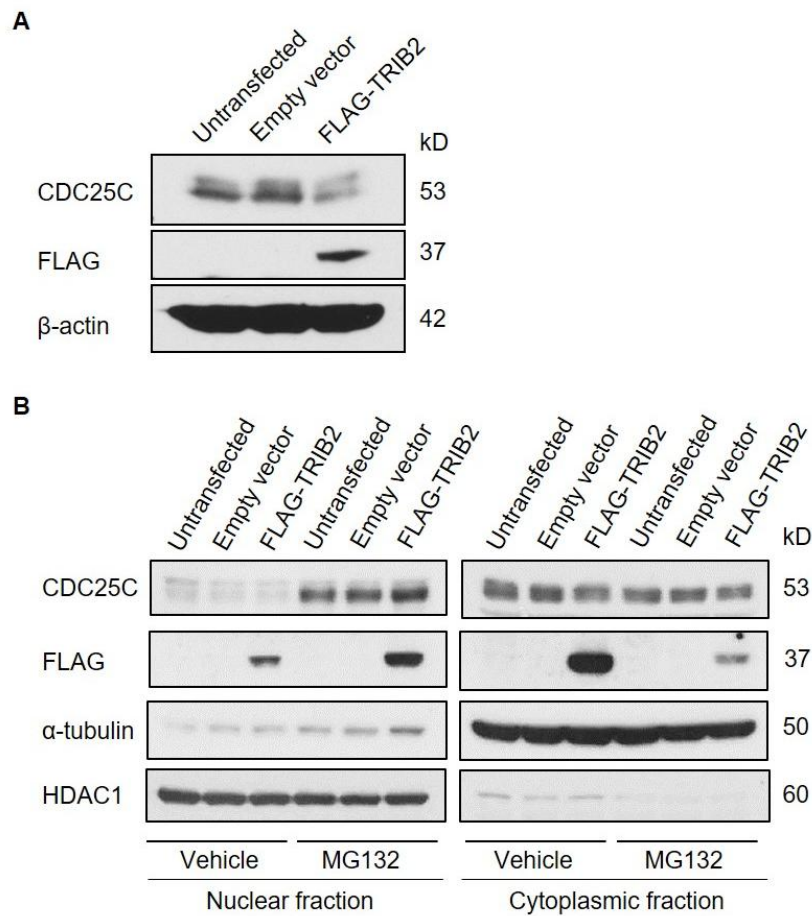
Figure 6.3 │ TRIB2 promotes proteasomal dependent degradation of CDC25C in the nucleus. (A) Whole cell lysates from FLAG-TRIB2-transfected cells and controls (untransfected and empty vector-transfected) were analyzed by Western blotting. **(B)** Cells were treated with DMSO (vehicle) or 10 µM of MG132 for 4 hours before subcellular fractionation for Western blotting analysis. α-tubulin and HDAC1 are cytoplasmic and nuclear markers respectively. For **A** and **B**, HeLa cells were used for the experiments. Panel A was a result from one experiment whereas panel **B** is a representative of two independent experiments.

TRIB2 is known to mediate the degradation of target proteins via ubiquitin proteasome system (Salome et al., 2015). Thus, we sought to determine if TRIB2 promotes ubiquitination of CDC25C. Indeed, we found that TRIB2 overexpression caused increased ubiquitination of both human and mouse CDC25C that were ectopically expressed in HeLa cells (Figure 6.4A). This is in accordance with the results of our co-immunoprecipitation assay that TRIB2 binds to both orthologs (Figure 6.2C). Furthermore, we demonstrated that TRIB2 promoted lysine (K)-48-linked polyubiquitination of endogenous CDC25C (Figure 6.4B and 6.4C). Protein ubiquitination via K48-linked ubiquitin chains is a specific cellular signal for proteasomal degradation (Komander, 2009). Hence, our results altogether suggest TRIB2 promotes polyubiquitination of CDC25C and this in turn increases proteasomal dependent degradation of CDC25C. TRIB2-mediated degradation of CEBPα requires the kinase-like domain and the C-terminal where COP1 binds to (Figure 1.3) (Keeshan et al., 2010). We performed a structure-function analysis of TRIB2 in HeLa cells to determine which domain of TRIB2 is essential for promotion of endogenous CDC25C ubiquitination. Like TRIB2 full length (FL) protein, overexpression of TRIB2 kinase-like domain (KD) alone was sufficient to drive CDC25C ubiquitination and deletion of either terminal (dN or dC) didn't affect TRIB2 function in this aspect (Figure 6.4D). Our preliminary result suggests only the kinase-like domain is crucial for TRIB2-mediated ubiquitination and possibly degradation of CDC25C.
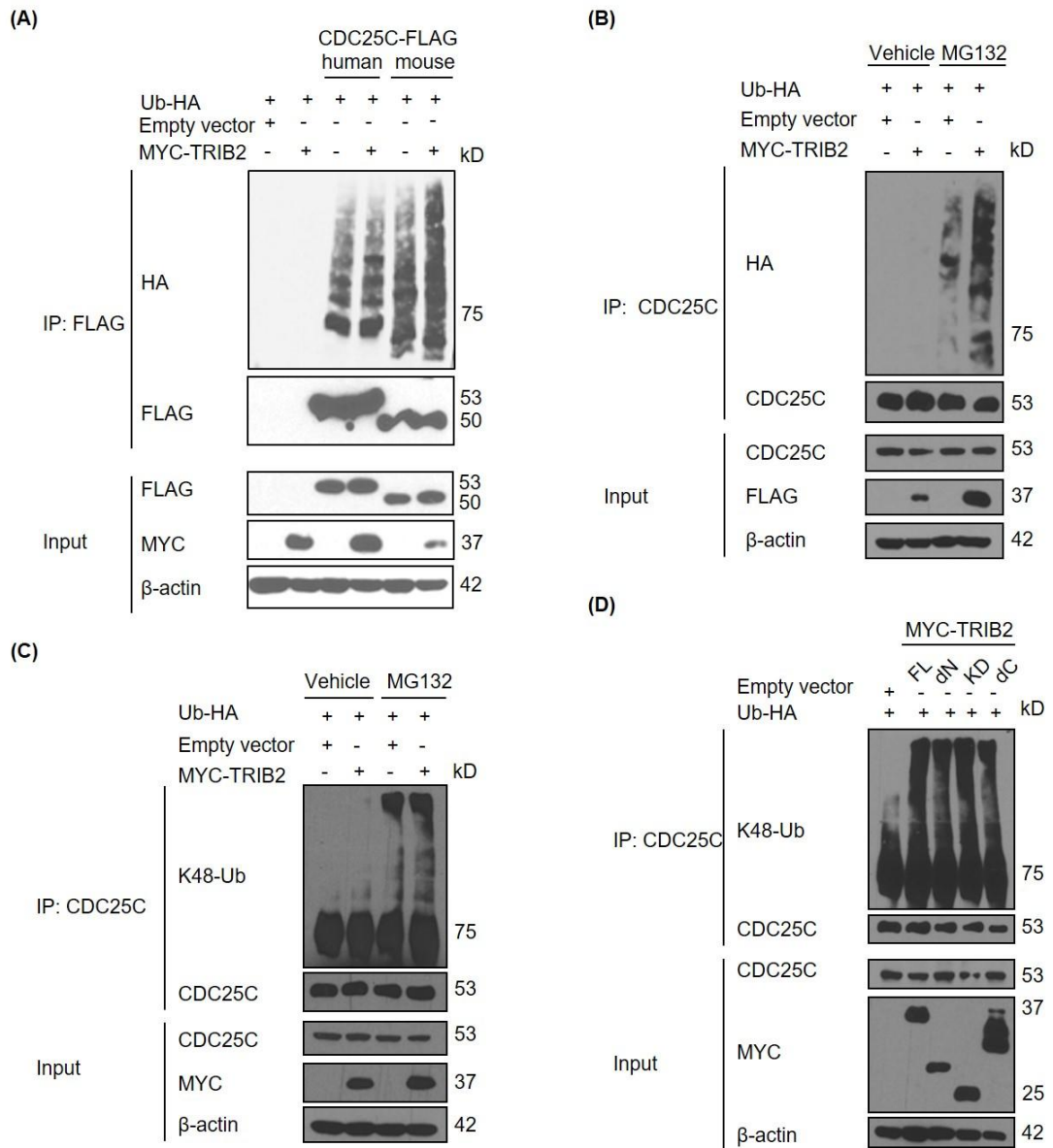
Figure 6.4 │ TRIB2 promotes K48-linked polyubiquitination of CDC25C. Impact of overexpression of MYC-tagged TRIB2 on HA-tagged ubiquitination of **(A)** human and mouse orthologs of FLAG-tagged CDC25C, and **(B)** endogenous CDC25C. Impact of overexpression of **(C)** MYC-tagged TRIB2 wild type and **(D)** different mutants on K48-linked ubiquitination of endogenous CDC25C. FL, full length; dN, N-terminal deleted; KD, only kinase domain expressed; dC, C-terminal deleted. For **A-D**, HeLa cells were used for the experiments. For **A** and **D**, all samples were treated with 10µM of MG132 for 7 hours prior cell lysis. Panel **A**, **B** and **C** are representatives of two independent experiments.

6.2.3 TRIB2 is tightly regulated during cell cycle phase progression.

Given the role of TRIB2 in regulation of CDC25B/C, we were interested to assess the expression of TRIB2 during cell cycle. We synchronized RPMI-8402, a T-ALL cell line by single thymidine block and monitored the level of *TRIB2 mRNA and* /TRIB2 protein levels as the synchronized cells resumed cell cycle following thymidine removal. DNA staining for samples collected at different time points confirmed the successful synchronization of cells. Cells were synchronized at G_1 to S phase transition (S0) by single thymidine block (Figure 6.5A). After removal of thymidine, cells entered and progressed through S phase (S12 and S15) synchronously (Figure 6.5A). At 20 hours onwards post thymidine removal, increasing fraction of cells were found in G_2/M and G_1 phases (Figure 6.5A). This was confirmed with detection of increased level of phosphorylated histone H3, a mitosis marker, in cells collected at 22 hours (S22) post thymidine removal (Figure 6.5B). We observed cyclic expression of TRIB2 protein despite no significant change at the mRNA level (Figure 6.5B and 6.5C). Increased level of TRIB2 protein was detected in S12, S17 and S22 where most of the synchronized cells were in S phase entry, S phase progression and mitotic phase respectively (Figure 6.5B). CDC25C protein level increased in S22 presumably due to its role in promoting mitotic entry (Figure 6.5B). Hence, increased expression of TRIB2 during mitotic phase could be important in regulating the activity of CDC25C.
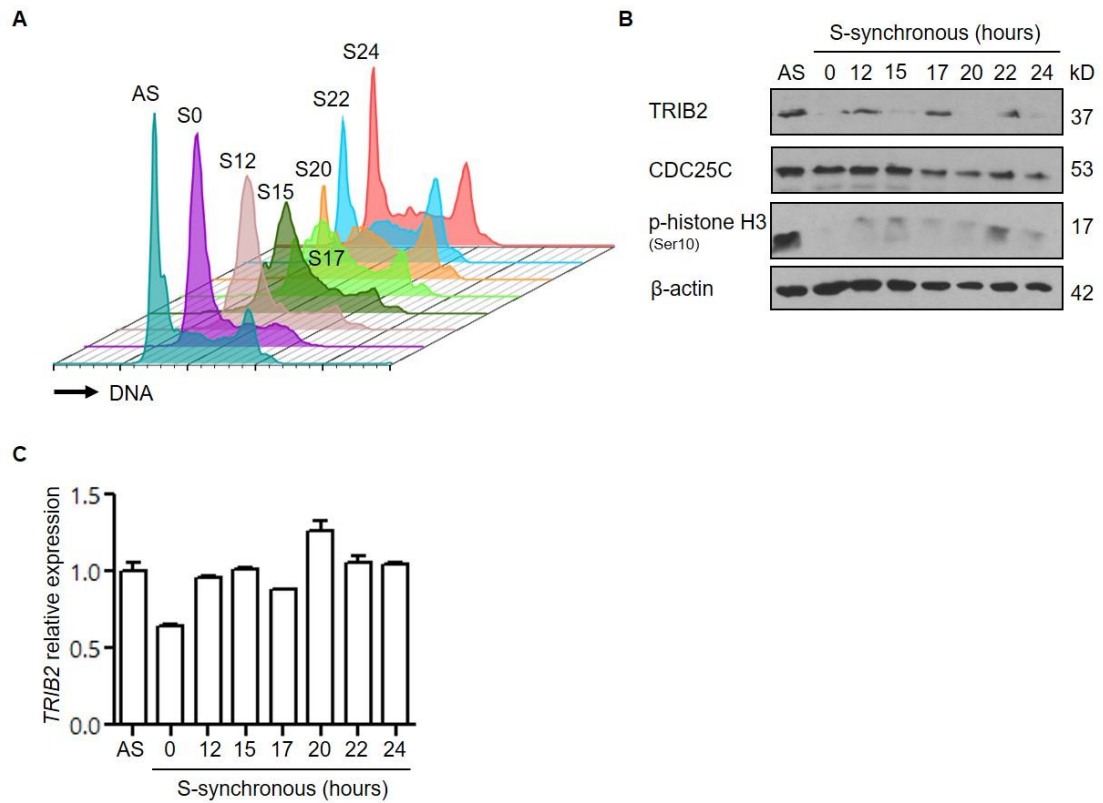
Figure 6.5 │ TRIB2 is regulated at protein level during cell cycle phase progression. Asynchronous (AS) RPMI-8402 cells were arrested by single thymidine block (S0) followed by release (S12-S24) to allow them to progress into different cell cycle phase synchronously. **(A)** Cell cycle analysis by flow cytometry. Histograms of cell cycle profile for all samples were staggered offset. **(B)** Western blotting analysis with p-histone H3 signal serves as a mitosis marker. **(C)** Expression of *TRIB2* measured by quantitative RT-PCR. All panels shown are representatives of two independent experiments.

6.3 Discussion

The relationship between TRIB2 and CDC25 family has not been studied before. Here, we showed that TRIB2 interacts physically with CDC25B/C. Similar to *Drosophila* Tribbles (Mata et al., 2000, Seher and Leptin, 2000, Grosshans and Wieschaus, 2000), we showed that TRIB2 promotes proteasomal dependent degradation of CDC25C. TRIB2 appears to degrade only active CDC25C in the nucleus and perhaps the pool of CDC25C available for TRIB2-mediated degradation may be smaller. In addition to that, we found the increase of CDC25C turnover is due to TRIB2 mediated K48-linked polyubiquitination of CDC25C. Hence, the function of *Drosophila* Tribbles is evolutionarily conserved in TRIB2.

Owing to the critical roles of CDC25 family in cell cycle regulation, the expression of CDC25 proteins is tightly regulated. CDC25C activity is controlled primarily by two mechanisms at the post-translational level. The first mechanism involves phosphorylation of CDC25C at Serine 216 which results in binding of CDC25C with 14-3-3 protein and subsequently CDC25C sequestration in the cytoplasm (Boutros et al., 2007). The other mechanism regulates CDC25C activity by proteasomal dependent degradation. Two E3 ubiquitin ligases have been identified so far that work independently of each other to regulate CDC25C at different cell cycle phase transitions. CDC25C is targeted by anaphase-promoting complex/cyclosome (APC/C) (Chen et al., 2002, Pfleger and Kirschner, 2000) for degradation upon mitotic exit whereas BRCA1 (Shabbeer et al., 2013) ubiquitinates CDC25C to prevent mitotic entry. We showed that TRIB2 promotes polyubiquitination and degradation of CDC25C. It is likely that TRIB2 functions as an adaptor for an as yet unidentified E3 ubiquitin ligase that ubiquitinates CDC25C. TRIB2 has previously been shown to function as an adaptor mediating the

degradation of CEBPα via COP1 E3 ligase in AML (Keeshan et al., 2010) or TRIM21 E3 ligase in lung cancer (Grandinetti et al., 2011).

CDC25C is tightly regulated in the steady state cell cycle as well as in response to stress such as DNA damage that induces G_2/M checkpoint (Boutros et al., 2007). The checkpoint following stress is important to allow cells to repair damaged DNA before resuming cell cycle. MAPK signalling appears to regulate CDC25C in both steady state cell cycle and checkpoint pathways. During cell cycle at steady state, phosphorylation of CDC25C at Threonine 48 by ERK leads to CDC25C activation and promotion of mitotic entry (Wang et al., 2007). We have shown that in cells lacking TRIB2 (Figure 5.4E), that there is loss of ERK activation. However, in response to stress and DNA damage, activated ERK has been shown to phosphorylate CDC25C at Serine 216 which in turn promotes CDC25C ubiquitination and proteasomal degradation (Eymin et al., 2006). In this study, the authors did not show whether the pool of ubiquitinated CDC25C was nuclear or cytoplasmic. JNK was shown to inactivate CDC25C by direct phosphorylation at Serine 168 to regulate mitotic entry and G_2/M DNA damage checkpoint (Gutierrez et al., 2010). Lastly, p38 induces cytoplasmic sequestration and thus inactivation of CDC25C indirectly via MAPK-activated protein kinase 2 (MK2) in response to DNA damage (Manke et al., 2005). In the previous chapter, we showed that TRIB2 controls T-ALL via MAPK modulation. Hence, further studies are warranted to examine TRIB2/MAPK/CDC25 axis in normal and malignant haemopoiesis.

The experimental works reported in this chapter help to provide a framework for strategic planning in further investigation of the cellular impacts of TRIB2 and CDC25C interaction. It remains to be clarified if TRIB2-CDC25C interaction affects a specific cell cycle phase transition and if the interaction underlies the anti-proliferative role of TRIB2 in immature developing thymocytes.

CHAPTER SEVEN: GENERAL DISCUSSION

A recent study that showed TRIB2 is capable of auto-phosphorylation challenges the current classification of Tribbles family as pseudokinases (Bailey et al., 2015). Like CASK (Mukherjee et al., 2008), TRIB2 could be an atypical kinase with specific substrates. Indeed, a screen for the physiological substrates of TRIB2 has not been documented although TRIB3 kinase activity had been assessed by *in vitro* kinase assay with selected substrates (Bowers et al., 2003). For TRIB2, substrate screening has been hindered by its unknown physiological role. Now, our works have uncovered a role for TRIB2 in the thymus where it regulates the proliferation of immature developing thymocytes. Hence, substrate screening for TRIB2 could be examined in the thymus and in these thymocytes where the physiological TRIB2-putative interacting proteins are expressed. This could be achieved with the recent development of kinase-interacting substrate screening (Amano et al., 2015) and is important for the elucidation of physiological TRIB2 signalling network in the thymus.

During *Drosophila* embryonic development, the anti-proliferative role of Tribbles is necessary to coordinate cellular proliferation and morphogenesis (Mata et al., 2000, Seher and Leptin, 2000, Grosshans and Wieschaus, 2000). In the thymus, we speculate that TRIB2 is important for the establishment of T-cell identity and the anti-proliferative role of TRIB2 is required to restrain self-renewal activity of uncommitted thymic progenitors (DN1 and DN2a) for T-cell specification and commitment. *Trib2* was shown to be regulated by transcription factors (PU.1, NOTCH and GATA3) that control a lympho-myeloid switch during early T-cell development (Del Real and Rothenberg, 2013). PU.1 is a progenitor cell transcription factor highly expressed initially in DN1 and DN2a progenitors where they retain multi-lineage plasticity but are repressed in DN2b stage where the

progenitors become committed to T-cell lineage (Yui et al., 2010). It is required for the expansion of DN1 and DN2 progenitors while restraining their differentiation by temporally restricting activation of the T-lineage developmental programme (Champhekar et al., 2015). Nevertheless, forced overexpression of PU.1 can divert these early uncommitted progenitors to a myeloid lineage which in normal conditions is inhibited by thymic NOTCH signalling (Franco et al., 2006). In contrast to PU.1, GATA3 is a T-lineage transcription factor. *Gata3* expression is turned on by NOTCH signalling in DN1 progenitors and remains stable at later stages (DP) of T-cell development. GATA3 is essential for development of the T-lineage as loss of GATA3 affects multiple T-cell developmental stages (Rothenberg and Scripture-Adams, 2008). To understand the myeloid versus T-cell fate choice, Del Real and colleagues studied the interactions between PU.1, GATA3 and NOTCH1 signalling in Scid.adh.2C2 cells, a DN3-like clonal early T-cell line that do not express endogenous PU.1 (Del Real and Rothenberg, 2013). *Trib2* was downregulated in diverted PU.1-overexpressing Scid.adh.2C2 cells which had increased expression of CD11b (Del Real and Rothenberg, 2013). This indicates *Trib2* is a T-lineage gene and is repressed by PU.1. Indeed, ChIP-seq analysis showed that *Trib2* is bound by PU.1 in DN1 and DN2a but not in DN2b T-lineage committed progenitors (Zhang et al., 2012d). In contrast, *Trib2* was upregulated by elevated NOTCH1 signalling in myeloid diversion-protected Scid.adh.2C2 cells that co-overexpressed PU.1 and ICN1 (Del Real and Rothenberg, 2013). This is not surprising as *Trib2* has been shown previously as a direct target of NOTCH1 (Wouters et al., 2007). Lastly, *Trib2* downregulation was dampened in PU.1-overexpressing Scid.adh.2C2 cells which had GATA3 knockdown and were more sensitive to myeloid diversion (Del Real and Rothenberg, 2013). This suggests regulation of *Trib2* by GATA3 and ChIP-seq analysis showed that *Trib2* is bound by GATA3 in uncommitted DN1, committed DN2b progenitors and DP mature cells (Zhang et al., 2012d). Intriguingly, a separate study aimed to characterize T cell lineage commitment

found that uncommitted DN1 and DN2a progenitors undergo similar extensive proliferation but committed DN2b cells proliferate at a slower rate, as assessed by carboxyfluorescein succinimidyl ester dilution, on OP9-DL1 co-culture system (Yui et al., 2010). This was not pursued further in the study but it highlights a potential coordination between cellular proliferation and commitment as the thymic progenitors develop. Given the anti-proliferative role of TRIB2 in these developing thymocytes and the connection of *Trib2* with PU.1, GATA3 and NOTCH1, future study is warranted to examine the role of *Trib2* in T-lineage commitment.

As mentioned in the third chapter, our data suggests that TRIB2 could have another distinct role in thymocytes beyond the DN stage. In the absence of TRIB2, increased number of DP thymocytes due to increased proliferation of DN thymocytes resulted in increased CD4 but not CD8 T cell maturation. However, this did not affect the size of peripheral T-cell pool. Hence, TRIB2 may impact on thymic selection, maturation of DP to SP thymocytes or thymic T-cell export. We speculate that the role of TRIB2 in the later stages of T-cell development (thymic selection and DP-SP maturation) is connected to its relationship with MAPK signalling. Thymic selection is a critical checkpoint at the DP stage for the generation of mature T-cells that can respond to foreign antigens without mounting an auto-immune response to self antigens. With low-avidity interactions between TCR and self-peptide-major histocompatibility complex (MHC) complexes, DP thymocytes that are normally destined to 'death-by-neglect' are signalled to survive and differentiate further (positive selection). However, high-avidity interactions between TCRs and self-peptide-MHC complexes lead to apoptosis induction instead (negative selection). MAPK signalling, initiated by TCR-ligand interactions, appears to be important in both selections. Positively-selecting ligands that promote survival generate a weaker but sustained activation of ERK signalling whereas negatively-selecting ligands that induce death generate a robust but transient activation of ERK

signalling (Daniels et al., 2006, McNeil et al., 2005). ERK expression is indispensable in positive selection (Fischer et al., 2005, Pages et al., 1999) compared to negative selection (McGargill et al., 2009) where p38 and JNK activation are more critical (Sugawara et al., 1998, Rincon et al., 1998). ERK and p38 are also important in the maturation of thymocytes from DP to SP stage. p38 activation (Fernandez, 2000) is required in the generation of both CD4 and CD8 SP T-cells whereas ERK activation (Sharp et al., 1997, Fischer et al., 2005) is important for the development of CD4 rather than CD8 SP T-cells. We demonstrated that TRIB2 is required for the regulation of MAPK signalling in leukaemic T-cells, and we showed reduced p38 signalling in $Trib2^{-/-}$ DN2 and $DN3_L$ thymocytes. Hence, future study should assess the impact of TRIB2 loss on thymic selection with further characterization of DP thymocytes (Mingueneau et al., 2013) and the MAPK status in these cells.

TRIB2 is highly conserved in mouse and human with 99.2% of similarity in amino acid sequences. Hence, study of TRIB2 in the mouse organism is important and relevant for the elucidation of its role in the human setting. So far, $Trib2$ knock out mouse models ($Trib2^{tm1Ryn}$ (Takasato et al., 2008), $Trib2^{tm1Lex}$ (Rishi et al., 2014) and $Trib2^{tm1Myam}$ (Satoh et al., 2013)) have been generated by germline deletion of $Trib2$. Stage or cell-type specific disruption of $Trib2$ could be useful in dissecting the role of TRIB2 in the development and differentiation of a specific haematopoietic lineage. This could be accomplished by CRE-recombinase mediated conditional deletion of $Lox-P$ site flanked $Trib2$ gene. Many different Cre-transgenic mouse lines have been developed where expression of Cre recombinase is under the control of cell-type specific promoter and hence enabling cell-type specific gene deletion. For example, $Vav1$ promoter driven Cre expression (Ogilvy et al., 1999) would allow deletion of $Trib2$ in HSCs and hence all their descendents whereas human $CD2$ promoter driven Cre expression (de Boer et al., 2003) would allow

deletion of *Trib2* in T- and B-lymphoid cells. Other mouse lines that are of relevance to study of TRIB2 in T-cell development include *Lck* proximal promoter and *Cd4* promoter/enhancer/silencer driven *Cre* expression which enable disruption of gene at DN and DP stage respectively (Lee et al., 2001).

In summary, the works presented in this thesis uncovered a previously unrecognized role for TRIB2 in negatively regulating the cell division kinetics of developing thymocytes. This is the first physiological role that we established for TRIB2 in steady state and stress haematopoiesis. We demonstrated that TRIB2 regulates the homeostasis of intrathymic T-cell development at steady state. The anti-proliferative role of TRIB2 is crucial to control the response of thymocytes to genotoxic stress. We showed that, in the absence of TRIB2, proliferative thymocytes are sensitized to 5-FU-induced apoptosis. The anti-proliferative role of TRIB2 is also essential for proper recovery of thymopoiesis after genotoxic stress. We found that loss of TRIB2 causes expansion of c-Kit⁻ DN1 thymic progenitors which in turn lead to accelerated thymopoietic recovery following 5-FU mediated genotoxic stress. Next, using a NOTCH1-induced T-ALL BM transplantation model, we provided evidence that TRIB2 possesses tumour suppression function in T-cell leukaemogenesis. In the absence of TRIB2, NOTCH1 is more potent in driving T-ALL initiation and the increased aggressiveness of *Trib2*⁻/⁻ T-ALL was enhanced by impaired activation of MAPK signalling. We performed GSEA analysis to extrapolate the experimental findings of TRIB2 role in murine T-ALL to different molecular subtypes of human T-ALL. *TRIB2* expression was elevated in LYL1⁺ immature human T-ALL enriched with MAPK signalling whereas its expression was suppressed in TLX1⁺ mature human T-ALL with defective MAPK signalling. Hence, TRIB2 could be tumour promoting or suppressing depending on the subtypes of T-ALL and this is related to its capability to modulate MAPK signalling. The tumour suppressing function of TRIB2 is novel and is a paradigm shift in the definition of

TRIB2 function in malignant haematopoiesis. Last but not least, we showed that the function of *Drosophila* Tribbles in promoting degradation of String is evolutionarily conserved in TRIB2. We identified CDC25B/C as new interacting partners of TRIB2. We demonstrated that TRIB2 targets CDC25C for K48-linked polyubiquitination and degradation via nuclear proteasome. This adds another layer to how TRIB2 could regulate cellular proliferation.

Bibliography

ADOLFSSON, J., MANSSON, R., BUZA-VIDAS, N., HULTQUIST, A., LIUBA, K., JENSEN, C. T., BRYDER, D., YANG, L., BORGE, O. J., THOREN, L. A., ANDERSON, K., SITNICKA, E., SASAKI, Y., SIGVARDSSON, M. & JACOBSEN, S. E. 2005. Identification of Flt3+ lympho-myeloid stem cells lacking erythro-megakaryocytic potential a revised road map for adult blood lineage commitment. *Cell,* 121**,** 295-306.

AKASHI, K., TRAVER, D., MIYAMOTO, T. & WEISSMAN, I. L. 2000. A clonogenic common myeloid progenitor that gives rise to all myeloid lineages. *Nature,* 404**,** 193-7.

ALLMAN, D., KARNELL, F. G., PUNT, J. A., BAKKOUR, S., XU, L., MYUNG, P., KORETZKY, G. A., PUI, J. C., ASTER, J. C. & PEAR, W. S. 2001. Separation of Notch1 promoted lineage commitment and expansion/transformation in developing T cells. *J Exp Med,* 194**,** 99-106.

ALTSCHUL, S. F., GISH, W., MILLER, W., MYERS, E. W. & LIPMAN, D. J. 1990. Basic local alignment search tool. *J Mol Biol,* 215**,** 403-10.

AMANO, M., HAMAGUCHI, T., SHOHAG, M. H., KOZAWA, K., KATO, K., ZHANG, X., YURA, Y., MATSUURA, Y., KATAOKA, C., NISHIOKA, T. & KAIBUCHI, K. 2015. Kinase-interacting substrate screening is a novel method to identify kinase substrates. *J Cell Biol,* 209**,** 895-912.

ANDERSEN, M. O., NYGAARD, J. V., BURNS, J. S., RAARUP, M. K., NYENGAARD, J. R., BUNGER, C., BESENBACHER, F., HOWARD, K. A., KASSEM, M. & KJEMS, J. 2010. siRNA nanoparticle functionalization of nanostructured scaffolds enables controlled multilineage differentiation of stem cells. *Mol Ther,* 18**,** 2018-27.

ANDERSON, G. & TAKAHAMA, Y. 2012. Thymic epithelial cells: working class heroes for T cell development and repertoire selection. *Trends Immunol,* 33**,** 256-63.

AQUINO ESPERANZA, J. A., AGUIRRE, M. V., AISPURU, G. R., LETTIERI, C. N., JUARISTI, J. A., ALVAREZ, M. A. & BRANDAN, N. C. 2008. In vivo 5-fluorouracil-[corrected]induced apoptosis on murine thymocytes: involvement of FAS, Bax and Caspase3. *Cell Biol Toxicol,* 24**,** 411-22.

ARBER, D. A., ORAZI, A., HASSERJIAN, R., THIELE, J., BOROWITZ, M. J., LE BEAU, M. M., BLOOMFIELD, C. D., CAZZOLA, M. & VARDIMAN, J. W. 2016. The 2016 revision to the World Health Organization classification of myeloid neoplasms and acute leukemia. *Blood,* 127**,** 2391-405.

ARGIROPOULOS, B., PALMQVIST, L., YUNG, E., KUCHENBAUER, F., HEUSER, M., SLY, L. M., WAN, A., KRYSTAL, G. & HUMPHRIES, R. K. 2008. Linkage of Meis1 leukemogenic activity to multiple downstream effectors including Trib2 and Ccl3. *Exp Hematol,* 36**,** 845-59.

ASHWELL, J. D., LU, F. W. & VACCHIO, M. S. 2000. Glucocorticoids in T cell development and function*. *Annu Rev Immunol,* 18**,** 309-45.

ASNAFI, V., BUZYN, A., THOMAS, X., HUGUET, F., VEY, N., BOIRON, J. M., REMAN, O., CAYUELA, J. M., LHERITIER, V., VERNANT, J. P., FIERE, D., MACINTYRE, E. & DOMBRET, H. 2005. Impact of TCR status and genotype on outcome in adult T-cell acute lymphoblastic leukemia: a LALA-94 study. *Blood,* 105**,** 3072-8.

ASNAFI, V., RADFORD-WEISS, I., DASTUGUE, N., BAYLE, C., LEBOEUF, D., CHARRIN, C., GARAND, R., LAFAGE-POCHITALOFF, M., DELABESSE, E., BUZYN, A., TROUSSARD, X. & MACINTYRE, E. 2003. CALM-AF10 is a common fusion transcript in T-ALL and is specific to the TCRgammadelta lineage. *Blood,* 102**,** 1000-6.

ASTER, J. C., BODNAR, N., XU, L., KARNELL, F., MILHOLLAND, J. M., MAILLARD, I., HISTEN, G., NAM, Y., BLACKLOW, S. C. & PEAR, W. S. 2011. Notch ankyrin repeat domain variation influences leukemogenesis and Myc transactivation. *PLoS One,* 6**,** e25645.

ASTER, J. C., XU, L., KARNELL, F. G., PATRIUB, V., PUI, J. C. & PEAR, W. S. 2000. Essential roles for ankyrin repeat and transactivation domains in induction of T-cell leukemia by notch1. *Mol Cell Biol,* 20**,** 7505-15.

AWONG, G., LAMOTTE-MOHS, R. & ZUNIGA-PFLUCKER, J. C. 2010. Key players for T-cell regeneration. *Curr Opin Hematol,* 17**,** 327-32.

BAILEY, F. P., BYRNE, D. P., ORUGANTY, K., EYERS, C. E., NOVOTNY, C. J., SHOKAT, K. M., KANNAN, N. & EYERS, P. A. 2015. The Tribbles 2 (TRB2) pseudokinase binds to ATP and autophosphorylates in a metal-independent manner. *Biochem J,* 467**,** 47-62.

BASH, R. O., HALL, S., TIMMONS, C. F., CRIST, W. M., AMYLON, M., SMITH, R. G. & BAER, R. 1995. Does activation of the TAL1 gene occur in a majority of patients with T-cell acute lymphoblastic leukemia? A pediatric oncology group study. *Blood,* 86**,** 666-76.

BEERMAN, I., BOCK, C., GARRISON, B. S., SMITH, Z. D., GU, H., MEISSNER, A. & ROSSI, D. J. 2013. Proliferation-dependent alterations of the DNA methylation landscape underlie hematopoietic stem cell aging. *Cell Stem Cell,* 12**,** 413-25.

BEGLEY, C. G., APLAN, P. D., DAVEY, M. P., NAKAHARA, K., TCHORZ, K., KURTZBERG, J., HERSHFIELD, M. S., HAYNES, B. F., COHEN, D. I., WALDMANN, T. A. & ET AL. 1989. Chromosomal translocation in a human leukemic stem-cell line disrupts the T-cell antigen receptor delta-chain diversity region and results in a previously unreported fusion transcript. *Proc Natl Acad Sci U S A,* 86**,** 2031-5.

BENNETT, J. M., CATOVSKY, D., DANIEL, M. T., FLANDRIN, G., GALTON, D. A., GRALNICK, H. R. & SULTAN, C. 1991. Proposal for the recognition of minimally differentiated acute myeloid leukaemia (AML-MO). *Br J Haematol,* 78**,** 325-9.

BENZ, C. & BLEUL, C. C. 2005. A multipotent precursor in the thymus maps to the branching point of the T versus B lineage decision. *J Exp Med,* 202**,** 21-31.

BENZ, C., MARTINS, V. C., RADTKE, F. & BLEUL, C. C. 2008. The stream of precursors that colonizes the thymus proceeds selectively through the early T lineage precursor stage of T cell development. *J Exp Med,* 205**,** 1187-99.

BERGER, R., DASTUGUE, N., BUSSON, M., VAN DEN AKKER, J., PEROT, C., BALLERINI, P., HAGEMEIJER, A., MICHAUX, L., CHARRIN, C., PAGES, M. P., MUGNERET, F., ANDRIEUX, J., TALMANT, P., HELIAS, C., MAUVIEUX, L., LAFAGE-POCHITALOFF, M., MOZZICONACCI, M. J., CORNILLET-LEFEBVRE, P., RADFORD, I., ASNAFI, V., BILHOU-NABERA, C., NGUYEN KHAC, F., LEONARD, C., SPELEMAN, F., POPPE, B., BASTARD, C., TAVIAUX, S., QUILICHINI, B., HERENS, C., GREGOIRE, M. J., CAVE, H., BERNARD, O. A. & GROUPE FRANCAIS DE CYTOGENETIQUE, H. 2003. t(5;14)/HOX11L2-positive T-cell acute lymphoblastic leukemia. A collaborative study of the Groupe Francais de Cytogenetique Hematologique (GFCH). *Leukemia,* 17**,** 1851-7.

BERGERON, J., CLAPPIER, E., RADFORD, I., BUZYN, A., MILLIEN, C., SOLER, G., BALLERINI, P., THOMAS, X., SOULIER, J., DOMBRET, H., MACINTYRE, E. A. & ASNAFI, V. 2007. Prognostic and oncogenic relevance of TLX1/HOX11 expression level in T-ALLs. *Blood,* 110**,** 2324-30.

BERKOWITZ, R. D., BECKERMAN, K. P., SCHALL, T. J. & MCCUNE, J. M. 1998. CXCR4 and CCR5 expression delineates targets for HIV-1 disruption of T cell differentiation. *J Immunol,* 161**,** 3702-10.

BERZINS, S. P., BOYD, R. L. & MILLER, J. F. 1998. The role of the thymus and recent thymic migrants in the maintenance of the adult peripheral lymphocyte pool. *J Exp Med,* 187**,** 1839-48.

BHANDOOLA, A. & SAMBANDAM, A. 2006. From stem cell to T cell: one route or many? *Nat Rev Immunol,* 6**,** 117-26.

BLOMBERG, I. & HOFFMANN, I. 1999. Ectopic expression of Cdc25A accelerates the G(1)/S transition and leads to premature activation of cyclin E- and cyclin A-dependent kinases. *Mol Cell Biol,* 19**,** 6183-94.

BOEHM, T. & SWANN, J. B. 2013. Thymus involution and regeneration: two sides of the same coin? *Nat Rev Immunol,* 13**,** 831-8.

BOETTCHER, S., ZIEGLER, P., SCHMID, M. A., TAKIZAWA, H., VAN ROOIJEN, N., KOPF, M., HEIKENWALDER, M. & MANZ, M. G. 2012. Cutting edge: LPS-induced emergency myelopoiesis depends on TLR4-expressing nonhematopoietic cells. *J Immunol,* 188**,** 5824-8.

BORGES, M., BARREIRA-SILVA, P., FLORIDO, M., JORDAN, M. B., CORREIA-NEVES, M. & APPELBERG, R. 2012. Molecular and cellular mechanisms of Mycobacterium avium-induced thymic atrophy. *J Immunol,* 189**,** 3600-8.

BOUTROS, R., LOBJOIS, V. & DUCOMMUN, B. 2007. CDC25 phosphatases in cancer cells: key players? Good targets? *Nat Rev Cancer,* 7**,** 495-507.

BOWERS, A. J., SCULLY, S. & BOYLAN, J. F. 2003. SKIP3, a novel Drosophila tribbles ortholog, is overexpressed in human tumors and is regulated by hypoxia. *Oncogene,* 22**,** 2823-35.

BREKELMANS, P., VAN SOEST, P., VOERMAN, J., PLATENBURG, P. P., LEENEN, P. J. & VAN EWIJK, W. 1994. Transferrin receptor expression as a marker of immature cycling thymocytes in the mouse. *Cell Immunol,* 159**,** 331-9.

BRENET, F., KERMANI, P., SPEKTOR, R., RAFII, S. & SCANDURA, J. M. 2013. TGFbeta restores hematopoietic homeostasis after myelosuppressive chemotherapy. *J Exp Med,* 210**,** 623-39.

BRENNER, A. K., REIKVAM, H., LAVECCHIA, A. & BRUSERUD, O. 2014. Therapeutic targeting the cell division cycle 25 (CDC25) phosphatases in human acute myeloid leukemia--the possibility to target several kinases through inhibition of the various CDC25 isoforms. *Molecules,* 19**,** 18414-47.

BROWN, L., CHENG, J. T., CHEN, Q., SICILIANO, M. J., CRIST, W., BUCHANAN, G. & BAER, R. 1990. Site-specific recombination of the tal-1 gene is a common occurrence in human T cell leukemia. *EMBO J,* 9**,** 3343-51.

BYEON, I. J., LI, H., SONG, H., GRONENBORN, A. M. & TSAI, M. D. 2005. Sequential phosphorylation and multisite interactions characterize specific target recognition by the FHA domain of Ki67. *Nat Struct Mol Biol,* 12**,** 987-93.

CABEZAS-WALLSCHEID, N. & TRUMPP, A. 2016. STEM CELLS. Potency finds its niches. *Science,* 351**,** 126-7.

CARLSON, K. M., VIGNON, C., BOHLANDER, S., MARTINEZ-CLIMENT, J. A., LE BEAU, M. M. & ROWLEY, J. D. 2000. Identification and molecular characterization of CALM/AF10fusion products in T cell acute lymphoblastic leukemia and acute myeloid leukemia. *Leukemia,* 14**,** 100-4.

CARPENTER, A. C. & BOSSELUT, R. 2010. Decision checkpoints in the thymus. *Nat Immunol,* 11**,** 666-73.

CARROLL, A. J., CRIST, W. M., LINK, M. P., AMYLON, M. D., PULLEN, D. J., RAGAB, A. H., BUCHANAN, G. R., WIMMER, R. S. & VIETTI, T. J. 1990. The t(1;14)(p34;q11) is nonrandom and restricted to T-cell acute lymphoblastic leukemia: a Pediatric Oncology Group study. *Blood,* 76**,** 1220-4.

CASERO, D., SANDOVAL, S., SEET, C. S., SCHOLES, J., ZHU, Y., HA, V. L., LUONG, A., PAREKH, C. & CROOKS, G. M. 2015. Long non-coding RNA profiling of human lymphoid progenitor cells reveals transcriptional divergence of B cell and T cell lineages. *Nat Immunol,* 16**,** 1282-91.

CAUWELIER, B., CAVE, H., GERVAIS, C., LESSARD, M., BARIN, C., PEROT, C., VAN DEN AKKER, J., MUGNERET, F., CHARRIN, C., PAGES, M. P., GREGOIRE, M. J., JONVEAUX, P., LAFAGE-POCHITALOFF, M., MOZZICCONACCI, M. J., TERRE, C., LUQUET, I., CORNILLET-LEFEBVRE, P., LAURENCE, B., PLESSIS, G., LEFEBVRE, C., LEROUX, D., ANTOINE-POIREL, H., GRAUX, C., MAUVIEUX, L., HEIMANN, P., CHALAS, C., CLAPPIER, E., VERHASSELT, B., BENOIT, Y., MOERLOOSE, B. D., POPPE, B., VAN ROY, N., KEERSMAECKER, K. D., COOLS, J., SIGAUX, F., SOULIER, J., HAGEMEIJER, A., PAEPE, A. D., DASTUGUE, N., BERGER, R. & SPELEMAN, F. 2007. Clinical, cytogenetic and molecular characteristics of 14 T-ALL patients carrying the TCRbeta-HOXA rearrangement: a study of the Groupe Francophone de Cytogenetique Hematologique. *Leukemia,* 21**,** 121-8.

CHAMPHEKAR, A., DAMLE, S. S., FREEDMAN, G., CAROTTA, S., NUTT, S. L. & ROTHENBERG, E. V. 2015. Regulation of early T-lineage gene expression and developmental progression by the progenitor cell transcription factor PU.1. *Genes Dev,* 29**,** 832-48.

CHAUDHURY, S. S., MORISON, J. K., GIBSON, B. E. & KEESHAN, K. 2015. Insights into cell ontogeny, age, and acute myeloid leukemia. *Exp Hematol,* 43**,** 745-55.

CHEN, F., ZHANG, Z., BOWER, J., LU, Y., LEONARD, S. S., DING, M., CASTRANOVA, V., PIWNICA-WORMS, H. & SHI, X. 2002. Arsenite-induced Cdc25C degradation is through the KEN-box and ubiquitin–

proteasome pathway. *Proceedings of the National Academy of Sciences,* 99**,** 1990-1995.

CHEN, M. S., HUROV, J., WHITE, L. S., WOODFORD-THOMAS, T. & PIWNICA-WORMS, H. 2001. Absence of apparent phenotype in mice lacking Cdc25C protein phosphatase. *Mol Cell Biol,* 21**,** 3853-61.

CHEN, Q., CHENG, J. T., TASI, L. H., SCHNEIDER, N., BUCHANAN, G., CARROLL, A., CRIST, W., OZANNE, B., SICILIANO, M. J. & BAER, R. 1990. The tal gene undergoes chromosome translocation in T cell leukemia and potentially encodes a helix-loop-helix protein. *EMBO J,* 9**,** 415-24.

CHIANG, M. Y., XU, M. L., HISTEN, G., SHESTOVA, O., ROY, M., NAM, Y., BLACKLOW, S. C., SACKS, D. B., PEAR, W. S. & ASTER, J. C. 2006. Identification of a conserved negative regulatory sequence that influences the leukemogenic activity of NOTCH1. *Mol Cell Biol,* 26**,** 6261-71.

CIMINO, G., SPROVIERI, T., RAPANOTTI, M. C., FOA, R., MECUCCI, C. & MANDELLI, F. 2001. Molecular evaluation of the NUP98/RAP1GDS1 gene frequency in adults with T-acute lymphoblastic leukemia. *Haematologica,* 86**,** 436-7.

CLAPPIER, E., CUCCUINI, W., CAYUELA, J. M., VECCHIONE, D., BARUCHEL, A., DOMBRET, H., SIGAUX, F. & SOULIER, J. 2006. Cyclin D2 dysregulation by chromosomal translocations to TCR loci in T-cell acute lymphoblastic leukemias. *Leukemia,* 20**,** 82-6.

CLEARY, M. L., MELLENTIN, J. D., SPIES, J. & SMITH, S. D. 1988. Chromosomal translocation involving the beta T cell receptor gene in acute leukemia. *J Exp Med,* 167**,** 682-7.

COBALEDA, C., JOCHUM, W. & BUSSLINGER, M. 2007. Conversion of mature B cells into T cells by dedifferentiation to uncommitted progenitors. *Nature,* 449**,** 473-7.

CREUTZIG, U., VAN DEN HEUVEL-EIBRINK, M. M., GIBSON, B., DWORZAK, M. N., ADACHI, S., DE BONT, E., HARBOTT, J., HASLE, H., JOHNSTON, D., KINOSHITA, A., LEHRNBECHER, T., LEVERGER, G., MEJSTRIKOVA, E., MESHINCHI, S., PESSION, A., RAIMONDI, S. C., SUNG, L., STARY, J., ZWAAN, C. M., KASPERS, G. J. & REINHARDT, D. 2012. Diagnosis and management of acute myeloid leukemia in children and adolescents: recommendations from an international expert panel. *Blood,* 120**,** 3187-205.

CVETKOVIC-LOPES, V., BAYER, L., DORSAZ, S., MARET, S., PRADERVAND, S., DAUVILLIERS, Y., LECENDREUX, M., LAMMERS, G. J., DONJACOUR, C. E., DU PASQUIER, R. A., PFISTER, C., PETIT, B., HOR, H., MUHLETHALER, M. & TAFTI, M. 2010. Elevated Tribbles homolog 2-specific antibody levels in narcolepsy patients. *J Clin Invest,* 120**,** 713-9.

D'ANGIO, M., VALSECCHI, M. G., TESTI, A. M., CONTER, V., NUNES, V., PARASOLE, R., COLOMBINI, A., SANTORO, N., VAROTTO, S., CANIGLIA, M., SILVESTRI, D., CONSARINO, C., LEVATI, L., MAGRIN, E., LOCATELLI, F., BASSO, G., FOA, R., BIONDI, A. & CAZZANIGA, G. 2015. Clinical features and outcome of SIL/TAL1-positive T-cell acute lymphoblastic leukemia in children and adolescents: a 10-year experience of the AIEOP group. *Haematologica,* 100**,** e10-3.

DAIL, M., LI, Q., MCDANIEL, A., WONG, J., AKAGI, K., HUANG, B., KANG, H. C., KOGAN, S. C., SHOKAT, K., WOLFF, L., BRAUN, B. S. & SHANNON, K. 2010. Mutant Ikzf1, KrasG12D, and Notch1 cooperate in T lineage leukemogenesis and modulate responses to targeted agents. *Proc Natl Acad Sci U S A,* 107**,** 5106-11.

DANIELS, M. A., TEIXEIRO, E., GILL, J., HAUSMANN, B., ROUBATY, D., HOLMBERG, K., WERLEN, G., HOLLANDER, G. A., GASCOIGNE, N. R. & PALMER, E. 2006. Thymic selection threshold defined by compartmentalization of Ras/MAPK signalling. *Nature,* 444**,** 724-9.

DE BOER, J., WILLIAMS, A., SKAVDIS, G., HARKER, N., COLES, M., TOLAINI, M., NORTON, T., WILLIAMS, K., RODERICK, K., POTOCNIK, A. J. & KIOUSSIS, D. 2003. Transgenic mice with hematopoietic and lymphoid specific expression of Cre. *Eur J Immunol,* 33**,** 314-25.

DE KEERSMAECKER, K., GRAUX, C., ODERO, M. D., MENTENS, N., SOMERS, R., MAERTENS, J., WLODARSKA, I., VANDENBERGHE, P., HAGEMEIJER, A., MARYNEN, P. & COOLS, J. 2005. Fusion of EML1 to ABL1 in T-cell acute lymphoblastic leukemia with cryptic t(9;14)(q34;q32). *Blood,* 105**,** 4849-52.

DEDHIA, P. H., KEESHAN, K., ULJON, S., XU, L., VEGA, M. E., SHESTOVA, O., ZAKS-ZILBERMAN, M., ROMANY, C., BLACKLOW, S. C. & PEAR, W. S. 2010. Differential ability of Tribbles family members to promote degradation of C/EBPalpha and induce acute myelogenous leukemia. *Blood,* 116**,** 1321-8.

DEL REAL, M. M. & ROTHENBERG, E. V. 2013. Architecture of a lymphomyeloid developmental switch controlled by PU.1, Notch and Gata3. *Development,* 140**,** 1207-19.

DIEHL, N. L., ENSLEN, H., FORTNER, K. A., MERRITT, C., STETSON, N., CHARLAND, C., FLAVELL, R. A., DAVIS, R. J. & RINCON, M. 2000. Activation of the p38 mitogen-activated protein kinase pathway arrests cell cycle progression and differentiation of immature thymocytes in vivo. *J Exp Med,* 191**,** 321-34.

DUBE, I. D., KAMEL-REID, S., YUAN, C. C., LU, M., WU, X., CORPUS, G., RAIMONDI, S. C., CRIST, W. M., CARROLL, A. J., MINOWADA, J. & ET AL. 1991. A novel human homeobox gene lies at the chromosome 10 breakpoint in lymphoid neoplasias with chromosomal translocation t(10;14). *Blood,* 78**,** 2996-3003.

DURINCK, K., GOOSSENS, S., PEIRS, S., WALLAERT, A., VAN LOOCKE, W., MATTHIJSSENS, F., PIETERS, T., MILANI, G., LAMMENS, T., RONDOU, P., VAN ROY, N., DE MOERLOOSE, B., BENOIT, Y., HAIGH, J., SPELEMAN, F., POPPE, B. & VAN VLIERBERGHE, P. 2015. Novel biological insights in T-cell acute lymphoblastic leukemia. *Exp Hematol*.

EDER, K., GUAN, H., SUNG, H. Y., FRANCIS, S. E., CROSSMAN, D. C. & KISS-TOTH, E. 2008a. LDL uptake by monocytes in response to inflammation is MAPK dependent but independent of tribbles protein expression. *Immunol Lett,* 116**,** 178-83.

EDER, K., GUAN, H., SUNG, H. Y., WARD, J., ANGYAL, A., JANAS, M., SARMAY, G., DUDA, E., TURNER, M., DOWER, S. K., FRANCIS, S. E., CROSSMAN, D. C. & KISS-TOTH, E. 2008b. Tribbles-2 is a novel regulator of inflammatory activation of monocytes. *Int Immunol,* 20**,** 1543-50.

EDGAR, B. A. & O'FARRELL, P. H. 1990. The three postblastoderm cell cycles of Drosophila embryogenesis are regulated in G2 by string. *Cell,* 62**,** 469-80.

EICHHORST, S. T., MUERKOSTER, S., WEIGAND, M. A. & KRAMMER, P. H. 2001. The chemotherapeutic drug 5-fluorouracil induces apoptosis in mouse thymocytes in vivo via activation of the CD95(APO-1/Fas) system. *Cancer Res,* 61**,** 243-8.

ELLISEN, L. W., BIRD, J., WEST, D. C., SORENG, A. L., REYNOLDS, T. C., SMITH, S. D. & SKLAR, J. 1991. TAN-1, the human homolog of the Drosophila notch gene, is broken by chromosomal translocations in T lymphoblastic neoplasms. *Cell,* 66**,** 649-61.

ERIKSON, J., FINGER, L., SUN, L., AR-RUSHDI, A., NISHIKURA, K., MINOWADA, J., FINAN, J., EMANUEL, B. S., NOWELL, P. C. & CROCE, C. M. 1986. Deregulation of c-myc by translocation of the alpha-locus of the T-cell receptor in T-cell leukemias. *Science,* 232**,** 884-6.

EYMIN, B., CLAVERIE, P., SALON, C., BRAMBILLA, C., BRAMBILLA, E. & GAZZERI, S. 2006. p14ARF Triggers G2 Arrest Through ERK-Mediated Cdc25C Phosphorylation, Ubiquitination and Proteasomal Degradation. *Cell Cycle,* 5**,** 759-765.

FALINI, B., MECUCCI, C., TIACCI, E., ALCALAY, M., ROSATI, R., PASQUALUCCI, L., LA STARZA, R., DIVERIO, D., COLOMBO, E., SANTUCCI, A., BIGERNA, B., PACINI, R., PUCCIARINI, A., LISO, A., VIGNETTI, M., FAZI, P., MEANI, N., PETTIROSSI, V., SAGLIO, G., MANDELLI, F., LO-COCO, F., PELICCI, P. G. & MARTELLI, M. F. 2005. Cytoplasmic nucleophosmin in acute myelogenous leukemia with a normal karyotype. *N Engl J Med,* 352**,** 254-66.

FERGUSON, A. M., WHITE, L. S., DONOVAN, P. J. & PIWNICA-WORMS, H. 2005. Normal cell cycle and checkpoint responses in mice and cells lacking Cdc25B and Cdc25C protein phosphatases. *Mol Cell Biol,* 25**,** 2853-60.

FERNANDEZ, E. 2000. Thymocyte development past the CD4(+)CD8(+) stage requires an active p38 mitogen-activated protein kinase. *Blood,* 95**,** 1356-61.

FERRANDO, A. A., HERBLOT, S., PALOMERO, T., HANSEN, M., HOANG, T., FOX, E. A. & LOOK, A. T. 2004. Biallelic transcriptional activation of oncogenic transcription factors in T-cell acute lymphoblastic leukemia. *Blood,* 103**,** 1909-11.

FERRANDO, A. A., NEUBERG, D. S., STAUNTON, J., LOH, M. L., HUARD, C., RAIMONDI, S. C., BEHM, F. G., PUI, C. H., DOWNING, J. R., GILLILAND, D. G., LANDER, E. S., GOLUB, T. R. & LOOK, A. T. 2002. Gene expression signatures define novel oncogenic pathways in T cell acute lymphoblastic leukemia. *Cancer Cell,* 1**,** 75-87.

FINGER, L. R., HARVEY, R. C., MOORE, R. C., SHOWE, L. C. & CROCE, C. M. 1986. A common mechanism of chromosomal translocation in T- and B-cell neoplasia. *Science,* 234**,** 982-5.

FISCHER, A. M., KATAYAMA, C. D., PAGES, G., POUYSSEGUR, J. & HEDRICK, S. M. 2005. The role of erk1 and erk2 in multiple stages of T cell development. *Immunity,* 23**,** 431-43.

FLACH, J., BAKKER, S. T., MOHRIN, M., CONROY, P. C., PIETRAS, E. M., REYNAUD, D., ALVAREZ, S., DIOLAITI, M. E., UGARTE, F., FORSBERG, E. C., LE BEAU, M. M., STOHR, B. A., MENDEZ, J., MORRISON, C. G. & PASSEGUE, E. 2014. Replication stress is a potent driver of functional decline in ageing haematopoietic stem cells. *Nature,* 512**,** 198-202.

FOUDI, A., HOCHEDLINGER, K., VAN BUREN, D., SCHINDLER, J. W., JAENISCH, R., CAREY, V. & HOCK, H. 2009. Analysis of histone 2B-GFP retention reveals slowly cycling hematopoietic stem cells. *Nat Biotechnol,* 27**,** 84-90.

FOX, C. S., WHITE, C. C., LOHMAN, K., HEARD-COSTA, N., COHEN, P., ZHANG, Y., JOHNSON, A. D., EMILSSON, V., LIU, C. T., CHEN, Y. D., TAYLOR, K. D., ALLISON, M., BUDOFF, M., ROTTER, J. I., CARR, J. J., HOFFMANN, U., DING, J., CUPPLES, L. A. & LIU, Y. 2012. Genome-wide association of pericardial fat identifies a unique locus for ectopic fat. *PLoS Genet,* 8**,** e1002705.

FRANCO, C. B., SCRIPTURE-ADAMS, D. D., PROEKT, I., TAGHON, T., WEISS, A. H., YUI, M. A., ADAMS, S. L., DIAMOND, R. A. & ROTHENBERG, E. V. 2006. Notch/Delta signaling constrains reengineering of pro-T cells by PU.1. *Proc Natl Acad Sci U S A,* 103**,** 11993-8.

FREIREICH, E. J., WIERNIK, P. H. & STEENSMA, D. P. 2014. The leukemias: a half-century of discovery. *J Clin Oncol,* 32**,** 3463-9.

FREY, J. R., ERNST, B., SURH, C. D. & SPRENT, J. 1992. Thymus-grafted SCID mice show transient thymopoiesis and limited depletion of V beta 11+ T cells. *J Exp Med,* 175**,** 1067-71.

GABRIELLI, B. G., DE SOUZA, C. P., TONKS, I. D., CLARK, J. M., HAYWARD, N. K. & ELLEM, K. A. 1996. Cytoplasmic accumulation of cdc25B phosphatase in mitosis triggers centrosomal microtubule nucleation in HeLa cells. *J Cell Sci,* 109 (Pt 5)**,** 1081-93.

GARCIA-CUELLAR, M. P., STEGER, J., FULLER, E., HETZNER, K. & SLANY, R. K. 2015. Pbx3 and Meis1 cooperate through multiple mechanisms to support Hox-induced murine leukemia. *Haematologica,* 100**,** 905-13.

GE, J., LIU, Y., LI, Q., GUO, X., GU, L., MA, Z. G. & ZHU, Y. P. 2013. Resveratrol induces apoptosis and autophagy in T-cell acute lymphoblastic leukemia cells by inhibiting Akt/mTOR and activating p38-MAPK. *Biomed Environ Sci,* 26**,** 902-11.

GILBY, D. C., SUNG, H. Y., WINSHIP, P. R., GOODEVE, A. C., REILLY, J. T. & KISS-TOTH, E. 2010. Tribbles-1 and-2 are tumour suppressors, down-regulated in human acute myeloid leukaemia. *Immunology Letters,* 130**,** 115-124.

GLATMAN ZARETSKY, A., ENGILES, J. B. & HUNTER, C. A. 2014. Infection-induced changes in hematopoiesis. *J Immunol,* 192**,** 27-33.

GODFREY, D. I., KENNEDY, J., SUDA, T. & ZLOTNIK, A. 1993. A developmental pathway involving four phenotypically and functionally distinct subsets of CD3-CD4-CD8- triple-negative adult mouse thymocytes defined by CD44 and CD25 expression. *J Immunol,* 150**,** 4244-52.

GOUNARI, F., AIFANTIS, I., MARTIN, C., FEHLING, H. J., HOEFLINGER, S., LEDER, P., VON BOEHMER, H. & REIZIS, B. 2002. Tracing lymphopoiesis with the aid of a pTalpha-controlled reporter gene. *Nat Immunol,* 3**,** 489-96.

GRABHER, C., VON BOEHMER, H. & LOOK, A. T. 2006. Notch 1 activation in the molecular pathogenesis of T-cell acute lymphoblastic leukaemia. *Nat Rev Cancer,* 6**,** 347-59.

GRANDINETTI, K. B., STEVENS, T. A., HA, S., SALAMONE, R. J., WALKER, J. R., ZHANG, J., AGARWALLA, S., TENEN, D. G., PETERS, E. C. & REDDY, V. A. 2011. Overexpression of TRIB2 in human lung cancers contributes to tumorigenesis through downregulation of C/EBPalpha. *Oncogene,* 30**,** 3328-35.

GRAUX, C., COOLS, J., MELOTTE, C., QUENTMEIER, H., FERRANDO, A., LEVINE, R., VERMEESCH, J. R., STUL, M., DUTTA, B., BOECKX, N., BOSLY, A., HEIMANN, P., UYTTEBROECK, A., MENTENS, N., SOMERS, R., MACLEOD, R. A., DREXLER, H. G., LOOK, A. T., GILLILAND, D. G., MICHAUX, L., VANDENBERGHE, P., WLODARSKA, I., MARYNEN, P. & HAGEMEIJER, A. 2004. Fusion of NUP214 to ABL1 on amplified episomes in T-cell acute lymphoblastic leukemia. *Nat Genet,* 36**,** 1084-9.

GRAUX, C., COOLS, J., MICHAUX, L., VANDENBERGHE, P. & HAGEMEIJER, A. 2006. Cytogenetics and molecular genetics of T-cell acute lymphoblastic leukemia: from thymocyte to lymphoblast. *Leukemia,* 20**,** 1496-510.

GREENBERG, J. M., BOEHM, T., SOFRONIEW, M. V., KEYNES, R. J., BARTON, S. C., NORRIS, M. L., SURANI, M. A., SPILLANTINI, M. G. & RABBITTS, T. H. 1990. Segmental and developmental regulation of a presumptive T-cell oncogene in the central nervous system. *Nature,* 344**,** 158-60.

GREGORJ, C., RICCIARDI, M. R., PETRUCCI, M. T., SCERPA, M. C., DE CAVE, F., FAZI, P., VIGNETTI, M., VITALE, A., MANCINI, M., CIMINO, G., PALMIERI, S., DI RAIMONDO, F., SPECCHIA, G., FABBIANO, F., CANTORE, N., MOSNA, F., CAMERA, A., LUPPI, M., ANNINO, L., MIRAGLIA, E., FIORITONI, G., RONCO, F., MELONI, G., MANDELLI, F., ANDREEFF, M., MILELLA, M., FOA, R., TAFURI, A. & PARTY, G. A. L. W. 2007. ERK1/2 phosphorylation is an independent predictor of complete remission in newly diagnosed adult acute lymphoblastic leukemia. *Blood,* 109**,** 5473-6.

GRIMWADE, D., IVEY, A. & HUNTLY, B. J. 2016. Molecular landscape of acute myeloid leukemia in younger adults and its clinical relevance. *Blood,* 127**,** 29-41.

GROSSHANS, J. & WIESCHAUS, E. 2000. A genetic link between morphogenesis and cell division during formation of the ventral furrow in Drosophila. *Cell,* 101**,** 523-31.

GUTIERREZ, G. J., TSUJI, T., CROSS, J. V., DAVIS, R. J., TEMPLETON, D. J., JIANG, W. & RONAI, Z. A. 2010. JNK-mediated phosphorylation of Cdc25C regulates cell cycle entry and G(2)/M DNA damage checkpoint. *J Biol Chem,* 285**,** 14217-28.

HAAS, S., HANSSON, J., KLIMMECK, D., LOEFFLER, D., VELTEN, L., UCKELMANN, H., WURZER, S., PRENDERGAST, A. M., SCHNELL, A., HEXEL, K., SANTARELLA-MELLWIG, R., BLASZKIEWICZ, S., KUCK, A., GEIGER, H., MILSOM, M. D., STEINMETZ, L. M., SCHROEDER, T., TRUMPP, A., KRIJGSVELD, J. & ESSERS, M. A. 2015. Inflammation-Induced Emergency Megakaryopoiesis Driven by Hematopoietic Stem Cell-like Megakaryocyte Progenitors. *Cell Stem Cell,* 17**,** 422-34.

HAFERLACH, T., KOHLMANN, A., WIECZOREK, L., BASSO, G., KRONNIE, G. T., BENE, M. C., DE VOS, J., HERNANDEZ, J. M., HOFMANN, W. K., MILLS, K. I., GILKES, A., CHIARETTI, S., SHURTLEFF, S. A., KIPPS, T. J., RASSENTI, L. Z., YEOH, A. E., PAPENHAUSEN, P. R., LIU, W. M., WILLIAMS, P. M. & FOA, R. 2010. Clinical utility of microarray-based gene expression profiling in the diagnosis and subclassification of leukemia: report from the International Microarray Innovations in Leukemia Study Group. *J Clin Oncol,* 28**,** 2529-37.

HAGEMEIJER, A. & GRAUX, C. 2010. ABL1 rearrangements in T-cell acute lymphoblastic leukemia. *Genes Chromosomes Cancer,* 49**,** 299-308.

HANAHAN, D. & WEINBERG, R. A. 2011. Hallmarks of cancer: the next generation. *Cell,* 144**,** 646-74.

HANNON, M. M., LOHAN, F., ERBILGIN, Y., SAYITOGLU, M., O'HAGAN, K., MILLS, K., OZBEK, U. & KEESHAN, K. 2012. Elevated TRIB2 with NOTCH1 activation in paediatric/adult T-ALL. *Br J Haematol,* 158**,** 626-34.

HANSEN-HAGGE, T. E., SCHAFER, M., KIYOI, H., MORRIS, S. W., WHITLOCK, J. A., KOCH, P., BOHLMANN, I., MAHOTKA, C., BARTRAM, C. R. & JANSSEN, J. W. 2002. Disruption of the RanBP17/Hox11L2 region by recombination with the TCRdelta locus in acute lymphoblastic leukemias with t(5;14)(q34;q11). *Leukemia,* 16**,** 2205-12.

HARRISON, D. E. & LERNER, C. P. 1991. Most primitive hematopoietic stem cells are stimulated to cycle rapidly after treatment with 5-fluorouracil. *Blood,* 78**,** 1237-40.

HATANO, M., ROBERTS, C. W., MINDEN, M., CRIST, W. M. & KORSMEYER, S. J. 1991. Deregulation of a homeobox gene, HOX11, by the t(10;14) in T cell leukemia. *Science,* 253**,** 79-82.

HEBESTREIT, K., GROTTRUP, S., EMDEN, D., VEERKAMP, J., RUCKERT, C., KLEIN, H. U., MULLER-TIDOW, C. & DUGAS, M. 2012. Leukemia gene atlas--a public platform for integrative exploration of genome-wide molecular data. *PLoS One,* 7**,** e39148.

HENG, T. S., GOLDBERG, G. L., GRAY, D. H., SUTHERLAND, J. S., CHIDGEY, A. P. & BOYD, R. L. 2005. Effects of castration on thymocyte development in two different models of thymic involution. *J Immunol,* 175**,** 2982-93.

HILL, R., KALATHUR, R. K., COLACO, L., BRANDAO, R., UGUREL, S., FUTSCHIK, M. & LINK, W. 2015. TRIB2 as a biomarker for diagnosis and progression of melanoma. *Carcinogenesis,* 36**,** 469-77.

HOFFMAN, E. S., PASSONI, L., CROMPTON, T., LEU, T. M., SCHATZ, D. G., KOFF, A., OWEN, M. J. & HAYDAY, A. C. 1996. Productive T-cell receptor

beta-chain gene rearrangement: coincident regulation of cell cycle and clonality during development in vivo. *Genes & Development,* 10**,** 948-962.

HOFFMANN, I., DRAETTA, G. & KARSENTI, E. 1994. Activation of the phosphatase activity of human cdc25A by a cdk2-cyclin E dependent phosphorylation at the G1/S transition. *EMBO J,* 13**,** 4302-10.

HOMMINGA, I., VUERHARD, M. J., LANGERAK, A. W., BUIJS-GLADDINES, J., PIETERS, R. & MEIJERINK, J. P. 2012. Characterization of a pediatric T-cell acute lymphoblastic leukemia patient with simultaneous LYL1 and LMO2 rearrangements. *Haematologica,* 97**,** 258-61.

HUSSEY, D. J., NICOLA, M., MOORE, S., PETERS, G. B. & DOBROVIC, A. 1999. The (4;11)(q21;p15) translocation fuses the NUP98 and RAP1GDS1 genes and is recurrent in T-cell acute lymphocytic leukemia. *Blood,* 94**,** 2072-9.

ISLAM, Z., NAGASE, M., YOSHIZAWA, T., YAMAUCHI, K. & SAKATO, N. 1998. T-2 toxin induces thymic apoptosis in vivo in mice. *Toxicol Appl Pharmacol,* 148**,** 205-14.

IZRAILIT, J., BERMAN, H. K., DATTI, A., WRANA, J. L. & REEDIJK, M. 2013. High throughput kinase inhibitor screens reveal TRB3 and MAPK-ERK/TGFbeta pathways as fundamental Notch regulators in breast cancer. *Proc Natl Acad Sci U S A,* 110**,** 1714-9.

JIANG, Q., LI, F., SHI, K., WU, P., AN, J., YANG, Y. & XU, C. 2013. ATF4 activation by the p38MAPK-eIF4E axis mediates apoptosis and autophagy induced by selenite in Jurkat cells. *FEBS Lett,* 587**,** 2420-9.

KATZAV, A., ARANGO, M. T., KIVITY, S., TANAKA, S., GIVATY, G., AGMON-LEVIN, N., HONDA, M., ANAYA, J. M., CHAPMAN, J. & SHOENFELD, Y. 2013. Passive transfer of narcolepsy: anti-TRIB2 autoantibody positive patient IgG causes hypothalamic orexin neuron loss and sleep attacks in mice. *J Autoimmun,* 45**,** 24-30.

KAWAKAMI, M., TSUTSUMI, H., KUMAKAWA, T., ABE, H., HIRAI, M., KUROSAWA, S., MORI, M. & FUKUSHIMA, M. 1990. Levels of serum granulocyte colony-stimulating factor in patients with infections. *Blood,* 76**,** 1962-4.

KAWASHIMA, M., LIN, L., TANAKA, S., JENNUM, P., KNUDSEN, S., NEVSIMALOVA, S., PLAZZI, G. & MIGNOT, E. 2010. Anti-Tribbles homolog 2 (TRIB2) autoantibodies in narcolepsy are associated with recent onset of cataplexy. *Sleep,* 33**,** 869-74.

KEESHAN, K., BAILIS, W., DEDHIA, P. H., VEGA, M. E., SHESTOVA, O., XU, L. W., TOSCANO, K., ULJON, S. N., BLACKLOW, S. C. & PEAR, W. S. 2010. Transformation by Tribbles homolog 2 (Trib2) requires both the Trib2 kinase domain and COP1 binding. *Blood,* 116**,** 4948-4957.

KEESHAN, K., HE, Y., WOUTERS, B. J., SHESTOVA, O., XU, L., SAI, H., RODRIGUEZ, C. G., MAILLARD, I., TOBIAS, J. W., VALK, P., CARROLL, M., ASTER, J. C., DELWEL, R. & PEAR, W. S. 2006. Tribbles homolog 2 inactivates C/EBPalpha and causes acute myelogenous leukemia. *Cancer Cell,* 10**,** 401-11.

KEESHAN, K., SHESTOVA, O., USSIN, L. & PEAR, W. S. 2008. Tribbles homolog 2 (Trib2) and HoxA9 cooperate to accelerate acute myelogenous leukemia. *Blood Cells Molecules and Diseases,* 40**,** 119-121.

KENNEDY, M. A., GONZALEZ-SARMIENTO, R., KEES, U. R., LAMPERT, F., DEAR, N., BOEHM, T. & RABBITTS, T. H. 1991. HOX11, a homeobox-containing T-cell oncogene on human chromosome 10q24. *Proc Natl Acad Sci U S A,* 88**,** 8900-4.

KINDLER, T., CORNEJO, M. G., SCHOLL, C., LIU, J., LEEMAN, D. S., HAYDU, J. E., FROHLING, S., LEE, B. H. & GILLILAND, D. G. 2008. K-RasG12D-induced T-cell lymphoblastic lymphoma/leukemias harbor Notch1 mutations and are sensitive to gamma-secretase inhibitors. *Blood,* 112**,** 3373-82.

KOMANDER, D. 2009. The emerging complexity of protein ubiquitination. *Biochem Soc Trans,* 37**,** 937-53.

KONDO, M., WEISSMAN, I. L. & AKASHI, K. 1997. Identification of clonogenic common lymphoid progenitors in mouse bone marrow. *Cell,* 91**,** 661-72.

KOSCHMIEDER, S., HALMOS, B., LEVANTINI, E. & TENEN, D. G. 2009. Dysregulation of the C/EBPalpha differentiation pathway in human cancer. *J Clin Oncol,* 27**,** 619-28.

KRISTJANSDOTTIR, K. & RUDOLPH, J. 2004. Cdc25 phosphatases and cancer. *Chem Biol,* 11**,** 1043-51.

KRUISWIJK, F., LABUSCHAGNE, C. F. & VOUSDEN, K. H. 2015. p53 in survival, death and metabolic health: a lifeguard with a licence to kill. *Nat Rev Mol Cell Biol,* 16**,** 393-405.

LACRONIQUE, V., BOUREUX, A., VALLE, V. D., POIREL, H., QUANG, C. T., MAUCHAUFFE, M., BERTHOU, C., LESSARD, M., BERGER, R., GHYSDAEL, J. & BERNARD, O. A. 1997. A TEL-JAK2 fusion protein with constitutive kinase activity in human leukemia. *Science,* 278**,** 1309-12.

LAVECCHIA, A., DI GIOVANNI, C., PESAPANE, A., MONTUORI, N., RAGNO, P., MARTUCCI, N. M., MASULLO, M., DE VENDITTIS, E. & NOVELLINO, E. 2012. Discovery of new inhibitors of Cdc25B dual specificity phosphatases by structure-based virtual screening. *J Med Chem,* 55**,** 4142-58.

LEE, P. P., FITZPATRICK, D. R., BEARD, C., JESSUP, H. K., LEHAR, S., MAKAR, K. W., PEREZ-MELGOSA, M., SWEETSER, M. T., SCHLISSEL, M. S., NGUYEN, S., CHERRY, S. R., TSAI, J. H., TUCKER, S. M., WEAVER, W. M., KELSO, A., JAENISCH, R. & WILSON, C. B. 2001. A critical role for Dnmt1 and DNA methylation in T cell development, function, and survival. *Immunity,* 15**,** 763-74.

LI, X., GOUNARI, F., PROTOPOPOV, A., KHAZAIE, K. & VON BOEHMER, H. 2008. Oncogenesis of T-ALL and nonmalignant consequences of overexpressing intracellular NOTCH1. *J Exp Med,* 205**,** 2851-61.

LI, X. & SLAYTON, W. B. 2013. Molecular mechanisms of platelet and stem cell rebound after 5-fluorouracil treatment. *Exp Hematol,* 41**,** 635-645 e3.

LI, Z., DORDAI, D. I., LEE, J. & DESIDERIO, S. 1996. A conserved degradation signal regulates RAG-2 accumulation during cell division and links V(D)J recombination to the cell cycle. *Immunity,* 5**,** 575-89.

LIANG, K. L., RISHI, L. & KEESHAN, K. 2013. Tribbles in acute leukemia. *Blood,* 121**,** 4265-70.

LIN, K. R., LEE, S. F., HUNG, C. M., LI, C. L., YANG-YEN, H. F. & YEN, J. J. 2007. Survival factor withdrawal-induced apoptosis of TF-1 cells involves a TRB2-Mcl-1 axis-dependent pathway. *J Biol Chem,* 282**,** 21962-72.

LIN, W. C. & DESIDERIO, S. 1994. Cell cycle regulation of V(D)J recombination-activating protein RAG-2. *Proc Natl Acad Sci U S A,* 91**,** 2733-7.

LINCOLN, A. J., WICKRAMASINGHE, D., STEIN, P., SCHULTZ, R. M., PALKO, M. E., DE MIGUEL, M. P., TESSAROLLO, L. & DONOVAN, P. J. 2002. Cdc25b phosphatase is required for resumption of meiosis during oocyte maturation. *Nat Genet,* 30**,** 446-9.

LITZOW, M. R. & FERRANDO, A. A. 2015. How we treat T-cell acute lymphoblastic leukemia in adults. *Blood.*

LIU, Y., GE, J., LI, Q., GUO, X., GU, L., MA, Z. G., LI, X. H. & ZHU, Y. P. 2014. Low-dose anisomycin sensitizes glucocorticoid-resistant T-acute lymphoblastic leukemia CEM-C1 cells to dexamethasone-induced apoptosis through activation of glucocorticoid receptor and p38-MAPK/JNK. *Leuk Lymphoma,* 55**,** 2179-88.

LONGLEY, D. B., HARKIN, D. P. & JOHNSTON, P. G. 2003. 5-fluorouracil: mechanisms of action and clinical strategies. *Nat Rev Cancer,* 3**,** 330-8.

LU, M., GONG, Z. Y., SHEN, W. F. & HO, A. D. 1991. The tcl-3 proto-oncogene altered by chromosomal translocation in T-cell leukemia codes for a homeobox protein. *EMBO J,* 10**,** 2905-10.

LUC, S., LUIS, T. C., BOUKARABILA, H., MACAULAY, I. C., BUZA-VIDAS, N., BOURIEZ-JONES, T., LUTTEROPP, M., WOLL, P. S., LOUGHRAN, S. J., MEAD, A. J., HULTQUIST, A., BROWN, J., MIZUKAMI, T., MATSUOKA, S., FERRY, H., ANDERSON, K., DUARTE, S., ATKINSON, D., SONEJI, S., DOMANSKI, A., FARLEY, A., SANJUAN-PLA, A., CARELLA, C., PATIENT, R., DE BRUIJN, M., ENVER, T., NERLOV, C., BLACKBURN, C., GODIN, I. & JACOBSEN, S. E. 2012. The earliest thymic T cell progenitors sustain B cell and myeloid lineage potential. *Nat Immunol,* 13**,** 412-9.

MAILAND, N., PODTELEJNIKOV, A. V., GROTH, A., MANN, M., BARTEK, J. & LUKAS, J. 2002. Regulation of G(2)/M events by Cdc25A through phosphorylation-dependent modulation of its stability. *EMBO J,* 21**,** 5911-20.

MANCINI, E., SANJUAN-PLA, A., LUCIANI, L., MOORE, S., GROVER, A., ZAY, A., RASMUSSEN, K. D., LUC, S., BILBAO, D., O'CARROLL, D., JACOBSEN, S. E. & NERLOV, C. 2012. FOG-1 and GATA-1 act sequentially to specify definitive megakaryocytic and erythroid progenitors. *EMBO J,* 31**,** 351-65.

MANKE, I. A., NGUYEN, A., LIM, D., STEWART, M. Q., ELIA, A. E. & YAFFE, M. B. 2005. MAPKAP kinase-2 is a cell cycle checkpoint kinase that regulates the G2/M transition and S phase progression in response to UV irradiation. *Mol Cell,* 17**,** 37-48.

MANNING, G., WHYTE, D. B., MARTINEZ, R., HUNTER, T. & SUDARSANAM, S. 2002. The protein kinase complement of the human genome. *Science,* 298**,** 1912-34.

MANZ, M. G. & BOETTCHER, S. 2014. Emergency granulopoiesis. *Nat Rev Immunol,* 14**,** 302-14.

MARTINS, V. C., BUSCH, K., JURAEVA, D., BLUM, C., LUDWIG, C., RASCHE, V., LASITSCHKA, F., MASTITSKY, S. E., BRORS, B., HIELSCHER, T., FEHLING, H. J. & RODEWALD, H. R. 2014. Cell competition is a tumour suppressor mechanism in the thymus. *Nature,* 509**,** 465-70.

MARTINS, V. C., RUGGIERO, E., SCHLENNER, S. M., MADAN, V., SCHMIDT, M., FINK, P. J., VON KALLE, C. & RODEWALD, H. R. 2012. Thymus-autonomous T cell development in the absence of progenitor import. *J Exp Med,* 209**,** 1409-17.

MASIERO, M., MINUZZO, S., PUSCEDDU, I., MOSERLE, L., PERSANO, L., AGNUSDEI, V., TOSELLO, V., BASSO, G., AMADORI, A. & INDRACCOLO, S. 2011. Notch3-mediated regulation of MKP-1 levels promotes survival of T acute lymphoblastic leukemia cells. *Leukemia,* 25**,** 588-98.

MATA, J., CURADO, S., EPHRUSSI, A. & RORTH, P. 2000. Tribbles coordinates mitosis and morphogenesis in Drosophila by regulating string/CDC25 proteolysis. *Cell,* 101**,** 511-22.

MAUCH, P., CONSTINE, L., GREENBERGER, J., KNOSPE, W., SULLIVAN, J., LIESVELD, J. L. & DEEG, H. J. 1995. Hematopoietic stem cell compartment: acute and late effects of radiation therapy and chemotherapy. *Int J Radiat Oncol Biol Phys,* 31**,** 1319-39.

MCGARGILL, M. A., CH'EN, I. L., KATAYAMA, C. D., PAGES, G., POUYSSEGUR, J. & HEDRICK, S. M. 2009. Cutting edge: Extracellular signal-related kinase is not required for negative selection of developing T cells. *J Immunol,* 183**,** 4838-42.

MCGUIRE, E. A., HOCKETT, R. D., POLLOCK, K. M., BARTHOLDI, M. F., O'BRIEN, S. J. & KORSMEYER, S. J. 1989. The t(11;14)(p15;q11) in a T-cell acute lymphoblastic leukemia cell line activates multiple transcripts, including Ttg-1, a gene encoding a potential zinc finger protein. *Mol Cell Biol,* 9**,** 2124-32.

MCKEITHAN, T. W., SHIMA, E. A., LE BEAU, M. M., MINOWADA, J., ROWLEY, J. D. & DIAZ, M. O. 1986. Molecular cloning of the breakpoint junction of a human chromosomal 8;14 translocation involving the T-cell receptor alpha-chain gene and sequences on the 3' side of MYC. *Proc Natl Acad Sci U S A,* 83**,** 6636-40.

MCNEIL, L. K., STARR, T. K. & HOGQUIST, K. A. 2005. A requirement for sustained ERK signaling during thymocyte positive selection in vivo. *Proc Natl Acad Sci U S A,* 102**,** 13574-9.

MELKUN, E., PILIONE, M. & PAULSON, R. F. 2002. A naturally occurring point substitution in Cdc25A, and not Fv2/Stk, is associated with altered cell-cycle status of early erythroid progenitor cells. *Blood,* 100**,** 3804-11.

MELLENTIN, J. D., SMITH, S. D. & CLEARY, M. L. 1989. lyl-1, a novel gene altered by chromosomal translocation in T cell leukemia, codes for a protein with a helix-loop-helix DNA binding motif. *Cell,* 58**,** 77-83.

MILLAR, J. B., BLEVITT, J., GERACE, L., SADHU, K., FEATHERSTONE, C. & RUSSELL, P. 1991. p55CDC25 is a nuclear protein required for the initiation of mitosis in human cells. *Proc Natl Acad Sci U S A,* 88**,** 10500-4.

MIN, H., MONTECINO-RODRIGUEZ, E. & DORSHKIND, K. 2004. Reduction in the developmental potential of intrathymic T cell progenitors with age. *J Immunol,* 173**,** 245-50.

MINGUENEAU, M., KRESLAVSKY, T., GRAY, D., HENG, T., CRUSE, R., ERICSON, J., BENDALL, S., SPITZER, M. H., NOLAN, G. P., KOBAYASHI, K., VON BOEHMER, H., MATHIS, D., BENOIST, C., BEST, A. J., KNELL, J., GOLDRATH, A., JOIC, V., KOLLER, D., SHAY, T., REGEV, A., COHEN, N., BRENNAN, P., BRENNER, M., KIM, F., NAGESWARA RAO, T., WAGERS, A., ROTHAMEL, K., ORTIZ-LOPEZ, A., BEZMAN, N. A., SUN, J. C., MIN-OO, G., KIM, C. C., LANIER, L. L., MILLER, J., BROWN, B., MERAD, M., GAUTIER, E. L., JAKUBZICK, C., RANDOLPH, G. J.,

MONACH, P., BLAIR, D. A., DUSTIN, M. L., SHINTON, S. A., HARDY, R. R., LAIDLAW, D., COLLINS, J., GAZIT, R., ROSSI, D. J., MALHOTRA, N., SYLVIA, K., KANG, J., FLETCHER, A., ELPEK, K., BELLEMARE-PELLETIER, A., MALHOTRA, D. & TURLEY, S. 2013. The transcriptional landscape of alphabeta T cell differentiation. *Nat Immunol,* 14**,** 619-32.

MOORE, A. J., SARMIENTO, J., MOHTASHAMI, M., BRAUNSTEIN, M., ZUNIGA-PFLUCKER, J. C. & ANDERSON, M. K. 2012. Transcriptional priming of intrathymic precursors for dendritic cell development. *Development,* 139**,** 373-84.

MUKHERJEE, K., SHARMA, M., JAHN, R., WAHL, M. C. & SUDHOF, T. C. 2010. Evolution of CASK into a Mg2+-sensitive kinase. *Sci Signal,* 3**,** ra33.

MUKHERJEE, K., SHARMA, M., URLAUB, H., BOURENKOV, G. P., JAHN, R., SUDHOF, T. C. & WAHL, M. C. 2008. CASK Functions as a Mg2+-independent neurexin kinase. *Cell,* 133**,** 328-39.

NAGEL, S., VENTURINI, L., PRZYBYLSKI, G. K., GRABARCZYK, P., SCHNEIDER, B., MEYER, C., KAUFMANN, M., SCHMIDT, C. A., SCHERR, M., DREXLER, H. G. & MACLEOD, R. A. 2011. Activation of Paired-homeobox gene PITX1 by del(5)(q31) in T-cell acute lymphoblastic leukemia. *Leuk Lymphoma,* 52**,** 1348-59.

NAIKI, T., SAIJOU, E., MIYAOKA, Y., SEKINE, K. & MIYAJIMA, A. 2007. TRB2, a mouse Tribbles ortholog, suppresses adipocyte differentiation by inhibiting AKT and C/EBPbeta. *J Biol Chem,* 282**,** 24075-82.

NAKAYAMA, K., OGAWA, A., MIYASHITA, H., TABARA, Y., IGASE, M., KOHARA, K., MIKI, T., KAGAWA, Y., YANAGISAWA, Y., KATASHIMA, M., ONDA, T., OKADA, K., FUKUSHIMA, S. & IWAMOTO, S. 2013. Positive natural selection of TRIB2, a novel gene that influences visceral fat accumulation, in East Asia. *Hum Genet,* 132**,** 201-17.

NAKAYAMA, T., KASPROWICZ, D. J., YAMASHITA, M., SCHUBERT, L. A., GILLARD, G., KIMURA, M., DIDIERLAURENT, A., KOSEKI, H. & ZIEGLER, S. F. 2002. The generation of mature, single-positive thymocytes in vivo is dysregulated by CD69 blockade or overexpression. *J Immunol,* 168**,** 87-94.

NOTTA, F., ZANDI, S., TAKAYAMA, N., DOBSON, S., GAN, O. I., WILSON, G., KAUFMANN, K. B., MCLEOD, J., LAURENTI, E., DUNANT, C. F., MCPHERSON, J. D., STEIN, L. D., DROR, Y. & DICK, J. E. 2016. Distinct routes of lineage development reshape the human blood hierarchy across ontogeny. *Science,* 351**,** aab2116.

NUNES-ALVES, C., NOBREGA, C., BEHAR, S. M. & CORREIA-NEVES, M. 2013. Tolerance has its limits: how the thymus copes with infection. *Trends Immunol,* 34**,** 502-10.

OGILVY, S., METCALF, D., GIBSON, L., BATH, M. L., HARRIS, A. W. & ADAMS, J. M. 1999. Promoter elements of vav drive transgene expression in vivo throughout the hematopoietic compartment. *Blood,* 94**,** 1855-63.

OKAMOTO, H., LATRES, E., LIU, R., THABET, K., MURPHY, A., VALENZEULA, D., YANCOPOULOS, G. D., STITT, T. N., GLASS, D. J. & SLEEMAN, M. W. 2007. Genetic deletion of Trb3, the mammalian Drosophila tribbles homolog, displays normal hepatic insulin signaling and glucose homeostasis. *Diabetes,* 56**,** 1350-6.

ORD, T., ORD, D., KUUSE, S. & PLAAS, M. 2012. Trib3 is regulated by IL-3 and affects bone marrow-derived mast cell survival and function. *Cell Immunol,* 280**,** 68-75.

OZEKI, Y., KANEDA, K., FUJIWARA, N., MORIMOTO, M., OKA, S. & YANO, I. 1997. In vivo induction of apoptosis in the thymus by administration of mycobacterial cord factor (trehalose 6,6'-dimycolate). *Infect Immun,* 65**,** 1793-9.

PAGES, G., GUERIN, S., GRALL, D., BONINO, F., SMITH, A., ANJUERE, F., AUBERGER, P. & POUYSSEGUR, J. 1999. Defective thymocyte maturation in p44 MAP kinase (Erk 1) knockout mice. *Science,* 286**,** 1374-7.

PALMA, C. A., AL SHEIKHA, D., LIM, T. K., BRYANT, A., VU, T. T., JAYASWAL, V. & MA, D. D. 2014. MicroRNA-155 as an inducer of apoptosis and cell differentiation in Acute Myeloid Leukaemia. *Mol Cancer,* 13**,** 79.

PALMER, D. B. 2013. The Effect of Age on Thymic Function. *Front Immunol,* 4**,** 316.

PANG, W. W., PRICE, E. A., SAHOO, D., BEERMAN, I., MALONEY, W. J., ROSSI, D. J., SCHRIER, S. L. & WEISSMAN, I. L. 2011. Human bone marrow hematopoietic stem cells are increased in frequency and myeloid-biased with age. *Proc Natl Acad Sci U S A,* 108**,** 20012-7.

PAUL, F., ARKIN, Y., GILADI, A., JAITIN, D. A., KENIGSBERG, E., KEREN-SHAUL, H., WINTER, D., LARA-ASTIASO, D., GURY, M., WEINER, A., DAVID, E., COHEN, N., LAURIDSEN, F. K., HAAS, S., SCHLITZER, A., MILDNER, A., GINHOUX, F., JUNG, S., TRUMPP, A., PORSE, B. T., TANAY, A. & AMIT, I. 2015. Transcriptional Heterogeneity and Lineage Commitment in Myeloid Progenitors. *Cell,* 163**,** 1663-77.

PEAR, W. S., ASTER, J. C., SCOTT, M. L., HASSERJIAN, R. P., SOFFER, B., SKLAR, J. & BALTIMORE, D. 1996. Exclusive development of T cell neoplasms in mice transplanted with bone marrow expressing activated Notch alleles. *J Exp Med,* 183**,** 2283-91.

PEAUDECERF, L., LEMOS, S., GALGANO, A., KRENN, G., VASSEUR, F., DI SANTO, J. P., EZINE, S. & ROCHA, B. 2012. Thymocytes may persist and differentiate without any input from bone marrow progenitors. *J Exp Med,* 209**,** 1401-8.

PFLEGER, C. M. & KIRSCHNER, M. W. 2000. The KEN box: an APC recognition signal distinct from the D box targeted by Cdh1. *Genes Dev,* 14**,** 655-65.

PORRITT, H. E., RUMFELT, L. L., TABRIZIFARD, S., SCHMITT, T. M., ZUNIGA-PFLUCKER, J. C. & PETRIE, H. T. 2004. Heterogeneity among DN1 prothymocytes reveals multiple progenitors with different capacities to generate T cell and non-T cell lineages. *Immunity,* 20**,** 735-45.

PRINZ, I., SANSONI, A., KISSENPFENNIG, A., ARDOUIN, L., MALISSEN, M. & MALISSEN, B. 2006. Visualization of the earliest steps of gammadelta T cell development in the adult thymus. *Nat Immunol,* 7**,** 995-1003.

PUI, J. C., ALLMAN, D., XU, L., DEROCCO, S., KARNELL, F. G., BAKKOUR, S., LEE, J. Y., KADESCH, T., HARDY, R. R., ASTER, J. C. & PEAR, W. S. 1999. Notch1 expression in early lymphopoiesis influences B versus T lineage determination. *Immunity,* 11**,** 299-308.

QI, L., HEREDIA, J. E., ALTAREJOS, J. Y., SCREATON, R., GOEBEL, N., NIESSEN, S., MACLEOD, I. X., LIEW, C. W., KULKARNI, R. N., BAIN, J., NEWGARD, C., NELSON, M., EVANS, R. M., YATES, J. & MONTMINY, M. 2006. TRB3 links the E3 ubiquitin ligase COP1 to lipid metabolism. *Science,* 312**,** 1763-6.

QIAO, Y., ZHANG, Y. & WANG, J. 2013. Ubiquitin E3 ligase SCF(beta-TRCP) regulates TRIB2 stability in liver cancer cells. *Biochem Biophys Res Commun,* 441**,** 555-9.

RADTKE, F., WILSON, A., STARK, G., BAUER, M., VAN MEERWIJK, J., MACDONALD, H. R. & AGUET, M. 1999. Deficient T cell fate specification in mice with an induced inactivation of Notch1. *Immunity,* 10**,** 547-58.

RANDALL, T. D. & WEISSMAN, I. L. 1997. Phenotypic and functional changes induced at the clonal level in hematopoietic stem cells after 5-fluorouracil treatment. *Blood,* 89**,** 3596-606.

RANDLE-BARRETT, E. S. & BOYD, R. L. 1995. Thymic microenvironment and lymphoid responses to sublethal irradiation. *Dev Immunol,* 4**,** 101-16.

REN, S. & ROLLINS, B. J. 2004. Cyclin C/cdk3 promotes Rb-dependent G0 exit. *Cell,* 117**,** 239-51.

REYA, T., MORRISON, S. J., CLARKE, M. F. & WEISSMAN, I. L. 2001. Stem cells, cancer, and cancer stem cells. *Nature,* 414**,** 105-11.

RINCON, M., WHITMARSH, A., YANG, D. D., WEISS, L., DERIJARD, B., JAYARAJ, P., DAVIS, R. J. & FLAVELL, R. A. 1998. The JNK pathway regulates the In vivo deletion of immature CD4(+)CD8(+) thymocytes. *J Exp Med,* 188**,** 1817-30.

RISHI, L., HANNON, M., SALOME, M., HASEMANN, M., FRANK, A. K., CAMPOS, J., TIMONEY, J., O'CONNOR, C., CAHILL, M. R., PORSE, B. & KEESHAN, K. 2014. Regulation of Trib2 by an E2F1-C/EBPalpha feedback loop in AML cell proliferation. *Blood,* 123**,** 2389-400.

RORTH, P., SZABO, K. & TEXIDO, G. 2000. The level of C/EBP protein is critical for cell migration during Drosophila oogenesis and is tightly controlled by regulated degradation. *Mol Cell,* 6**,** 23-30.

ROSSI, D. J., BRYDER, D., ZAHN, J. M., AHLENIUS, H., SONU, R., WAGERS, A. J. & WEISSMAN, I. L. 2005. Cell intrinsic alterations underlie hematopoietic stem cell aging. *Proc Natl Acad Sci U S A,* 102**,** 9194-9.

ROTHENBERG, E. V. & SCRIPTURE-ADAMS, D. D. 2008. Competition and collaboration: GATA-3, PU.1, and Notch signaling in early T-cell fate determination. *Semin Immunol,* 20**,** 236-46.

SAKA, Y. & SMITH, J. C. 2004. A Xenopus tribbles orthologue is required for the progression of mitosis and for development of the nervous system. *Dev Biol,* 273**,** 210-25.

SAKAI, S., OHOKA, N., ONOZAKI, K., KITAGAWA, M., NAKANISHI, M. & HAYASHI, H. 2010. Dual mode of regulation of cell division cycle 25 A protein by TRB3. *Biol Pharm Bull,* 33**,** 1112-6.

SALLAN, S. E. 2006. Myths and lessons from the adult/pediatric interface in acute lymphoblastic leukemia. *Hematology Am Soc Hematol Educ Program*, 128-32.

SALOME, M., CAMPOS, J. & KEESHAN, K. 2015. TRIB2 and the ubiquitin proteasome system in cancer. *Biochem Soc Trans,* 43**,** 1089-94.

SANDA, T., LAWTON, L. N., BARRASA, M. I., FAN, Z. P., KOHLHAMMER, H., GUTIERREZ, A., MA, W., TATAREK, J., AHN, Y., KELLIHER, M. A., JAMIESON, C. H., STAUDT, L. M., YOUNG, R. A. & LOOK, A. T. 2012. Core transcriptional regulatory circuit controlled by the TAL1 complex in human T cell acute lymphoblastic leukemia. *Cancer Cell,* 22**,** 209-21.

SATOH, T., KIDOYA, H., NAITO, H., YAMAMOTO, M., TAKEMURA, N., NAKAGAWA, K., YOSHIOKA, Y., MORII, E., TAKAKURA, N., TAKEUCHI, O. & AKIRA, S. 2013. Critical role of Trib1 in differentiation of tissue-resident M2-like macrophages. *Nature,* 495**,** 524-8.

SCHLENNER, S. M., MADAN, V., BUSCH, K., TIETZ, A., LAUFLE, C., COSTA, C., BLUM, C., FEHLING, H. J. & RODEWALD, H. R. 2010. Fate mapping reveals separate origins of T cells and myeloid lineages in the thymus. *Immunity,* 32**,** 426-36.

SCHOOLMEESTERS, A., BROWN, D. D. & FEDOROV, Y. 2012. Kinome-wide functional genomics screen reveals a novel mechanism of TNFalpha-induced nuclear accumulation of the HIF-1alpha transcription factor in cancer cells. *PLoS One,* 7**,** e31270.

SEHER, T. C. & LEPTIN, M. 2000. Tribbles, a cell-cycle brake that coordinates proliferation and morphogenesis during Drosophila gastrulation. *Curr Biol,* 10**,** 623-9.

SEITAN, V. C., HAO, B., TACHIBANA-KONWALSKI, K., LAVAGNOLLI, T., MIRA-BONTENBAL, H., BROWN, K. E., TENG, G., CARROLL, T., TERRY, A., HORAN, K., MARKS, H., ADAMS, D. J., SCHATZ, D. G., ARAGON, L.,

FISHER, A. G., KRANGEL, M. S., NASMYTH, K. & MERKENSCHLAGER, M. 2011. A role for cohesin in T-cell-receptor rearrangement and thymocyte differentiation. *Nature,* 476**,** 467-71.

SERWOLD, T., EHRLICH, L. I. & WEISSMAN, I. L. 2009. Reductive isolation from bone marrow and blood implicates common lymphoid progenitors as the major source of thymopoiesis. *Blood,* 113**,** 807-15.

SHABBEER, S., OMER, D., BERNEMAN, D., WEITZMAN, O., ALPAUGH, A., PIETRASZKIEWICZ, A., METSUYANIM, S., SHAINSKAYA, A., PAPA, M. Z. & YARDEN, R. I. 2013. BRCA1 targets G2/M cell cycle proteins for ubiquitination and proteasomal degradation. *Oncogene,* 32**,** 5005-16.

SHAO, L., FENG, W., LI, H., GARDNER, D., LUO, Y., WANG, Y., LIU, L., MENG, A., SHARPLESS, N. E. & ZHOU, D. 2014. Total body irradiation causes long-term mouse BM injury via induction of HSC premature senescence in an Ink4a- and Arf-independent manner. *Blood,* 123**,** 3105-15.

SHARP, L. L., SCHWARZ, D. A., BOTT, C. M., MARSHALL, C. J. & HEDRICK, S. M. 1997. The influence of the MAPK pathway on T cell lineage commitment. *Immunity,* 7**,** 609-18.

SHIMA, E. A., LE BEAU, M. M., MCKEITHAN, T. W., MINOWADA, J., SHOWE, L. C., MAK, T. W., MINDEN, M. D., ROWLEY, J. D. & DIAZ, M. O. 1986. Gene encoding the alpha chain of the T-cell receptor is moved immediately downstream of c-myc in a chromosomal 8;14 translocation in a cell line from a human T-cell leukemia. *Proc Natl Acad Sci U S A,* 83**,** 3439-43.

SHIN, J. Y., HU, W., NARAMURA, M. & PARK, C. Y. 2014. High c-Kit expression identifies hematopoietic stem cells with impaired self-renewal and megakaryocytic bias. *J Exp Med,* 211**,** 217-31.

SMITH, S. D., MORGAN, R., GEMMELL, R., AMYLON, M. D., LINK, M. P., LINKER, C., HECHT, B. K., WARNKE, R., GLADER, B. E. & HECHT, F.

1988. Clinical and biologic characterization of T-cell neoplasias with rearrangements of chromosome 7 band q34. *Blood,* 71**,** 395-402.

SOULIER, J., CLAPPIER, E., CAYUELA, J. M., REGNAULT, A., GARCIA-PEYDRO, M., DOMBRET, H., BARUCHEL, A., TORIBIO, M. L. & SIGAUX, F. 2005. HOXA genes are included in genetic and biologic networks defining human acute T-cell leukemia (T-ALL). *Blood,* 106**,** 274-86.

SPELEMAN, F., CAUWELIER, B., DASTUGUE, N., COOLS, J., VERHASSELT, B., POPPE, B., VAN ROY, N., VANDESOMPELE, J., GRAUX, C., UYTTEBROECK, A., BOOGAERTS, M., DE MOERLOOSE, B., BENOIT, Y., SELLESLAG, D., BILLIET, J., ROBERT, A., HUGUET, F., VANDENBERGHE, P., DE PAEPE, A., MARYNEN, P. & HAGEMEIJER, A. 2005. A new recurrent inversion, inv(7)(p15q34), leads to transcriptional activation of HOXA10 and HOXA11 in a subset of T-cell acute lymphoblastic leukemias. *Leukemia,* 19**,** 358-66.

SPITS, H. 2002. Development of alphabeta T cells in the human thymus. *Nat Rev Immunol,* 2**,** 760-72.

STEIN, E. M. & TALLMAN, M. S. 2016. Emerging therapeutic drugs for AML. *Blood,* 127**,** 71-8.

STEIN, S. J., MACK, E. A., ROME, K. S., PAJCINI, K. V., OHTANI, T., XU, L., LI, Y., MEIJERINK, J. P., FARYABI, R. B. & PEAR, W. S. 2016. Trib2 Suppresses Tumor Initiation in Notch-Driven T-ALL. *PLoS One,* 11**,** e0155408.

SUBRAMANIAN, A., TAMAYO, P., MOOTHA, V. K., MUKHERJEE, S., EBERT, B. L., GILLETTE, M. A., PAULOVICH, A., POMEROY, S. L., GOLUB, T. R., LANDER, E. S. & MESIROV, J. P. 2005. Gene set enrichment analysis: a knowledge-based approach for interpreting genome-wide expression profiles. *Proc Natl Acad Sci U S A,* 102**,** 15545-50.

SUDO, K., EMA, H., MORITA, Y. & NAKAUCHI, H. 2000. Age-associated characteristics of murine hematopoietic stem cells. *J Exp Med,* 192**,** 1273-80.

SUGAWARA, T., MORIGUCHI, T., NISHIDA, E. & TAKAHAMA, Y. 1998. Differential roles of ERK and p38 MAP kinase pathways in positive and negative selection of T lymphocytes. *Immunity,* 9**,** 565-74.

SUN, D., LUO, M., JEONG, M., RODRIGUEZ, B., XIA, Z., HANNAH, R., WANG, H., LE, T., FAULL, K. F., CHEN, R., GU, H., BOCK, C., MEISSNER, A., GOTTGENS, B., DARLINGTON, G. J., LI, W. & GOODELL, M. A. 2014. Epigenomic profiling of young and aged HSCs reveals concerted changes during aging that reinforce self-renewal. *Cell Stem Cell,* 14**,** 673-88.

SUNG, H. Y., GUAN, H., CZIBULA, A., KING, A. R., EDER, K., HEATH, E., SUVARNA, S. K., DOWER, S. K., WILSON, A. G., FRANCIS, S. E., CROSSMAN, D. C. & KISS-TOTH, E. 2007. Human tribbles-1 controls proliferation and chemotaxis of smooth muscle cells via MAPK signaling pathways. *J Biol Chem,* 282**,** 18379-87.

TAGHON, T., WAEGEMANS, E. & VAN DE WALLE, I. 2012. Notch signaling during human T cell development. *Curr Top Microbiol Immunol,* 360**,** 75-97.

TAGHON, T., YUI, M. A., PANT, R., DIAMOND, R. A. & ROTHENBERG, E. V. 2006. Developmental and molecular characterization of emerging beta- and gammadelta-selected pre-T cells in the adult mouse thymus. *Immunity,* 24**,** 53-64.

TAKASATO, M., KOBAYASHI, C., OKABAYASHI, K., KIYONARI, H., OSHIMA, N., ASASHIMA, M. & NISHINAKAMURA, R. 2008. Trb2, a mouse homolog of tribbles, is dispensable for kidney and mouse development. *Biochem Biophys Res Commun,* 373**,** 648-52.

TAKEDA, S., RODEWALD, H. R., ARAKAWA, H., BLUETHMANN, H. & SHIMIZU, T. 1996. MHC class II molecules are not required for survival of newly

generated CD4+ T cells, but affect their long-term life span. *Immunity, 5***,** 217-28.

TAN, S. H., YAM, A. W., LAWTON, L. N., WONG, R. W., YOUNG, R. A., LOOK, T. A. & SANDA, T. 2015. TRIB2 reinforces the oncogenic transcriptional program controlled by the TAL1 complex in T-cell acute lymphoblastic leukemia. *Leukemia.*

TOYODA, H., TANAKA, S., MIYAGAWA, T., HONDA, Y., TOKUNAGA, K. & HONDA, M. 2010. Anti-Tribbles homolog 2 autoantibodies in Japanese patients with narcolepsy. *Sleep,* 33**,** 875-8.

TYCKO, B., SMITH, S. D. & SKLAR, J. 1991. Chromosomal translocations joining LCK and TCRB loci in human T cell leukemia. *J Exp Med,* 174**,** 867-73.

VAN LIMBERGEN, H., BEVERLOO, H. B., VAN DRUNEN, E., JANSSENS, A., HAHLEN, K., POPPE, B., VAN ROY, N., MARYNEN, P., DE PAEPE, A., SLATER, R. & SPELEMAN, F. 2001. Molecular cytogenetic and clinical findings in ETV6/ABL1-positive leukemia. *Genes Chromosomes Cancer,* 30**,** 274-82.

VAN VLIERBERGHE, P., AMBESI-IMPIOMBATO, A., DE KEERSMAECKER, K., HADLER, M., PAIETTA, E., TALLMAN, M. S., ROWE, J. M., FORNE, C., RUE, M. & FERRANDO, A. A. 2013. Prognostic relevance of integrated genetic profiling in adult T-cell acute lymphoblastic leukemia. *Blood,* 122**,** 74-82.

VAN VLIERBERGHE, P. & FERRANDO, A. 2012. The molecular basis of T cell acute lymphoblastic leukemia. *J Clin Invest,* 122**,** 3398-406.

VAN VLIERBERGHE, P., VAN GROTEL, M., BEVERLOO, H. B., LEE, C., HELGASON, T., BUIJS-GLADDINES, J., PASSIER, M., VAN WERING, E. R., VEERMAN, A. J., KAMPS, W. A., MEIJERINK, J. P. & PIETERS, R. 2006. The cryptic chromosomal deletion del(11)(p12p13) as a new activation

mechanism of LMO2 in pediatric T-cell acute lymphoblastic leukemia. *Blood,* 108**,** 3520-9.

VARDIMAN, J. W., HARRIS, N. L. & BRUNNING, R. D. 2002. The World Health Organization (WHO) classification of the myeloid neoplasms. *Blood,* 100**,** 2292-302.

VARDIMAN, J. W., THIELE, J., ARBER, D. A., BRUNNING, R. D., BOROWITZ, M. J., PORWIT, A., HARRIS, N. L., LE BEAU, M. M., HELLSTROM-LINDBERG, E., TEFFERI, A. & BLOOMFIELD, C. D. 2009. The 2008 revision of the World Health Organization (WHO) classification of myeloid neoplasms and acute leukemia: rationale and important changes. *Blood,* 114**,** 937-51.

VOGEL, A. B., HAASBACH, E., REILING, S. J., DROEBNER, K., KLINGEL, K. & PLANZ, O. 2010. Highly pathogenic influenza virus infection of the thymus interferes with T lymphocyte development. *J Immunol,* 185**,** 4824-34.

WANG, J., JANI-SAIT, S. N., ESCALON, E. A., CARROLL, A. J., DE JONG, P. J., KIRSCH, I. R. & APLAN, P. D. 2000. The t(14;21)(q11.2;q22) chromosomal translocation associated with T-cell acute lymphoblastic leukemia activates the BHLHB1 gene. *Proc Natl Acad Sci U S A,* 97**,** 3497-502.

WANG, J., PARK, J. S., WEI, Y., RAJURKAR, M., COTTON, J. L., FAN, Q., LEWIS, B. C., JI, H. & MAO, J. 2013a. TRIB2 acts downstream of Wnt/TCF in liver cancer cells to regulate YAP and C/EBPalpha function. *Mol Cell,* 51**,** 211-25.

WANG, J., ZHANG, Y., WENG, W., QIAO, Y., MA, L., XIAO, W., YU, Y., PAN, Q. & SUN, F. 2013b. Impaired phosphorylation and ubiquitination by p70 S6 kinase (p70S6K) and Smad ubiquitination regulatory factor 1 (Smurf1) promote tribbles homolog 2 (TRIB2) stability and carcinogenic property in liver cancer. *J Biol Chem,* 288**,** 33667-81.

WANG, P. Y., SUN, Y. X., ZHANG, S., PANG, M., ZHANG, H. H., GAO, S. Y., ZHANG, C., LV, C. J. & XIE, S. Y. 2013c. Let-7c inhibits A549 cell

195

proliferation through oncogenic TRIB2 related factors. *FEBS Lett,* 587**,** 2675-81.

WANG, R., HE, G., NELMAN-GONZALEZ, M., ASHORN, C. L., GALLICK, G. E., STUKENBERG, P. T., KIRSCHNER, M. W. & KUANG, J. 2007. Regulation of Cdc25C by ERK-MAP kinases during the G2/M transition. *Cell,* 128**,** 1119-32.

WANG, X., XIAO, G., ZHANG, Y., WEN, X., GAO, X., OKADA, S. & LIU, X. 2008. Regulation of Tcrb recombination ordering by c-Fos-dependent RAG deposition. *Nat Immunol,* 9**,** 794-801.

WEI, S. C., ROSENBERG, I. M., CAO, Z., HUETT, A. S., XAVIER, R. J. & PODOLSKY, D. K. 2012. Tribbles 2 (Trib2) is a novel regulator of toll-like receptor 5 signaling. *Inflamm Bowel Dis,* 18**,** 877-88.

WENG, A. P., FERRANDO, A. A., LEE, W., MORRIS, J. P. T., SILVERMAN, L. B., SANCHEZ-IRIZARRY, C., BLACKLOW, S. C., LOOK, A. T. & ASTER, J. C. 2004. Activating mutations of NOTCH1 in human T cell acute lymphoblastic leukemia. *Science,* 306**,** 269-71.

WILSON, A., LAURENTI, E., OSER, G., VAN DER WATH, R. C., BLANCO-BOSE, W., JAWORSKI, M., OFFNER, S., DUNANT, C. F., ESHKIND, L., BOCKAMP, E., LIO, P., MACDONALD, H. R. & TRUMPP, A. 2008. Hematopoietic stem cells reversibly switch from dormancy to self-renewal during homeostasis and repair. *Cell,* 135**,** 1118-29.

WOUTERS, B. J., JORDA, M. A., KEESHAN, K., LOUWERS, I., ERPELINCK-VERSCHUEREN, C. A., TIELEMANS, D., LANGERAK, A. W., HE, Y., YASHIRO-OHTANI, Y., ZHANG, P., HETHERINGTON, C. J., VERHAAK, R. G., VALK, P. J., LOWENBERG, B., TENEN, D. G., PEAR, W. S. & DELWEL, R. 2007. Distinct gene expression profiles of acute myeloid/T-lymphoid leukemia with silenced CEBPA and mutations in NOTCH1. *Blood,* 110**,** 3706-14.

XIA, Y., BROWN, L., YANG, C. Y., TSAN, J. T., SICILIANO, M. J., ESPINOSA, R., 3RD, LE BEAU, M. M. & BAER, R. J. 1991. TAL2, a helix-loop-helix gene activated by the (7;9)(q34;q32) translocation in human T-cell leukemia. *Proc Natl Acad Sci U S A,* 88**,** 11416-20.

XIE, S., XIE, N., LI, Y., WANG, P., ZHANG, C., LI, Q., LIU, X., DENG, J., ZHANG, C. & LV, C. 2012. Upregulation of TRB2 induced by miR-98 in the early lesions of large artery of type-2 diabetic rat. *Molecular and Cellular Biochemistry,* 361**,** 305-314.

XIN, J. X., YUE, Z., ZHANG, S., JIANG, Z. H., WANG, P. Y., LI, Y. J., PANG, M. & XIE, S. Y. 2013. miR-99 inhibits cervical carcinoma cell proliferation by targeting TRIB2. *Oncol Lett,* 6**,** 1025-1030.

YAMAMOTO, R., MORITA, Y., OOEHARA, J., HAMANAKA, S., ONODERA, M., RUDOLPH, K. L., EMA, H. & NAKAUCHI, H. 2013. Clonal analysis unveils self-renewing lineage-restricted progenitors generated directly from hematopoietic stem cells. *Cell,* 154**,** 1112-26.

YOKOYAMA, T., KANNO, Y., YAMAZAKI, Y., TAKAHARA, T., MIYATA, S. & NAKAMURA, T. 2010. Trib1 links the MEK1/ERK pathway in myeloid leukemogenesis. *Blood,* 116**,** 2768-75.

YOKOYAMA, T. & NAKAMURA, T. 2011. Tribbles in disease: Signaling pathways important for cellular function and neoplastic transformation. *Cancer Sci,* 102**,** 1115-22.

YOKOYAMA, T., TOKI, T., AOKI, Y., KANEZAKI, R., PARK, M. J., KANNO, Y., TAKAHARA, T., YAMAZAKI, Y., ITO, E., HAYASHI, Y. & NAKAMURA, T. 2012. Identification of TRIB1 R107L gain-of-function mutation in human acute megakaryocytic leukemia. *Blood,* 119**,** 2608-11.

YOSHIMURA, F. K., WANG, T. & CANKOVIC, M. 1999. Sequences between the enhancer and promoter in the long terminal repeat affect murine leukemia virus pathogenicity and replication in the thymus. *J Virol,* 73**,** 4890-8.

YUI, M. A., FENG, N. & ROTHENBERG, E. V. 2010. Fine-scale staging of T cell lineage commitment in adult mouse thymus. *J Immunol,* 185**,** 284-93.

YUI, M. A. & ROTHENBERG, E. V. 2014. Developmental gene networks: a triathlon on the course to T cell identity. *Nat Rev Immunol,* 14**,** 529-45.

YUSUF, I. & FRUMAN, D. A. 2003. Regulation of quiescence in lymphocytes. *Trends Immunol,* 24**,** 380-6.

ZANELLA, F., RENNER, O., GARCIA, B., CALLEJAS, S., DOPAZO, A., PEREGRINA, S., CARNERO, A. & LINK, W. 2010. Human TRIB2 is a repressor of FOXO that contributes to the malignant phenotype of melanoma cells. *Oncogene,* 29**,** 2973-82.

ZEDIAK, V. P., MAILLARD, I. & BHANDOOLA, A. 2007. Multiple prethymic defects underlie age-related loss of T progenitor competence. *Blood,* 110**,** 1161-7.

ZHANG, C., CHI, Y. L., WANG, P. Y., WANG, Y. Q., ZHANG, Y. X., DENG, J., LV, C. J. & XIE, S. Y. 2012a. miR-511 and miR-1297 inhibit human lung adenocarcinoma cell proliferation by targeting oncogene TRIB2. *PLoS One,* 7**,** e46090.

ZHANG, H., PHOTIOU, A., GROTHEY, A., STEBBING, J. & GIAMAS, G. 2012b. The role of pseudokinases in cancer. *Cell Signal,* 24**,** 1173-1184.

ZHANG, H. H., PANG, M., DONG, W., XIN, J. X., LI, Y. J., ZHANG, Z. C., YU, L., WANG, P. Y., LI, B. S. & XIE, S. Y. 2014. miR-511 induces the apoptosis of radioresistant lung adenocarcinoma cells by triggering BAX. *Oncol Rep,* 31**,** 1473-9.

ZHANG, J., DING, L., HOLMFELDT, L., WU, G., HEATLEY, S. L., PAYNE-TURNER, D., EASTON, J., CHEN, X., WANG, J., RUSCH, M., LU, C., CHEN, S. C., WEI, L., COLLINS-UNDERWOOD, J. R., MA, J., ROBERTS, K. G., POUNDS, S. B., ULYANOV, A., BECKSFORT, J., GUPTA, P., HUETHER, R., KRIWACKI, R. W., PARKER, M., MCGOLDRICK, D. J., ZHAO, D., ALFORD, D., ESPY, S., BOBBA, K. C., SONG, G., PEI, D.,

CHENG, C., ROBERTS, S., BARBATO, M. I., CAMPANA, D., COUSTAN-SMITH, E., SHURTLEFF, S. A., RAIMONDI, S. C., KLEPPE, M., COOLS, J., SHIMANO, K. A., HERMISTON, M. L., DOULATOV, S., EPPERT, K., LAURENTI, E., NOTTA, F., DICK, J. E., BASSO, G., HUNGER, S. P., LOH, M. L., DEVIDAS, M., WOOD, B., WINTER, S., DUNSMORE, K. P., FULTON, R. S., FULTON, L. L., HONG, X., HARRIS, C. C., DOOLING, D. J., OCHOA, K., JOHNSON, K. J., OBENAUER, J. C., EVANS, W. E., PUI, C. H., NAEVE, C. W., LEY, T. J., MARDIS, E. R., WILSON, R. K., DOWNING, J. R. & MULLIGHAN, C. G. 2012c. The genetic basis of early T-cell precursor acute lymphoblastic leukaemia. *Nature,* 481**,** 157-63.

ZHANG, J. A., MORTAZAVI, A., WILLIAMS, B. A., WOLD, B. J. & ROTHENBERG, E. V. 2012d. Dynamic transformations of genome-wide epigenetic marking and transcriptional control establish T cell identity. *Cell,* 149**,** 467-82.

ZHANG, L., LI, X., KE, Z., HUANG, L., LIANG, Y., WU, J., ZHANG, X., CHEN, Y., ZHANG, H. & LUO, X. 2013. MiR-99a may serve as a potential oncogene in pediatric myeloid leukemia. *Cancer Cell Int,* 13**,** 110.

ZHANG, P., NELSON, S., BAGBY, G. J., SIGGINS, R., 2ND, SHELLITO, J. E. & WELSH, D. A. 2008. The lineage-c-Kit+Sca-1+ cell response to Escherichia coli bacteremia in Balb/c mice. *Stem Cells,* 26**,** 1778-86.

ZHANG, Y., DAVIS, J. L. & LI, W. 2005. Identification of tribbles homolog 2 as an autoantigen in autoimmune uveitis by phage display. *Mol Immunol,* 42**,** 1275-81.

ZHENG, Y. S., ZHANG, H., ZHANG, X. J., FENG, D. D., LUO, X. Q., ZENG, C. W., LIN, K. Y., ZHOU, H., QU, L. H., ZHANG, P. & CHEN, Y. Q. 2012. MiR-100 regulates cell differentiation and survival by targeting RBSP3, a phosphatase-like tumor suppressor in acute myeloid leukemia. *Oncogene,* 31**,** 80-92.

ZHOU, M. H., GAO, L., JING, Y., XU, Y. Y., DING, Y., WANG, N., WANG, W., LI, M. Y., HAN, X. P., SUN, J. Z., WANG, L. L. & YU, L. 2012. Detection of ETV6 gene rearrangements in adult acute lymphoblastic leukemia. *Ann Hematol,* 91**,** 1235-43.

ZUNA, J., ZALIOVA, M., MUZIKOVA, K., MEYER, C., LIZCOVA, L., ZEMANOVA, Z., BREZINOVA, J., VOTAVA, F., MARSCHALEK, R., STARY, J. & TRKA, J. 2010. Acute leukemias with ETV6/ABL1 (TEL/ABL) fusion: poor prognosis and prenatal origin. *Genes Chromosomes Cancer,* 49**,** 873-84.